Imbalance minimization in Virtual Power Plants using Industrial Demand Response

R.F.J. Tetteroo

Master of Science Thesis

TU Delft Delft University of Technology

Intelligent Electrical Power Grids

Imbalance minimization in Virtual Power Plants using Industrial Demand Response

Master of Science Thesis

For the degree of Master of Science in Sustainable Energy Technology
at Delft University of Technology

R.F.J. Tetteroo
4046315

July 9, 2021

Dr. Miloš Cvetković	Supervisor
Prof. Peter Palensky	Supervisor
Msc. Digvijay Gusain	Daily supervisor
Dr. Rudi Santbergen	External reader

Faculty of Electrical Engineering, Mathematics and Computer Science (EEMCS) · Delft University of Technology

Abstract

The growing number of distributed energy resources (DER) connected to the low- and medium voltage grid has prompted the development of Virtual Power Plants. Virtual Power Plants can aggregate and dispatch DER to gain revenue in the Day-Ahead market, however as a Balancing Responsible Party it can risk imbalance cost due to the errors between the Day-Ahead forecast and actual production of renewable energy. Industrial loads can provide demand response by making deliberate changes to their energy consumption which can assist in the reduction of imbalances in a Virtual Power Plant portfolio. This thesis provides a technical analysis of the ability of industrial processes to minimize the imbalances in Virtual Power Plants due to Day-Ahead forecast errors of renewable energy.

Literature on industrial demand response was reviewed to identify the advantages and disadvantages of major industrial processes to operate as a flexible load in a short-term redispatch scheme. Suitable processes included refrigerated warehouses, chlor-alkali-, hydrogen- and aluminum production plants, owing to their high ramp-rate, low complexity, fast response time or ability to shift load consumption in time. On the other hand, less suitable processes included the steel-making, cement production and paper & pulp industry due to inefficiencies at partial load, significant inter-dependencies of processes or high utilization rates.

An analysis was performed on the capability of the chlor-alkali and hydrogen industry to minimize imbalances in a Virtual Power Plant. To this purpose, a simulation setup was developed in Python of a Virtual Power Plant comprising PV (300 MW) and onshore wind energy (300 MW), a chlor-alkali (203.5 MW) and hydrogen plant (193.4 MW), and a controller based on Model Predictive Control (MPC). The industrial plants were modelled in detail using OpenModelica which could be simulated in Python as Functional Mock-up Units. An innovative MPC was developed with the objective to minimize imbalances due to the errors between Day-Ahead bids and actual energy production by adjusting the energy consumption of the industrial plants. The industrial process dynamics were successfully implemented in the MPC by integrating Hammerstein Wiener models based on simulated input-output data of the chlor-alkali and hydrogen plant. Historical data was used to provide a realistic presentation of the Day-Ahead forecast errors in a renewable energy portfolio. A simulation study was performed for the month of October and the results show that industrial demand response by the chlor-alkali and hydrogen plant can significantly reduce imbalances from 12947 MWh to

1277 MWh (-90.1%). The major cause for the remaining imbalances is the limited capacity of the hydrogen and chlorine storage, whereas imbalances did not result from operation at a high utilization rate or from ramp-rate limitations of the industrial plants. The MPC could adequately adjust the energy consumption of the industrial plant while ensuring that constraints on process variables were respected.

A sensitivity analysis showed that the imbalances are strongly affected by the storage capacity. Halving the storage capacity of the industrial plants compared to the base-case significantly increased the imbalances to 4149 MWh (+225%) since storage level limits were reached more frequently. Doubling the storage capacity nearly eliminated the imbalances (-99%) as the storage levels limits were not reached. The utilization rate of the industrial plants showed minor effects on the imbalance minimization between 80 to 90%, whilst from 95% imbalances increased significantly up to 2891 MWh (+126%) due the lack of regulation capacity for reducing positive imbalances. Furthermore, it was shown that without a correction to the Day-Ahead bids to guide storage levels towards the midway level, the imbalances rise majorly to 6643 MWh (+420%) as a result of continuously positive or negative Day-Ahead errors. Prediction horizon length and the accuracy of the imbalance forecast had no influence on the imbalance minimization ability of the MPC owing to the favorably high ramp rate of the industrial plants. Finally, the imbalance minimization performance of the industrial plants could be maintained successfully even when restricting the ramp frequency of individual production units by increasing the number of separately controllable electrolyser sub-groups.

This study shows there is a significant potential for industrial processes to minimize imbalances in Virtual Power Plants. The results of this research can assist in the development of Virtual Power Plants that aim at reducing their imbalances and it can contribute to a wider participation of industrial processes in distributed energy systems.

Table of Contents

List of Figures

List of Tables

Acknowledgements

This thesis marks the end of my study period at the Technical University of Delft for the master Sustainable Energy Technology. It would not have been possible without the support of several important people.

I would like to start by thanking my supervisor dr. Miloš Cvetković. It was a great pleasure to perform my master thesis in the Intelligent Electrical Power Grids group under your guidance and I much enjoyed the fruitful discussions that helped improve the scientific quality of this research. Furthermore, the support and guidance of professor Peter Palensky has been greatly appreciated. Your enthusiasm for the research topic was a great motivating factor during this thesis process. In addition, I am very grateful for the participation of dr. Rudi Santbergen in the examination committee and his interest in taking part in the thesis defense. Finally, I want to thank my daily supervisor Digvijay Gusain. It has been a real pleasure to collaborate with you on this topic. Your enthusiasm, helpful feedback and openness for new ideas have made this thesis process a great learning experience.

Additionally, I have had support from my parents, my stepmother and my vast number of brothers and sisters whom have always been there throughout my studies and during this project. I also appreciate the help of Alex for proofreading the thesis and providing me with his useful comments. During my study period, there have also been multiple great friends of which I can only mention a few. I want to thank Arjan and Marleen for the interesting and fun dinners we have had together and for the sportive skating rounds that kept me off my chair. Furthermore, I am grateful for having had Veikko and Alessia with me as they provided a listening ear or much needed distraction from studying when needed. Additionally, I appreciate the relaxing times with Ron throughout my studies that kept giving me a fresh perspective and I enjoyed the talks with Ludwig on optimization and control theory which greatly boosted my understanding of these subjects.

Finally, I would very much like to thank Thalia. Your continuous love and support has been invaluable and I am grateful for having spent both the great and more difficult times of this journey with you.

Delft, University of Technology
July 9, 2021

R.F.J. Tetteroo

Chapter 1

Introduction

1-1 Background issue

In 2015, countries around the world have signed the Paris Agreement in order to restrict the global temperature rise to 2 degrees [1]. One of the main trajectories to reduce the greenhouse gas emissions and thereby limit the increase of global temperature is the transition from a carbon-intensive to a low-carbon and renewable energy system. The intended transition faces some challenges, however, notably regarding the integration of renewable energy in the power system and the phasing out of conventional power generators [2]. Renewable energy resources such as solar and wind energy are significantly influenced by environmental and climatic factors. Therefore, their output is strongly volatile and uncertain which makes balancing energy demand and supply in the grid increasingly difficult. Furthermore, the traditional power system is designed for power flow in a single direction. Namely, large-scale conventional generators produce power which is transported by the high-voltage network and then distributed by a medium-voltage and low-voltage network where it is used by consumers. Renewable resources increasingly feed power directly into the medium-voltage or low-voltage networks which can lead to technical issues such as transmission congestion and voltage and frequency instabilities [3]. Moreover, the conventional synchronous generators perform an important function by providing ancillary services, such as frequency restoration and reserve power provision, which helps protect the power system reliability [4]. Replacing the conventional generators with renewable energy sources will require new entities to provide ancillary services. The challenges mentioned above motivate the development of innovative power plants based on renewable energy resources that can produce energy for wholesale markets and/or provide ancillary services to protect the power system reliability. The Virtual Power Plant is a concept that could meet the above mentioned criteria.

1-2 Literature review

A Virtual Power plant (VPP) is an aggregation of distributed energy resources connected in a single system. At the core of the Virtual Power Plant is the energy management system which

dispatches the energy resources in order to maximize profit in wholesale electricity markets or to support the power system reliability. Virtual Power Plants integrate distributed energy resources (DER) which are electric power resources directly connected to the medium-voltage and low-voltage distribution networks, rather than the high voltage transmission network [5]. DER comprise a wide variety of energy technologies including generation units (i.e. wind and solar energy), storage devices (i.e. batteries), energy conversion systems (i.e. fuel cells and electrolysers) and controllable loads.

Several motivations and incentives drive the development of Virtual Power Plants. As mentioned, a rising number of DER are being connected to the low-voltage and medium-voltage grids which can cause network reliability issues if their dispatch is uncontrolled [5]. Virtual Power Plants aggregate multiple DER in a single portfolio and can coordinate their dispatch such that network constraints are not violated [6]. Furthermore, the aggregation of DER in a Virtual Power Plants grant small-scale DER access to the wholesale markets. This can improve the revenue per DER unit and, additionally, increase the visibility of DER to the network operators [7]. Virtual Power Plants are also able to integrate large shares of renewable energy resources in their portfolio while still being a reliable and secure source of energy [7]. To be more specific, the variability and uncertainty of renewable energy can be compensated by intelligently dispatching the controllable DER units in the Virtual Power Plant. Finally, Virtual Power Plants can be designed to provide ancillary services, such as frequency control, voltage control and black start capability, similar to conventional generators [8]. With its ability to provide both energy for wholesale electricity markets and ancillary services, Virtual Power Plants can hence assist in the phasing-out of conventional fossil fuel based generators [7].

Virtual Power Plants can participate in the Day-Ahead Energy market to make revenue [9]. The Day-Ahead market is a wholesale electricity market where producers and consumers can buy/sell energy a day before the delivery [10]. Participants in the Day-Ahead market need to send bids for each of the 24 hours of the next day before a market deadline, which is 12.00 CET in the Netherlands. After the deadline, the market operator determines the Day-Ahead price for each hour and contracts the nominated bids of the consumers/producers. In literature, Virtual Power Plants are often assumed to be a Balancing Responsible Party [11, 9, 12]. BRP's are obliged to execute the Day-Ahead market schedule and they are held financially responsible for any deviations from the schedule. These deviations are known as imbalances and can be defined as the difference between the planned energy consumption/production in the Day-Ahead market and actual energy exchange with the grid during an Imbalance Settlement Period (ISP) [13]. An Imbalance Settlement Period consists of 15 minutes. The sum of all imbalances of BRP's comprise the system imbalance which the Transmission System Operator (TSO) needs to eliminate by activating balancing power. BRP's are incentivized to minimize their individual imbalances through the imbalance pricing system. A BRP will be remunerated if its individual imbalances help restore the total system imbalance, however it is penalized if the imbalances increased the total system imbalance in an ISP [10]. The remuneration/penalty depends on the imbalance price which is highly volatile and difficult to predict [10].

Virtual Power Plants with renewable energy resources rely on energy forecasts to determine the bids on the Day-Ahead market. Because of errors in this Day-Ahead forecast due to uncertainty of renewable energy production, a deviation between the actual renewable energy production and the Day-Ahead bid can occur leading to imbalances. With the volatile and

uncertain imbalance price, Virtual Power Plants may risk high imbalance cost and therefore multiple studies have started focusing on the minimization of imbalance cost or volumes. In Ref. [11], a scheduling strategy was developed for a Virtual Power Plant with renewable energy generation, energy storage and controllable loads that operates in the Day-Ahead market. The anticipated imbalance cost due to Day-Ahead forecast errors were minimized during the Day-Ahead bidding phase by using stochastic optimization. In Ref. [14], an optimal bidding strategy for the Day-Ahead market was developed for a Virtual Power Plant with wind energy, energy storage and controllable loads. In this study, the intraday market was also used to correct the deviations between the Day-Ahead bid and the actual energy exchange with the grid. Various studies have applied a control system that can continuously redispatch flexible resources in the Virtual Power Plant close to real-time in order to minimize imbalance costs or volumes. A control system known as Model Predictive Control (MPC) is often utilized to this purpose which relies on the rolling horizon principle. The term rolling horizon refers to the repeated solving of a time-dependent model to determine control inputs over a planning horizon, of which only the first input is implemented, and moving the planning horizon a step forward in time after each solution step. In Ref. [12], a two-staged optimization was developed for a Virtual Power Plant with wind energy and a biomass CHP. In the first stage, stochastic optimization is used to calculate the Day-Ahead bids and in the second phase a Model Predictive Control unit continuously redispatches a biomass plant to minimize imbalance cost. A similar two-stage optimization was developed in Ref. [15], but in this case flexible micro-CHP systems were used to minimize balancing cost. In Ref. [13], a Model Predictive Control unit was developed to minimize imbalances in a Virtual Power Plant by redispatching controllable loads.

As shown in the references above [13, 11, 14], several types of flexible resources can be integrated in a Virtual Power Plant portfolio which can be redispatched close to real-time. These flexible resources include energy storage, flexible generation units and controllable loads amongst others. Controllable loads can make deliberate changes to their energy consumption from their regular demand profile which is known as Demand Response (DR). The industrial sector hosts several processes with the ability to provide demand response [16]. Furthermore, industrial processes also possess favorable characteristics for implementing demand response such as a high energy intensity per actor and availability of necessary infrastructure such as sensors, metering technologies and personal operators [17]. Thus far, research on industrial demand response in Virtual Power Plants is limited [18, 19, 20]. In Ref. [18], a scheduling algorithm for a Virtual Power Plant with wind energy, conventional generators, and industrial loads (iron melting and steel companies) was developed. Mixed Integer Non-Linear Programming was used to schedule the generators and industrial loads such that profits in multiple energy markets were maximized. In Ref. [19] and Ref. [20], the same Virtual Power Plant setup as in [18] was used, however in [19] different types of demand response programs were evaluated and in [20] a risk management study in the case of contingencies was included.

Recently, studies on demand response in the industrial sector have highlighted the importance of integrating nonlinear dynamics of the industrial process during the scheduling [21, 22, 23, 24]. This is necessary in order to avoid generating load schedules that would result in a violation of constraints of the industrial process. In Ref. [21], a MPC was developed to schedule industrial air separation units under time-varying prices such that operational cost can be minimized. Data-driven, low-order models for the MPC were developed using input-output data of complex, high fidelity models such that lower computation times could be

achieved while still including the relevant nonlinear dynamics of the plant. In Ref. [23] the scheduling of air separation units was examined in more detail with the aim of minimizing operational costs in the Day-Ahead market and the Californian real-time market. In Ref. [22], a first-principles model was developed of a chlor-alkali plant which was used in a scheduling algorithm to minimize operational cost in the Day-Ahead market. Finally, in Ref. [24] input and output data of the first principles chlor-alkali model of Ref. [22] was used to identify a data-driven model that could be solved with less computational effort and the model was used in an optimization to maximize profits in the Day-Ahead and Real-Time market.

1-3 Research goals

Virtual Power Plants can trade in the Day-Ahead market to gain revenue, however as a Balancing Responsible Party it can risk high balancing cost due to errors in the Day-Ahead forecast of renewable energy. In order to minimize imbalances, Virtual Power Plants can integrate resources in the portfolio that can be dispatched near real-time [13, 15, 12] including flexible industrial processes which can provide demand response [17]. The present research on demand response in Virtual Power Plants, however, mainly focuses on the residential sector [13, 11, 14] whilst studies that use demand response provided by industrial processes are limited [19, 18, 20]. Furthermore, the focus of these limited studies is mainly on economic factors such as profit maximization in wholesale markets rather than on the technical ability of these industries to minimize imbalances. In addition, the studies generally apply simplistic process models in the optimization problem that may neglect important dynamics and could generate schedules that violate process constraints. Based on the current research it is evident that a thorough technical analysis of the ability of industrial demand response to minimize imbalances in Virtual Power Plants is lacking.

Therefore, the research objective of this study is:

Investigating the ability of Industrial Demand Response to Minimize Energy Imbalances in Virtual Power Plants due to renewable energy forecast errors.

This main research objective will be addressed with the following three research questions:

1. What are the advantages and disadvantages of major processes in the industrial sector to provide demand response for the minimization of imbalances?
2. What is the capability of the chlor-alkali and hydrogen production process to minimize energy imbalances in Virtual Power Plants caused by Day-Ahead forecast errors of renewable energy?
3. What is the effect of important parameters of the control system and the industrial plants on the minimization of imbalances?

The contribution of the thesis consists of the following:

1. The integration of nonlinear dynamics of industrial processes in the control model of a Model Predictive Control unit to enable scheduling without violating process constraints.

2. An analysis of the ability of two major chemical industries to minimize energy imbalances of a renewable energy based Virtual Power Plant.

3. An innovative control algorithm that can reschedule industrial loads while limiting the ramping frequency of the individual production units.

1-4 Research approach

The first research question will be answered by reviewing the literature on demand response provided by major industrial processes. The processes will be evaluated based on their suitability to operate in a short-term redispatch control system which is necessary for imbalance minimization. Based on the literature two processes are chosen to be integrated in the Virtual Power Plant in this thesis, namely the chlor-alkali and hydrogen process, which are realistic plants operating in the Port of Rotterdam. The second research question will be answered by modelling and simulating a Virtual Power Plant using open-source software as much as possible. The Virtual Power Plant consists of renewable energy, the two industrial plants and a controller based on Model Predictive Control (MPC) that redispatches the industrial plants to minimize imbalances. The third research question is answered by simulating the Virtual Power Plant with varying values of relevant parameters of the controller and industrial plants.

1-5 Thesis structure

This thesis is structured as followed: Chapter 1 provides the research topic, literature review, research objectives and research approach. In Chapter 2, the background on Virtual Power Plants and Model Predictive Control is explained, and literature on industrial demand response is described. Chapter 3 introduces the setup of the Virtual Power Plant and describes the modelling of the renewable resources and the chlor-alkali and hydrogen plant in the Virtual Power Plant. In Chapter 4, the development of the MPC is described which will minimize the imbalances in the Virtual Power Plant. Chapter 5 presents the results of the base-case simulation and the effect of varying parameters on the minimization of imbalances. Finally, in Chapter 6 the conclusion of the thesis will be described and recommendations for further study are included.

Chapter 2

Background

2-1 Virtual Power Plants

Virtual Power Plant are distributed energy systems that can coordinate the dispatch of Distributed Energy Resources (DER) to maximize profits in energy wholesale markets or protect the grid reliability. These DER are energy technologies connected to the medium- and low-voltage networks, rather than the high-voltage networks. This section will elaborate on the concept of the Virtual Power Plant by describing the definition, components and operation in electricity markets.

2-1-1 Definition

The Virtual Power Plant is still in the development phase and its definition is not yet harmonized in scientific literature. For instance in Ref. [25], a Virtual Power Plant is defined as "a cluster of dispersed generation units (either fossil fuel and/or renewable energy based), flexible loads and storage systems that are grouped to operate as a single entity". In Ref. [26] a Virtual Power Plant is a ""A portfolio of Distributed Energy Resources, which are connected by a control system based on information and communication technology (ICT). The VPP acts as a single visible entity in the power system, is always grid-tied and can be either static or dynamic". Most of the definitions share that a VPP is an aggregation of distributed energy resources that are coordinated by a single entity with the goal to provide grid services and/or make revenue in wholesale markets.

In this thesis, the comprehensive definition by the Fenix project in Europe is used [27]:

"A Virtual Power Plant (VPP) aggregates the capacity of many diverse DERs, it creates a single operating profile from a composite of the parameters characterizing each DERs and can incorporate the impact of the network on aggregate DERs output. A VPP is a flexible representation of a portfolio of DERs that can be used to make contracts in the wholesale market and to offer services to the system operator"

Virtual Power Plants have several similarities with microgrids [6]. Microgrids are a set of electrical loads, generation units and storage units that are connected to the electric grid by means of a single point of connection and linked by a control system [28]. However, there are two main differences, namely: 1) Virtual Power Plants are always grid-tied whereas microgrids can operate in islandic mode, disconnected from the main grid, and 2) Virtual Power Plants can aggregate DER that are geographically dispersed, whilst in microgrids the DER are located in the same geographic area [6]. Some other differences have been mentioned in Ref. [28], namely that the capacity of microgrids is often smaller (KW to several MW) than that of Virtual Power Plants, and microgrids have a stronger focus on serving local consumption whereas Virtual Power Plants see consumption as a flexibility resource to be offered in energy markets.

The definition of Virtual Power Plants often strongly overlaps, if not coincides, with that of Aggregators. For instance in ref. [29], an aggregator is defined as "a company who acts as an intermediary between electricity end-users and DER owners and the power system participants who wish to serve these end-users or exploit the services provided by these DERs", which does not provide a clear distinction with a Virtual Power Plant. Thus far no academic work has attempted to either unify or distinguish Aggregators and Virtual Power Plants, hence scientific literature [30, 31], companies [32] and institutions [33] often use the terms interchangeably. To remain consistent, this thesis applies the term Virtual Power Plant and the term Aggregator will not be used further on.

2-1-2 Components

Virtual Power Plants consist of energy resources, namely distributed generation, energy storage and flexible loads, and an Energy Management System [34]. These components are described briefly below.

- Distributed generation units produce electricity and consist of renewable energy resources and conventional energy sources. Examples of distributed renewable energy resources are wind, PV and small hydropower systems, whereas examples of conventional energy resources include diesel generators, micro-gas turbines and biodiesel or biogas generators.
- Energy storage technologies convert power into an energy form that can be stored and reconverted back to electrical energy. Common examples are flywheels, batteries and hydrogen storage systems. The storage technologies can have different applications depending on their technical characteristics such as response rate, energy and power density, and storage capacity.
- Flexible loads are energy consumers that can make deliberate changes to their consumption pattern, for instance in response to varying prices or financial incentives. Making deliberate changes to the consumption pattern is known as Demand Response which will be explained further in Section 2-3.
- The Energy Management System (EMS) is responsible for the scheduling and dispatch of the Virtual Power Plant energy resources. An EMS can perform multiple functions such as providing forecasts of energy generation, load consumption and energy prices,

and coordinating power flow between components. The objectives of the EMS can be widespread, including maximizing profits, improving the power quality, and minimizing greenhouse gas emissions.

2-1-3 Electricity markets and imbalances

Virtual Power Plants can participate in various electricity markets to gain revenue. In this thesis, two markets are considered namely the Day-Ahead and Imbalance market. The timeline of these markets are shown in Figure 2-1. In the Day-Ahead market, participants can buy/sell energy for the next day [10]. The energy is traded in hourly products and it should be produced/consumed at the hour for which the energy has been sold/bought. Every day, participants bid the minimum/maximum price for which it wants to sell/buy a certain energy quantity at each hour of the next day before the market deadline. In the Netherlands, this deadline is at 12:00 CET [10]. After the deadline, the market operator takes all bids into account and it calculates the market clearing price. If the production/consumption bid of the market participant is below/above the market clearing price, the bid is nominated and the participant is required to produce or take-off the amount of energy it has bid in that particular hour.

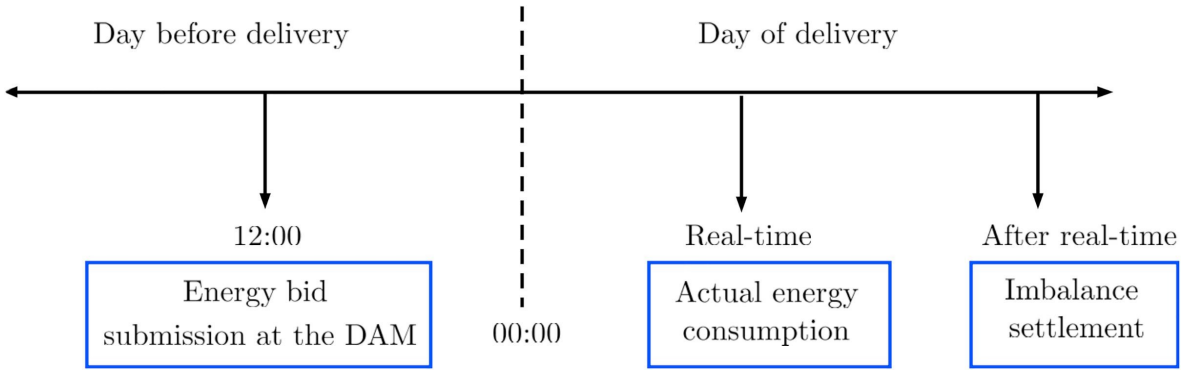

Figure 2-1: Day-Ahead and Imbalance market timeline

The imbalance market takes place in real-time and operates with time periods of 15 minutes which are known as Imbalance Settlement Periods (ISP) [10]. An imbalance is the difference between the Day-Ahead market bid of a market participant and its actual energy exchanged with the power system within an ISP [13]. Imbalances can be negative if the market participant has a shortage, or positive if the participant has a surplus compared to the Day-Ahead bid. The system imbalance is the net sum of all individual imbalances of market participants per ISP [13]. To eliminate the system imbalance, the Transmission System Operator (TSO) needs to activate balancing power thereby ensuring that demand and supply are balanced at all times.

Participants in the Imbalance Market are known as Balancing Responsible Parties (BRP) [35]. In most countries, every consumer/producer connected to the power system should be part of a BRP. BRP's are financially responsible for their imbalances and they are incentivized to minimize imbalances in their portfolio by means of the imbalance price mechanism [36]. Through this mechanism, a BRP receives an imbalance price if their individual imbalances

helped reduce the system imbalance, however it pays an imbalance price if the individual imbalances aggravated the system imbalance within an ISP. The imbalance price is determined during the Imbalance Settlement period and it depends on the cost the TSO made for activating the balancing power that eliminates the system imbalance [36]. Because the imbalance price is volatile and difficult to predict, imbalances can be a significant cost for BRP's.

In between the Imbalance and Day-Ahead market, there is an Intraday market. In the Intraday market of the Netherlands, participants can buy/sell energy as quarter hourly products throughout the day up to 5 minutes before the actual consumption/production time and it can be used for the correction of the imbalance position of a BRP. The Intraday market is not taken into account in this thesis due to its low liquidity.

2-1-4 Internal balancing

Literature often assumes a Virtual Power Plant is a single BRP that is financially responsible for its individual imbalances. An important source of imbalances in Virtual Power Plants are the errors between the Day-Ahead forecast of renewable energy and the actual production [15]. Therefore, various studies focus on minimizing imbalance volumes or costs in Virtual Power Plants which can be achieved by redispatching flexible components near real-time. This is known as internal balancing [15] and a common control method to perform this rescheduling is Model Predictive Control [15].

2-2 Model Predictive Control

Model Predictive Control is a method to control a process or system while satisfying constraints and it is used in a wide range of applications such as chemical processing, indoor climate regulation and vehicle control. MPC consists of solving an optimization problem at each time-step to calculate control inputs for a process [37]. To make predictions about the behaviour of process, the MPC integrates a simplified internal model in the optimization. Unlike other control approaches, MPC can integrate set-points, specific goals and dynamics of the system in the control algorithm. Furthermore, a very important advantage of MPC is the ability to take constraints into account explicitly. In Figure 2-2 a diagram is shown of a Model Predictive Control unit. The term 'plant' is often used for the process that is controlled by the MPC and this term is also used in this thesis. For the internal model of the MPC, this thesis will adopt the term 'control model'.

A key feature of MPC is the rolling horizon principle. A rolling horizon means that each time-step the MPC calculates optimal control actions over a certain prediction horizon. Only the first control input is implemented by the plant after which the MPC shifts a step forward in time and the optimization is performed again. By using this rolling horizon principle, a MPC can take into account the most recent predictions and integrate feedback from the plant to determine the optimal control signals. In Figure 2-3 the rolling horizon principle of a MPC is shown.

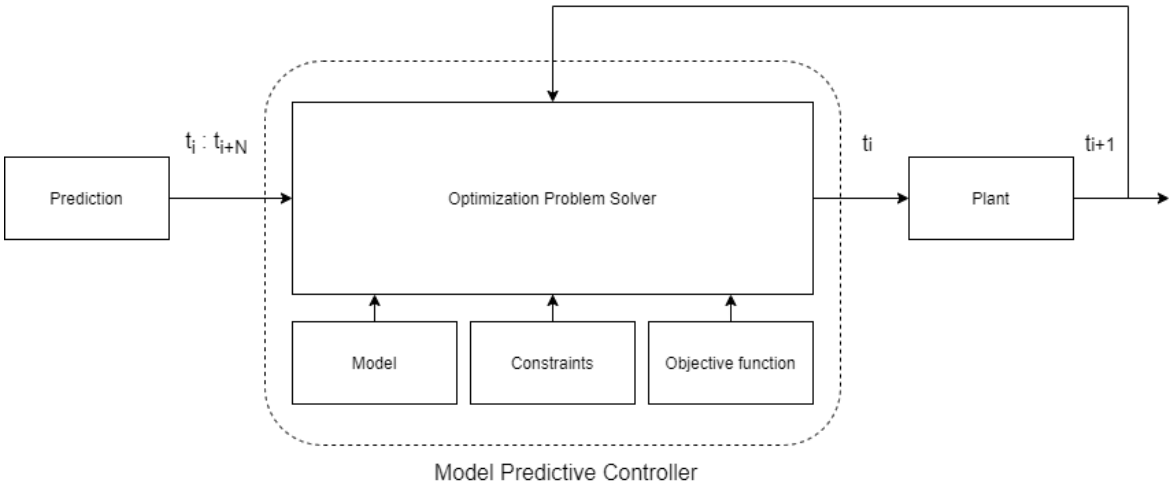

Figure 2-2: Model Predictive Control scheme

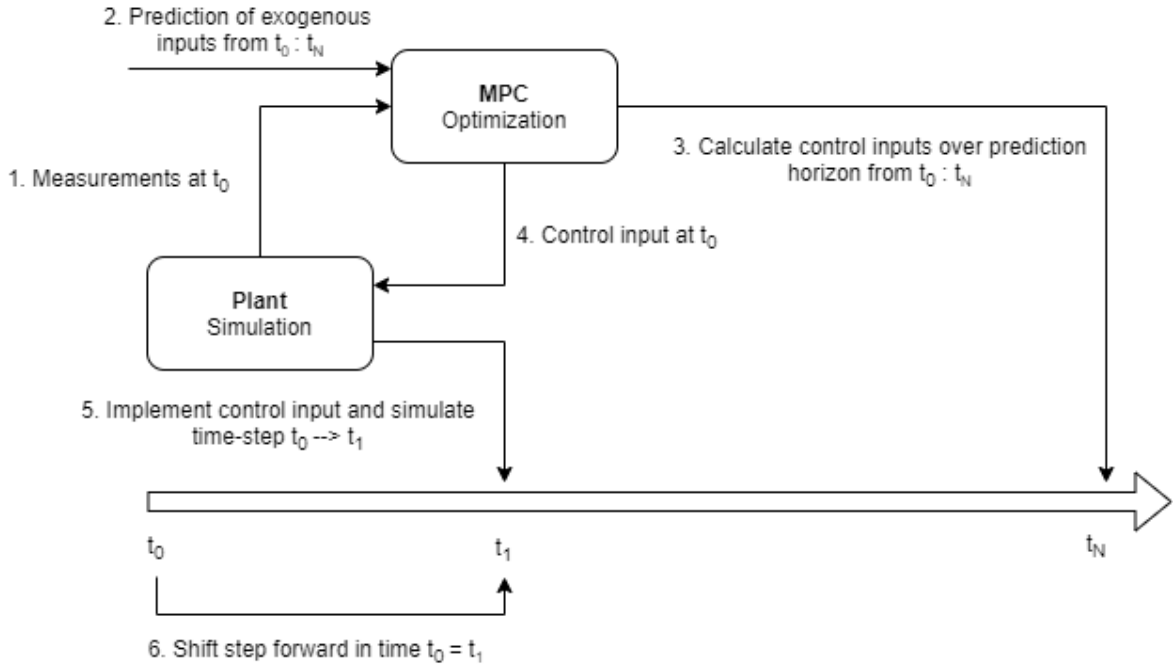

Figure 2-3: Rolling horizon principle in Model Predictive Control

2-3 Demand Response: a suitability analysis of major industries

This section will explain the concept of demand response and provide an analysis of the suitability of major industries to perform demand response in a short-term redispatch scheme as well as a discussion on the industries to be integrated in the Virtual Power Plant of this thesis.

2-3-1 Definition and Classification

Demand Response can be defined as changes to the electricity consumption of end-use customers from their regular consumption profile. It comprises all the intended modifications meant to adjust the timing/level of instantaneous demand, or to change the total electricity consumption of end-use customers [38]. Demand response is part of a collection of actions referred to as Demand Side Management (DSM) [39]. Four types of demand response actions are possible on the end-use consumer side, of which two examples are shown in Figure 2-4:

Load reduction or increasing refers to the deliberate temporary decrease, or increase, of the energy consumption of the end-use customer without changing their energy consumption during other periods [38].

Load shifting refers to moving the energy consumption within time. Load shifting does not result in lost production for consumers, however costs for the rescheduling may still apply especially for industrial consumers.

Generation decreasing or increasing is the temporary up- or down regulation of production capacity at consumers [38].

Changing the consumed energy carrier is a relatively new type of demand response. It can be performed by consumers with technologies that can operate flexibly with different energy carriers (i.e. hybrid boilers that can switch between using electricity or gas to produce heat) [40].

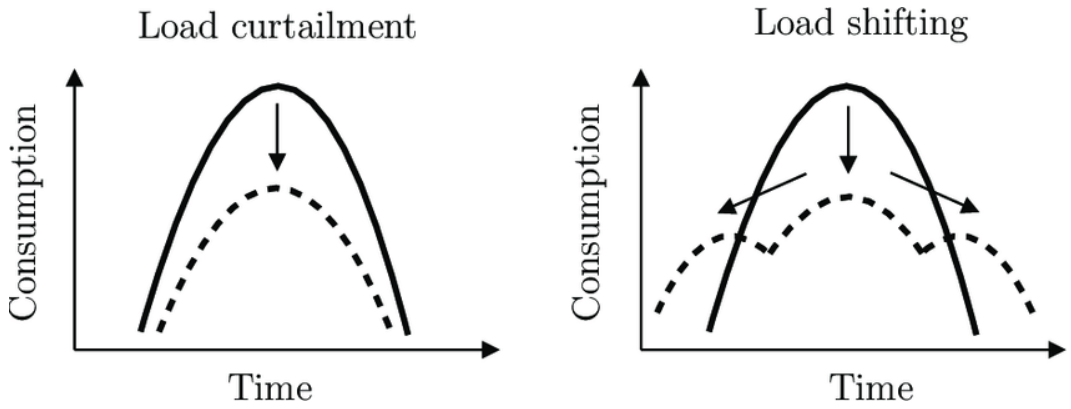

Figure 2-4: Example of load curtailment and load shifting

Demand Response can be organized in price-based and incentive-based programs. In price-based programs, participants are exposed to dynamic energy prices that reflect the real-time cost of electricity [41]. In incentive-based programs, participants receive a monetary reward for partaking in a demand response program [38]. An incentive-based program known as Direct Load Control (DLC) is applied in the Virtual Power Plant in this thesis. In DLC programs, utilities such as Virtual Power Plants can remotely control the energy consumption of equipment of actors participating in the program.

2-3-2 Demand Response in the Industrial Sector

The industrial or secondary sector consists of the companies and activities that process raw materials to develop products which are sold by the tertiary sector to consumers. Industrial processes have a high technical potential to provide demand response and often have much of the necessary infrastructure already installed [17]. This section provides an overview of the advantages and disadvantages of major industries in providing demand response and a discussion on the industries that will be integrated in the Virtual Power Plant.

Refrigerated Warehouses

Refrigerated warehouses consist of facilities and premises dedicated to store refrigerated products. In the Netherlands, refrigerated warehouses consume around 0.34 PJ [42] and there are around 45 large refrigerated warehouses with a power consumption above 0.5 MW [43]. Refrigerated warehouses can be used for load shedding by turning off cooling equipment or lightning and for load shifting by pre- or post cooling thereby making use of the high thermal capacity of the products. There are several beneficial characteristics of refrigerated warehouses related to demand response including the high energy consumption of the sector especially during peak periods, the limited effect of short-term interruptions of power consumption on the product quality owing to the high thermal inertia of products and the relatively simple processes involved in refrigeration [17]. Furthermore, refrigerated warehouses only require a notification time of 15 minutes, hence they can respond relatively rapidly to demand response requests [44], and their control systems are suitable for automated demand response programs [17]. On the other hand, implementing demand response in refrigerated warehouses meets with various challenges, such as the small temperature band that is allowed in many products [45] and the difficulty to establish a baseline energy consumption profile [46]. Furthermore, refrigerated warehouses can require a relatively long time after a demand response event to return to the desired warehouse temperature [47].

Cement Mills

Cement milling is an energy intensive industry which consists of grinding cement klinker and combining it with other compounds to produce cement. In the Netherlands, there are two cement plants with a combined electrical energy consumption of around 478.5 TJ [48]. The grinding process requires most of the electrical energy consumption, namely 70% of total electricity consumption in most plants and 90-100% in the Netherlands specifically. Potential advantages of cement mills for providing demand response include that grinders can be started/stopped within minutes and the control system of cement plants can be automated which allows for participating in automated demand response programs [17]. Furthermore, multiple studies [49, 50] and actual plants [51] have shown cement mills can perform load shifting. On the other hand, there are some disadvantages as well. Interviews with actual cement plant owners performed in Ref. [16], indicate that cement milling is mostly considered for load shedding rather than shifting because of high utilization rates, limited storage capacities and up/downstream process dependencies. In addition, the grinding process in cement mills is an on/off process which results in a poor granularity of the demand response energy provided

[52]. Finally, the grinding process is preferably operated at steady-state and interruptions should weigh up against start-up/shut-down cost[51].

Metal production industry

Steel manufacturing - Steel manufacturing is highly energy intensive and responsible for nearly 7 percent of the global total carbon dioxide emissions globally [53]. Most energy is used in the scrap melting process which can be performed by blast or electric arc furnaces [54]. Electric arc furnaces can be used for demand response, but blast furnaces cannot since there is no electricity consumption. The single steel manufacturing plant in the Netherlands is located in Ijmuiden (Tata Steel) which consumes around 3% of the total Dutch electricity consumption [54]. There are some challenges with demand response in steel manufacturing. Steel manufacturing has a high interdependence of processes making it one of the most difficult industries to schedule for demand response [17]. Furthermore, most processes run at 100% capacity and require long start-up and shut-down times. These interruptions can not be recovered via load shifting and losing production by load shedding is not considered financially attractive [55]. In the Netherlands, Tata Steel uses blast furnaces which do not rely on electricity and can therefore not be scheduled for load shedding or shifting [55].

Aluminium production - The main energy consuming process in the aluminium production is smelting which is an electrolytic process that converts alumina to aluminium [17]. Smelting of alumina occurs in high-temperature pots onto which a DC current is applied. The current to individual pots can be finely regulated and also complete pot lines can be turned on/off. In the Netherlands, nearly all of the electricity for aluminium production is consumed by the company Aldel. It consumes around 150 MW power at full load and about 6.6 PJ of electricity per year in total [56]. Aldel is currently operating as a 'virtual' battery by providing 15 MW up- and 15 MW down regulation in the ancillary services market [57]. Aluminium production seems a very suitable industry for providing demand response. Firstly, aluminum production is not a complicated process to schedule, as opposed to many other industrial processes such as cement production or steel manufacturing [17]. Furthermore, power consumption of the process can be adjusted within seconds with a high degree of granularity and with high ramp-rates. Additionally, short-term power interruptions have limited effects on product quality owing to the high thermal mass of the pots [17]. Also with new technical developments aluminium production can not only reduce load consumption, but also increase their consumption [58]. A major disadvantage is the high utilization rate, therefore load shedding is more commonly considered for aluminium production than load shifting [59, 16].

Chlor-Alkali process

The chlor-alkali process uses electrolysis to produce chlorine, hydrogen and sodium-hydroxide (caustic soda). The Netherlands has three chlor-alkali facilities which are located in Rotterdam and Delfgauw (Nouryon) and Bergen op Zoom (Sabic) and together they consume around 6.6 PJ of electricity per year [60]. The plant in the Port of Rotterdam is responsible for a considerable power consumption of 200 MW. The chlor-alkali process has several advantageous features for providing demand response. Firstly, the chlor-alkali process can rapidly respond

to demand response requests since the current to the electrolysers can be quickly reduced or increased and it has a high ramp-rate. For instance, ramping from minimum to maximum power consumption can be achieved within 30 minutes according to [61]. Furthermore, the chlor-alkali process has potential to perform load shifting by using the intermediate chlorine storage [22, 24, 62, 63]. However, load shifting does require an overcapacity of electrolysers. Recently, some chlor-alkali companies are actually installing additional electrolyser capacity to enable load shifting. For instance, Nouryon is adding production capacity to the Rotterdam plant such that the chlorine production can be adjusted based on a variable energy supply [64]. Challenges with the use of the chlor-alkali process for demand response are the high utilization rate (>80% [16]) which can limit the potential for load shifting. Furthermore, the chlorine storage size is generally restricted for safety regulations [62]. Although the storage size could be limited, recently it was discussed that the storage size could be considered larger if the chlorine is converted to other chemical intermediates [65].

Paper & Pulp industry

The paper & pulp industry comprise the factories involved in the production of paper and cardboard. In the Netherlands, there are around 20 factories with a total electricity and heat consumption of 4.7 PJ and 11.9 PJ respectively [66]. One major flexibility potential in pulp production can be found in the mechanical process known as refining which consumes most of the electricity. According to ref. [16], advantages of paper & pulp plants for providing demand response are the high energy consumption per actor and availability of storage tanks which would allow for load shifting. However, challenges are involving with demand response in the paper & pulp industry, including the longer ramp-up time and unreliability of start-ups of refiners whenever the mechanical process has been shut down. Furthermore, paper quality can deteriorate significantly by operating refiners at partial load. Demand response could also be provided by installing electric boilers to cover the thermal demand as was shown in Ref. [67], however the paper & pulp industry currently relies mostly on gas-fired boilers and CHP systems.

Hydrogen plants

The Dutch Climate Agreement states the ambition to realize a hydrogen electrolysis capacity of 500 MW by 2025 and 3-4 GW by 2030 which is to be powered by renewable energy resources [68]. Considering 3000 full-load hours per year [69], this would mean the electricity consumption of hydrogen electrolysis would be 5.4 PJ in 2025. Currently, there are two types of market-ready electrolysers for hydrogen production, namely Proton Exchange Membrane (PEM) and Alkaline electrolysers. Important advantages of PEM over alkaline electrolysis are the higher power density, increased cell efficiency, and rapid dynamic performance. On the other hand, alkaline electrolysis is a more established technology and it is still less expensive [70]. PEM electrolysers are able to ramp up/down to minimum/maximum loads within seconds, which makes it particularly suitable for integration with renewable energy resources and providing demand response on a short notice. Challenges with the development of large-scale hydrogen from electrolysis are the high cost. However, some reports state that costs may significantly drop owing to economies of scale and technological improvements and prices for hydrogen from electrolysis might therefore become competitive with fossil-based hydrogen

by 2030 [71]. Storage of hydrogen is also challenging because of the low density and low condensation point of gaseous hydrogen. Hydrogen can be stored above ground in domes at elevated pressure and this is expected to be the main storage method in the initial development stage of the hydrogen infrastructure in the Netherlands [72]. In the future, when the increased share of renewable energy will require more hydrogen infrastructure, more large-scale storage facilities will be required such as empty gas fields and salt caverns.

2-3-3 Discussion on industrial processes for integration in Virtual Power Plant

In this thesis, two industrial processes will be integrated in the Virtual Power Plant to perform demand response such that energy imbalances can be minimized. Several criteria have been set-up for deciding on the industrial process:

1. **The process can perform load shifting**. This thesis aims to follow the approach of [73] in which chemical plants are used as grid-level batteries by using an overcapacity of production units and intermediate storage tanks. A benefit of load shifting is that it limits the need for focusing on the costs since there is no loss of production such as with load shedding.
2. **The process is located within the Port of Rotterdam**. The Port of Rotterdam is the largest industrial cluster in the Netherlands and representative of an industrial site. Selecting processes within an actual industrial cluster increases the applicability of this thesis.
3. **The process can ramp-up/down power significantly within an ISP**. Since imbalance volumes in Virtual Power Plants are changing every ISP of 15 minutes, the industrial process needs to be able to ramp up/down significantly during this time period.

Based on the literature review, which is summarized in Table 4-2, and the above mentioned criteria, the chlor-alkali process and hydrogen plant were chosen to be integrated in the Virtual Power Plant. Although the steel industry has a high nominal power consumption, the interdependence of processes, long response-rate and lack of options for load shifting make the industry less suitable for dispatching close to real-time. Additionally, there is no steel plant located in the Port of Rotterdam. The aluminum industry has significant advantages such as the ability for part-load operation, limited process complexity and high ramp-rates. Yet, the aluminum plant of Aldel is also not located in the Port of Rotterdam. For cement mills, the poor granularity of the adjustable power consumption limits the ability to minimize imbalances in a Virtual Power Plant. In the paper & pulp industry, a major disadvantage is the longer time for starting-up which would not be suitable for mitigating imbalances that change every 15 minutes. Furthermore, there can be a negative effect of part-load operation on the required paper quality. Refrigerated warehouses are suitable candidates for application in the Virtual Power Plant owing to the fast response rate and potential for load shifting. However, a major challenge is determining a baseline energy consumption which is outside the scope of this study.

The chlor-alkali process has a fast-response and high ramp rate. There is also a chlor-alkali plant of Nouryon located in the Port of Rotterdam which has a high electricity consumption

(200 MW) and may thereby serve demand response for a large Virtual Power Plant. Furthermore, the Nouryon plant is currently increasing their production capacity to provide demand response and to keep up production during maintenance, which indicates an overcapacity of the production units could be assumed. Moreover, there is an intermediate storage tank present to store the chlorine which allows for load shifting.

Hydrogen plants based on electrolysis also display high ramp rates which allows them to quickly change their power consumption. Although currently the hydrogen plant developments in the Port of Rotterdam are in the feasibility study phase, it is the vision to built around 500 MW of hydrogen electrolysis capacity by 2025 including a 200 MW plant of Shell. Since these hydrogen plants will be powered by renewable energy, it may be assumed that an overcapacity of electrolysers will be present. Furthermore, the current plans indicate an intermediate storage will be available onsite [72] which combined with the overcapacity would allow for load shifting.

Industry	Energy consumption	Located in Port of Rotterdam	Response rate	Advantages	Disadvantages
Refrigerated warehouse	0.34 PJ	Yes	15 min	+ Fast response time + Load shifting potential + Automated DR possible	- Difficulty establishing baseline energy consumption - Limited availability of demand response during recovery periods - Limited energy consumption per actor
Cement Mills	0.48 PJ	Yes	Minutes	+ Fast response time + Load shifting potential + Automated DR possible + High consumption per actor	- Poor granularity in providing demand response - High utilization rate / load shedding more common
Steel manufacturing	N/A	No	N/A	+ High consumption per actor	- Slow start-up/shut down - High process interdependency - High utilization rates / only load shedding
Aluminum production	6.6 PJ	No	Seconds	+ Fast response time + Load shifting potential + High consumption per actor	- Load shedding more common - High utilization rate / load shedding more common
Paper & Pulp	4.7 PJ	No	N/A	+ Load shifting potential + High consumption per actor	- Difficulty in start-up of equipment - Partial load can reduce product quality - High utilization rate / load shedding more common
Chlor-Alkali	6.6 PJ [60]	Yes	Minutes	+ Fast response rate + Load shifting potential + High consumption per actor	- Storage size restricted by regulations - Load shedding more common - High utilization rate / load shedding more common
Hydrogen electrolysis	5.4 PJ by 2025 [69]	Yes	Seconds to minutes	+ Fast response rate + Load shifting potential	- Storage size could be limited by cost

Table 2-1: Advantages and disadvantages of major industries for providing demand response

Chapter 3

Virtual Power Plant

3-1 Virtual Power Plant system

The Virtual Power Plant in this thesis consist of renewable energy resources, two industrial plants, and a Model Predictive Control unit. The renewable resources are a portfolio of 300 MW PV and 300 MW onshore wind power and the industrial plants are a 203.5 MW chlor-alkali plant of Nouryon and 193.4 MW hydrogen plant of Shell as shown in Figure 3-1.

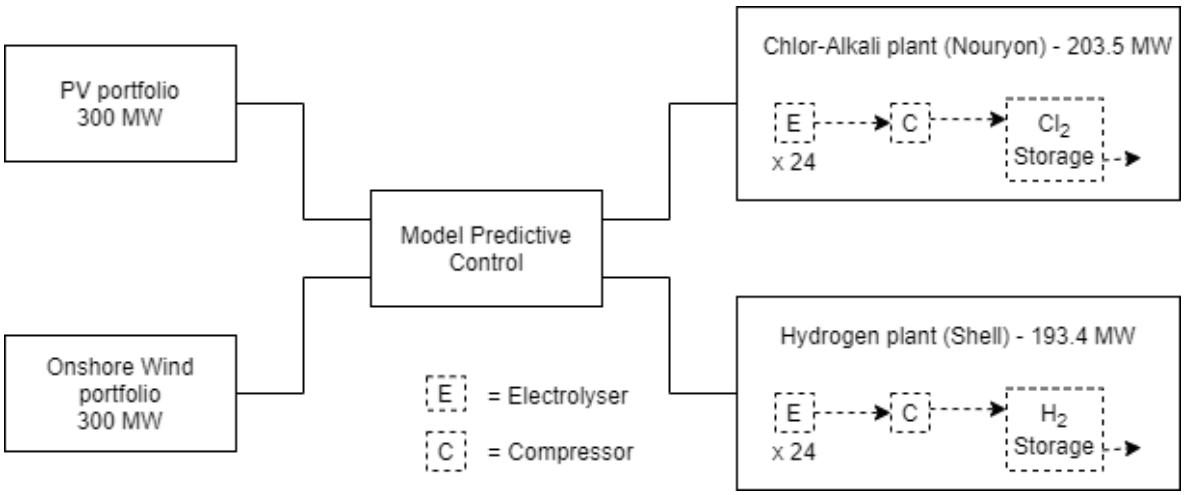

Figure 3-1: Virtual Power Plant with renewable energy, an MPC and industrial plants

Several assumptions based on literature are applied to the Virtual Power Plant in this thesis:

- The Virtual Power Plant sells energy on the Day-Ahead market. It is assumed all Day-Ahead energy bids are accepted since renewable energy is prioritized on merit-order owing to its low marginal cost [74].

- The Virtual Power Plant is considered to be a Balancing Responsible Party (BRP) following [15]. The imbalances of the Virtual Power Plant are defined as the difference between the Day-Ahead bid and the actual energy exchanged with the grid within an ISP [13].
- The flexible industrial plants are contracted by the Virtual Power Plant in a Direct Load Control program [75]. Following the USEF Whitepaper for Aggregators [76], it is assumed that the Virtual Power Plant can have control over sub-processes rather than the complete chlor-alkali and hydrogen plant. In this thesis, the Virtual Power Plant will be able to control 24 chlor-alkali and 24 hydrogen electrolysers, the compressors and the storage tanks.
- The chlor-alkali and hydrogen plant provide demand response by temporarily increasing/decreasing chlorine and hydrogen production respectively and storing the chemicals in an intermediate storage. They thereby operate as a grid-level battery as described in [73, 22]. The demand response energy quantity provided to the Virtual Power Plant is the difference between the plant's nominal and actual energy consumption during an ISP [77].
- A Model Predictive Control unit of the Virtual Power Plant is responsible for adjusting the energy consumption the industrial plants such that imbalances are minimized while preventing violation of important process constraints.

The objective of this thesis is to analyse the ability of the chlor-alkali and hydrogen plant to minimize imbalances caused by the deviation between the Day-Ahead bids and actual renewable energy generation in a Virtual Power Plant. To this purpose, a Model Predictive Control (MPC) unit has been developed which will be explained in Chapter 4. The physical components of the Virtual Power Plant will be accurately represented by using historical data for the renewable energy resources and detailed first-principles models for the chlor-alkali and hydrogen plant. The development of these components is described in detail in the following Sections 3-2 and 3-3.

3-2 Renewable Energy - Day-Ahead forecast and actual production

Imbalances in the Virtual Power Plant portfolio result from the error between the Day-Ahead forecast and actual production of renewable energy. Following the approach of [15], historical renewable energy data is used to generate the Day-Ahead error time-series for the Virtual Power Plant. The data consists of time-series of Day-Ahead forecast and actual renewable energy generation of PV and onshore wind in 2020 from Belgium which was extracted from the website of Elia, the Belgium Transmission System Operator [78, 79]. The data-set has a granularity of 15 minutes which coincides with the length of an Imbalance Settlement Period (ISP). The Day-Ahead forecast and actual production time-series have been normalized and scaled to meet the size of a 300 MW solar and 300 MW onshore wind portfolio using the following formulas [15]:

$$P_{PV,VPP}(t) = \frac{P_{PVData,Elia(t)}}{NationalPVCapacity} \cdot 300MW \tag{3-1}$$

$$P_{Wind,VPP}(t) = \frac{P_{WindData,Elia(t)}}{NationalWindCapacity} \cdot 300MW \tag{3-2}$$

Also, the Day-Ahead forecast data has been averaged at each hour such that the energy production at each ISP within an hour is equal. This averaging has been performed since the Day-Ahead market operates with hourly bids and the Transmission System Operator assumes that the energy production of a BRP per ISP is equal to a quarter of the hourly bid. By differencing the actual renewable energy production and the Day-Ahead forecast, the Day-Ahead forecast errors can be calculated as shown with the following formula:

$$P_{DA,error}(t) = P_{RE,actual}(t) - P_{RE,DAforecast}(t) \tag{3-3}$$

These Day-Ahead forecast errors will directly result in imbalances in the Virtual Power Plant unless demand response is provided by the industrial plants.

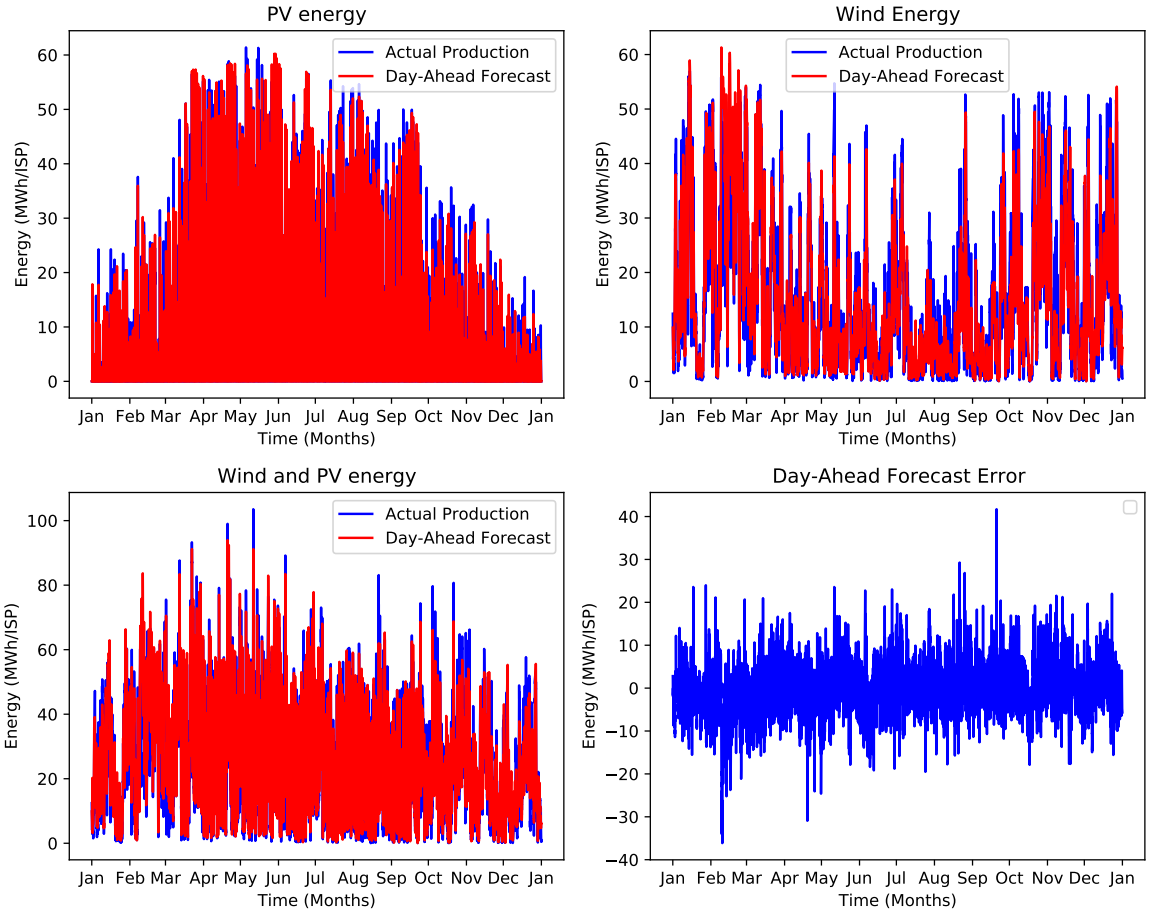

Figure 3-2: Renewable energy Day-Ahead forecasts and actual production

The renewable energy time-series used in this thesis are shown in Figure 3-2. Note that power production (MW) has been converted to energy production per ISP (MWh/ISP) by multiplying the 15-minute power data by $\frac{1}{4}$. The top-left plot shows the PV Day-Ahead

energy forecast and actual production of the Virtual Power Plant. The PV production is higher in spring/summer than in autumn/winter owing to the higher position of the sun above the horizon which increases the solar irradiation per squared meter. In the top-right plot, the wind energy forecast and production is shown. The wind energy production is higher in autumn/winter than in spring/summer. This can be explained by the higher average wind speeds during the autumn/winter and the lower air temperature which increases the density of the air passing through the rotor swept area. The bottom-left plot shows the sum of the PV and onshore wind Day-Ahead energy forecast and actual production of the Virtual Power Plant. Although there is not a clear trend, it can be seen that somewhat more energy is produced during February-June, than during July-January. Finally, the bottom-right plot shows the difference between the total Day-Ahead forecast and actual power production which are the Day-Ahead forecast errors.

These Day-Ahead forecast errors have been fitted to a probability density distribution function as shown in Figure 3-3. It is evident from the figure that the Cauchy distribution provides a good fit. Based on the data, the mean Day-Ahead forecast error is 0.16 MWh/ISP with a standard deviation of 5.63 MWh. The mean indicates that the positive and negative imbalances over the course of the year cancel each-other out. Finally, the minimum and maximum Day-Ahead forecast error is -36.13 MWh/ISP and 41.71 MWh/ISP respectively.

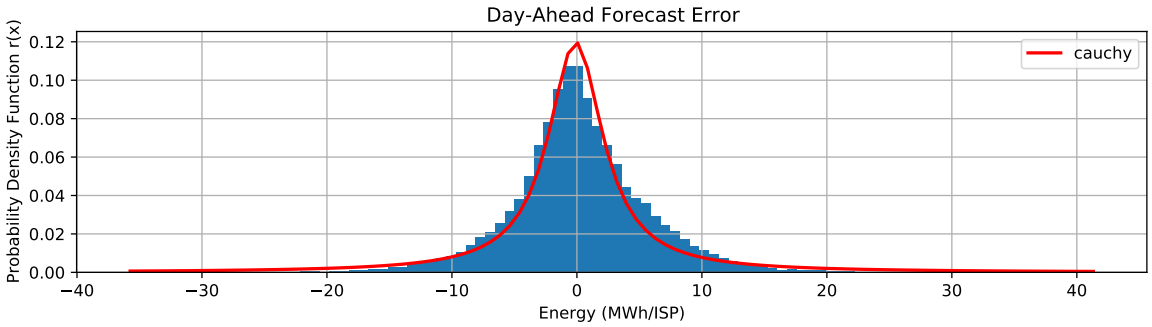

Figure 3-3: Renewable energy forecast errors fitted with a Cauchy probability distribution

There are other options to create Day-Ahead forecast error time-series, such as through developing prediction models based on ARMA, ARIMA, SARIMA or Neural-Networks. However the development of prediction models is not a goal in this thesis. Furthermore, the scaled national data provides a good representation of a Virtual Power Plant portfolio with PV and onshore wind energy resources that are geographically dispersed.

3-3 Industrial plants

This section describes the modeling of the chlor-alkali and hydrogen plants in the Virtual Power Plant. The plants have been developed in OpenModelica, which is an open-source software for modelling, simulation and optimization of dynamic systems. The plants are high-fidelity, non-linear models that closely represent the actual chlor-alkali and hydrogen production process. These OpenModelica plants will serve two purposes in this thesis. The first purpose is to simulate the actual plant response to control signals calculated by the

MPC. This can validate the ability of the MPC controller to dispatch complex plants without violating important process constraints. The second purpose of the plants is to generate realistic input-output data that is needed for the identification of the control model of the MPC.

3-3-1 Chlor-Alkali plant

The most important components of a chlor-alkali plant are the electrolysers which produce chlorine and caustic soda [80]. Currently, the main electrolyser type in the industry is the membrane electrolyser [81] which is comprised of a stack of individual chlor-alkali cells. The electrolyser cells contain an anode that is fed with $NaCl(aq)$ and a cathode which is fed with $NaOH(aq)$. By applying a voltage difference on the cell, the following reactions occur:

$$\textbf{Anode} \quad 2Cl^{-}(aq) \rightarrow Cl_2(g) + 2e^{-}$$
$$\textbf{Cathode} \quad 2H_2O(l) + 2e^{-} \rightarrow H_2(g) + 2OH^{-}(aq)$$
$$\textbf{Total Reaction} \quad 2NaCl(aq) + 2H_2O(l) \rightarrow Cl_2(g) + H_2(g) + 2NaOH(aq)$$

In order to maintain electrical balance in the cell, sodium ions are able to travel through the membrane from the cathode to the anode. The produced chlorine gas exits the electrolyser and then goes through a liquification process, which requires a compression step, after which it is stored in a tank.

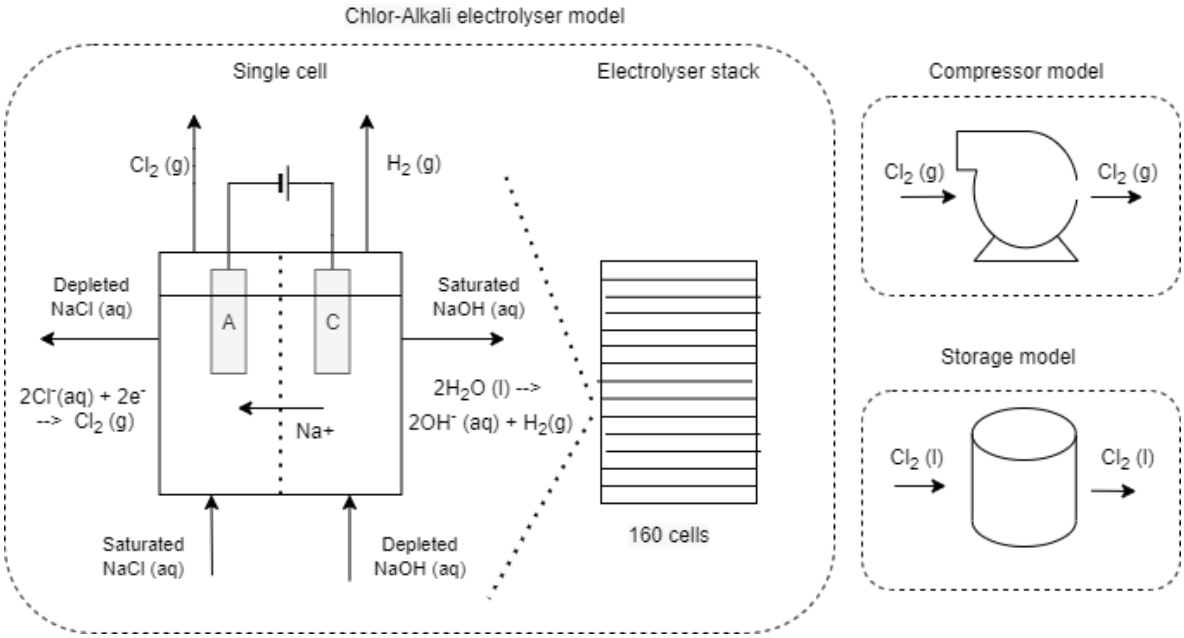

Figure 3-4: Components of a chlor-alkali simulator developed in OpenModelica

The next sections describe the modelling and validation of a detailed chlor-alkali simulator developed in OpenModelica which is based on [22, 82]. The simulator consists of a chlor-alkali

membrane electrolyser with 160 cells, a compressor and a storage model. The simulators can be multiplied as many times as desired to match the number of electrolysers in the whole plant, which is 24 electrolysers in this thesis. Note that the subscript $_c$ has been added to several variables to avoid overlap with the hydrogen simulator described in Section 3-3-2. An overview of the parameters and variables for the OpenModelica model can be found in Table A-1 in the Appendix.

Electrolyser - Electrochemical model

The voltage in a chlor-alkali cell consists of three components, namely the thermodynamic, kinetic and ohmic voltage [22].

$$V_{cell,c} = V_{equ,c} + V_{act,c} + V_{ohm,c} \tag{3-4}$$

The thermodynamic voltage, or equilibrium voltage, is described with the Nernst equation which calculates the reduction potential of an electrochemical reaction using the standard electrode potential, temperature and activities of the chemical compounds [82, 80]:

$$V_{equ,c} = V_{rev,c} + \frac{R \cdot T_c}{2 \cdot F \cdot \alpha} \left(\left(\ln \frac{\sqrt{P_{Cl_2}^{ano}}}{C_{Cl}^{ano}} \right) + 2.302 \cdot (14 + \log (C_{OH}^{cat})) \right) \tag{3-5}$$

where, $V_{equ,c}$ is the equilibrium voltage, $V_{rev,c}$ is the reversible voltage, R is the universal gas constant, T_c is the cell temperature, F is the Faraday constant, α is a multiplication factor, $P_{Cl_2}^{ano}$ is the partial pressure of gaseous chlorine and C_{Cl}^{ano} is the concentration of chlorine ions in the anode and C_{OH}^{cat} is the concentration of hydroxide ions in the cathode.

The kinetic or activation voltage results from a resistance to the kinetics of the electrochemical reactions in the anode and cathode [80]:

$$V_{act,c} = 0.03 \cdot \left(\log \frac{I_c}{A_{e,c}} - \log (12) \right) + 0.05 \cdot \left(\log \frac{I_c}{A_{e,c}} - \log (30) \right) \tag{3-6}$$

where, $V_{act,c}$ is the kinetic or activation voltage, I_c is the current through the electrolyser cell and $A_{e,c}$ is the surface area of the electrolyser cell.

The ohmic voltage $V_{ohm,c}$ is caused by the resistance across the electrolyte, the separator and cell hardware, and is it described with the following equation [22, 83]:

$$V_{ohm,c} = I_c \cdot \frac{2.6125 \cdot 10^{-4} - 1.75 \cdot 10^{-6}(T_c - 273)}{A_{e,c}} \tag{3-7}$$

Electrolyser - Material balance model

The production of H_2 and Cl_2 in the chlor-alkali electrolyser stack is described with Faraday's law:

$$\dot{N}_{H_2,c}^{cat,out} = \dot{N}_{Cl_2}^{ano,out} = \frac{\eta_F \cdot N_{cells,c} \cdot I_c}{2 \cdot F} \tag{3-8}$$

The molar flows $\dot{N}_{Cl_2}^{ano,out}$ and $\dot{N}_{H_2,c}^{cat,out}$ indicate the total production of chlorine and hydrogen of an electrolyser stack comprising $N_{cells,c}$ cells [22]. Under the operating temperature of the chlor-alkali electrolysers in this thesis there is no build-up of gas in the cell due to the low solubility of H_2 and Cl_2 [84].

The mass balance of chloride ions in the anode is described by [22]:

$$\frac{dn_{cl}^{ano}}{dt} = C_{NaCl}^{ano,in} \cdot \dot{V}_{in} - C_{NaCl}^{ano} \cdot \dot{V} - 2 \cdot \dot{n}_{Cl_2}^{ano,out} \tag{3-9}$$

where, n_{Cl}^{ano} is the amount of moles of Cl^{-1} ions in the anolyte, $C_{NaCl}^{ano,in}$ is the concentration of NaCl in the inlet flow $\dot{V}_{in}$, C_{NaCl}^{ano} is the concentration of NaCl in the outflow $\dot{V}$, and $\dot{n}_{Cl_2}^{ano,out}$ is the molar production of $Cl_2(g)$. The number 2 in front indicates that per mole Cl_2 produced, two moles of Cl^{-1} ions are consumed.

The hydroxide ion balance in the cathode is governed by:

$$\frac{dn_{OH}^{cat}}{dt} = C_{NaOH}^{cat,in} \cdot \dot{V}_{in} - C_{NaOH}^{cat} \cdot \dot{V} + 2 \cdot \dot{n}_{Cl_2}^{ano,out} \tag{3-10}$$

where, n_{OH}^{cat} is the amount of moles of OH^{-1} in the catholyte, $C_{NaOH}^{cat,in}$ is the concentration of $NaOH$ in the inlet flow $\dot{V}_{in}$ and C_{NaOH}^{cat} is the concentration of $NaOH$ in the outlet flow $\dot{V}$. The last part of the equation, $2\dot{n}_{Cl_2}^{ano,out}$, indicates that per mole of Cl_2 produced, two moles of OH^{-1} ions are produced.

The water balance equations for the anode and cathode compartment are as followed [22]:

$$\frac{dn_{H_2O}^{ano}}{dt} = (55.56{\cdot}10^3 - C_{ano,in}^{NaCl}){\cdot}\dot{V}_{in} - \dot{V}{\cdot}\frac{n_{H_2O}^{ano}}{V} + \frac{D_{H_2O} \cdot A_{e,c}}{\delta V}(n_{H_2O}^{cat} - n_{H_2O}^{ano}) - 0.6{\cdot}\dot{n}_{Cl_2}^{ano,out} \tag{3-11}$$

$$\frac{dn_{H_2O}^{cat}}{dt} = (55.56 \cdot 10^3 - C_{cat,in}^{NaOH}) \cdot \dot{V}_{in} - \dot{V} \cdot \frac{n_{H_2O}^{cat}}{V} - \frac{D_{H_2O} \cdot A_{e,c}}{\delta V} \cdot (n_{H_2O}^{cat} - n_{H_2O}^{ano}) - 2.3 \cdot \dot{n}_{Cl_2}^{ano,out} \tag{3-12}$$

where $n_{H_2O}^{ano}$ and $n_{H_2O}^{cat}$ are the number of moles of H_2O in the anolyte and catholyte respectively, D_{H_2O} is the diffusivity of water molecules across the membrane, $A_{e,c}$ is the electrode surface area of the cell, δV is the membrane thickness. At the anode, the $-0.6 \cdot \dot{n}_{Cl_2}^{ano,out}$ indicates that 0.6 moles of water evaporates per produced mole of Cl_2. At the cathode, the -2.3 $\dot{n}_{Cl_2}^{ano,out}$ consists of the evaporation of 0.3 moles of water and the consumption of 2 moles of water per mol of Cl_2 produced.

The flow rates into and out of the cell are the same ($\dot{V}_{in} = \dot{V}$), hence the cell volume V remains constant.

Electrolyser - Thermal model

The thermal model of the electrolyser is described with a lumped heat capacity equation, since the production of gaseous Cl_2 and H_2 can provide enough mixing to assume a uniform temperature in the electrolyser [22]:

$$N_{cells,c} \cdot n_t \cdot C_{pt} \cdot \frac{dT_c}{dt} = N_{cells,c} \cdot (\dot{n}_t^{in} \cdot C_{pt,c}^{in} \cdot T_{in,c} - \dot{n}_t^{out} \cdot C_{pt,c} \cdot T_c) - \dot{Q}_{rxn} - \dot{Q}_{evp} - \dot{Q}_{loss,c} + \dot{Q}_{gen,c} \tag{3-13}$$

where n_t is the total number of moles inside the electrolyser and $C_{pt,c}$ and $C_{pt,c}^{in}$ are the lumped heat capacities of the cell and inlet flow rate respectively.

The part between brackets is the sensible heat loss due to electrolyte flowing in and out of the cell. The heat capacities $C_{pt,c}$ and $C_{pt,c}^{in}$ are calculated by summing the contribution of each species [22]:

$$C_{pt,c} = \sum_i x_i \cdot C_{p,i} \tag{3-14}$$

where x_i indicates the mole fraction of species i, and $C_{p,i}$ is the heat capacity of species i. $\dot{Q}_{rxn}$ refers to the heat generated because of the chemical reactions:

$$\dot{Q}_{rxn} = \dot{N}_{Cl_2}^{ano,out} \cdot \Delta H_{rxn} \tag{3-15}$$

where $\dot{N}_{Cl_2}^{ano,out}$ refers to the production of chlorine gas and ΔH_{rxn} indicates the enthalpy of the reaction.

The term $\dot{Q}_{evp}$ integrates the heat loss due to gases leaving the cell. The major contribution to this heat loss is the evaporation of water, which can be described with the following formula [22]:

$$\dot{Q}_{evp} = 0.9 \cdot \dot{N}_{Cl_2}^{ano,out} \cdot \Delta H_{vap} \tag{3-16}$$

where, ΔH_{vap} is the latent heat loss per mol of water. The value of 0.9 is the sum of the water evaporating from the anode (0.6 mol) and cathode (0.3 mol).

The electrolyser stack also experiences a heat loss to the environment, because of the difference between the stack and the ambient temperature. This heat loss is captured by the component $\dot{Q}_{loss,c}$ as follows [22]:

$$\dot{Q}_{loss,c} = \frac{1}{R_{th,c}} \cdot (T_c - T_{amb}) \tag{3-17}$$

where $R_{th,c}$ the thermal resistance of the stack of cells and T_{amb} is the ambient temperature.

The heat generation due to a current flowing through an electrolyser with resistance is described with $\dot{Q}_{gen,c}$. This heat generation component is equal to the electrical power input of the chlor-alkali electrolyser.

$$\dot{Q}_{gen,c} = P_c = N_{cells,c} \cdot V_{cell,c} \cdot I_c \tag{3-18}$$

where, P_c is the power consumed by the electrolyser.

Compressor

A compressor increases the pressure of the chlorine gas from atmopheric pressure to 0.3 MPa during the liquification process [22]. The expression that describes how the temperature of the chlorine gas depends on the initial temperature, and initial and final pressure is shown below:

$$T_{f,c} = T_{i,c} \left[\frac{P_{f,c}}{P_{i,c}} \right]^{\frac{n_c - 1}{n_c}} \tag{3-19}$$

where $T_{i,c}$ and $T_{f,c}$ are the initial temperature before compression and final temperature after compression respectively, $P_{i,c}$ and $P_{f,c}$ are the pressure before and after compression respective and n_c is the polytropic exponent. By assuming the chlorine gas behaves as an ideal gas, the work that needs to be performed to achieve the compression is [22]:

$$W^{th}_{comp,c} = R \cdot T_{i,c} \cdot \frac{n_c}{n_c - 1} \left(\left[\frac{P_{f,c}}{P_{i,c}}^{\frac{n_c - 1}{n_c}} \right] - 1 \right) \tag{3-20}$$

where $W^{th}_{comp,c}$ is the theoretical energy required for the compression of a mol of produced chlorine gas and R is the universal gas constant. The electrical input needed for the compressor can be found by dividing the theoretical work with the polytropic efficiency:

$$W^{elec}_{comp,c} = \frac{W^{th}_{comp,c}}{\eta_{pc}} \tag{3-21}$$

where $W^{elec}_{comp,c}$ is the actual energy required for the compression of a mol of Cl_2 and η_{pc} is the polytropic efficiency. The polytropic efficiency can be calculated using the polytropic exponent n and the adiabatic exponent k.

$$\eta_{pc} = \frac{(k-1)/k}{(n_c - 1)/n_c} \tag{3-22}$$

where the adiabatic exponent of diatomic gases k is calculated as follows:

$$k = \frac{C_p}{C_v} = 1.4 \tag{3-23}$$

Storage model

The storage model can be described by a simple mass balance using the following equation [22]:

$$\frac{dM_{s,c}}{dt} = \dot{M}_{in,c} - \dot{M}_{out,c} \tag{3-24}$$

where $M_{s,c}$ is the total amount of moles of Cl_2 stored in the pressured storage, and $\dot{M}_{in,c}$ and $\dot{M}_{out,c}$ are the molar flow rates of Cl_2 in and out of the storage. A constant molar outflow is assumed, which is equal to the Cl_2 production at nominal production.

Validation

The OpenModelica simulator in this thesis was validated with the chlor-alkali electrolyser that was developed in Ref. [22, 82] in the dynamic modelling software gProms. In Figure 3-5, the effect of current density step from 0.4 to 0.5 $\frac{A}{cm^2}$ on the cell voltage, temperature and $NaCl$ concentration is shown. After the current density step, the cell voltage rises instantaneously because the current in the ohmic voltage $V_{ohm,c}$ equation is immediately increased. Then the cell voltages reduces slightly, since the temperature rise in the cell causes the ohmic resistance to drop. Furthermore, the step in current density increases the consumption of Cl^- ions thereby lowering the concentration of $NaCl$ in the anolyte until a new equilibrium is reached. Moreover, when increasing the current density the heat production increases which causes the cell temperature to rise until there is a new temperature equilibrium. The OpenModelica model in this thesis coincides well with the model developed in gProms by [82]. This is because several improvements to the model in literature of [22] were implemented in the OpenModelica model in this thesis. These improvements were suggested to and adopted by the authors of Ref. [22] after which they published a corrigendum with the improvements in [82]. During further correspondence, the simulation results of their updated gProms model and the OpenModelica model of this thesis were compared which showed both models are completely in agreement.

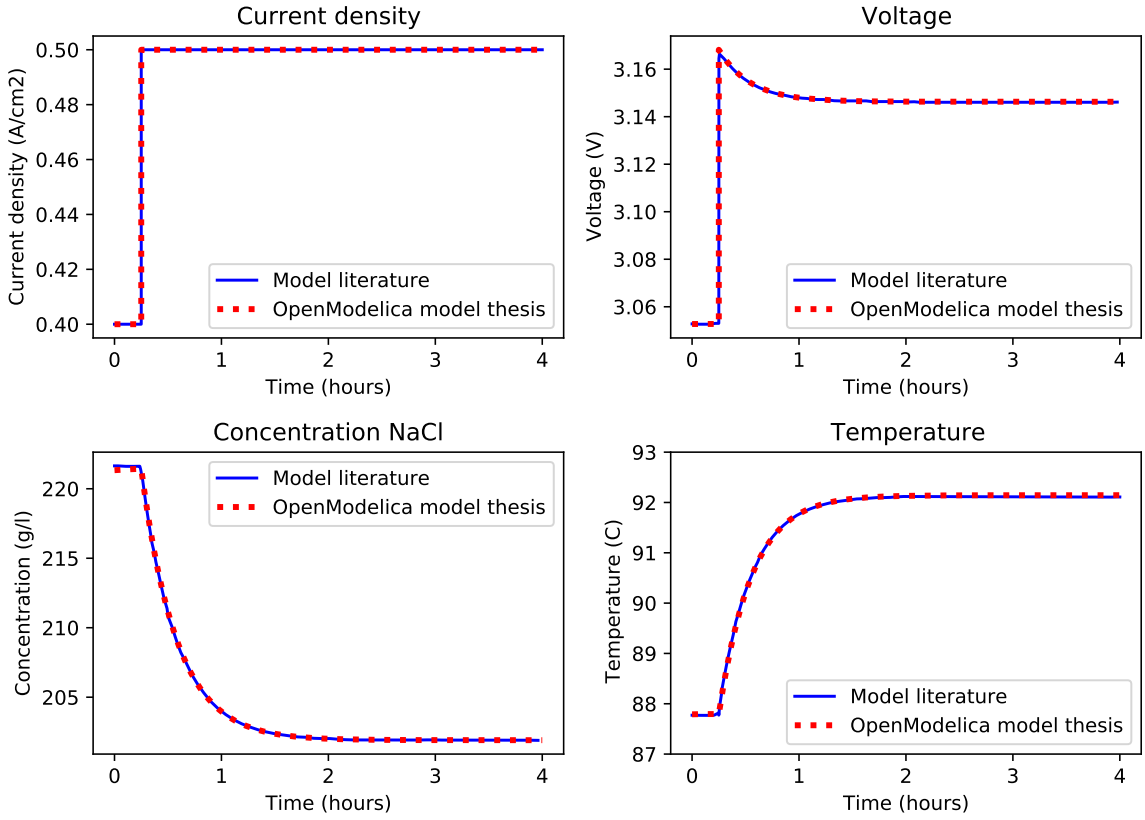

Figure 3-5: Responses of the OpenModelica model and literature model to a step increase of current density from 0.4 to 0.5 $\frac{A}{cm^2}$

When performing a steady state simulation at the rated current density of 0.6 $\frac{A}{cm2}$ and a cell temperature of 90 °C, it was shown that the power consumption per electrolyser is 8.48 MW. Hence for a plant with 24 electrolysers this amounts to 203.5 MW which well represents the 200 MW chlor-alkali plant of Nouryon. The compressor power needed for the whole plant is 1.1 MW which is less than 0.6% of the total plant power consumption. For simplification, the power consumption of the compressor model has been omitted in the simulation study in this thesis.

3-3-2 Hydrogen plant

The hydrogen plant in this thesis consists of twenty-four Proton Exchange Membrane (PEM) electrolysers, a compressor and a storage unit. The electrolyser is based on a 46 KW PEM electrolyser that was experimentally tested and modeled in [85] and [86]. This is a high pressure electrolyser with 60 PEM cells in series each with a cell area of 290 cm^2. The reactions taking place in a PEM electrolyser resulting from an applied voltage difference are as followed:

$$\textbf{Anode} \quad H_2O(l) \rightarrow 2H^+ + \frac{1}{2}O_2(g) + 2e^-$$
$$\textbf{Cathode} \quad 2H^+(aq) + 2e^- \rightarrow H_2(g)$$
$$\textbf{Total Reaction} \quad H_2O(l) \rightarrow H_2(g) + \frac{1}{2}O_2(g)$$

After production, the hydrogen at the outlet of the PEM electrolysers is compressed to 100 bar to allow for above-ground storage [87]. Since the 46 KW PEM electrolyser has a much smaller capacity than the chlor-alkali electrolyser, it is assumed that one hydrogen electrolyser unit in this thesis consists of a series of 160 x 46 KW PEM electrolysers as shown in Figure 3-6 below.

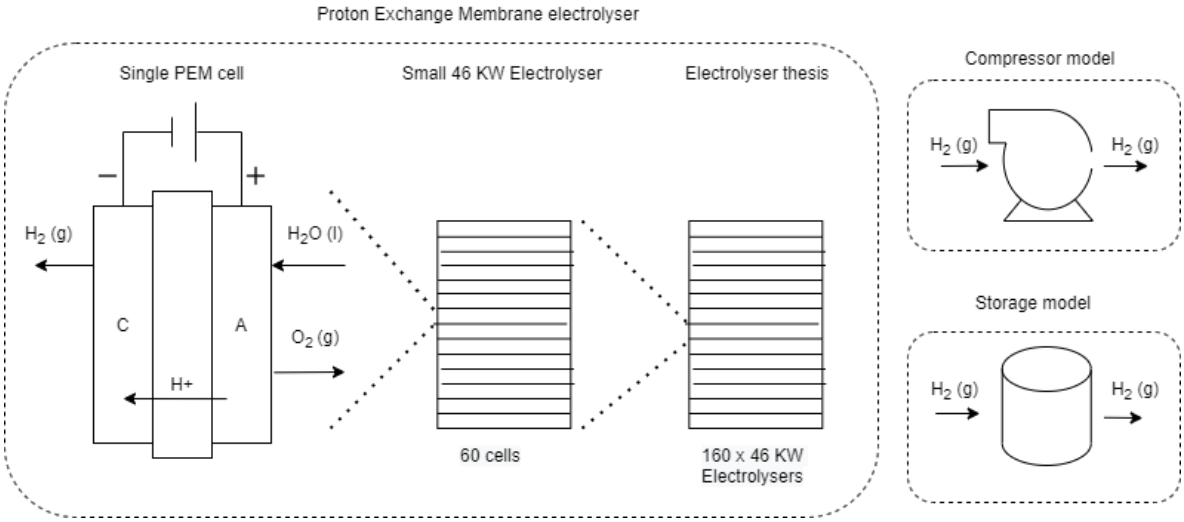

Figure 3-6: Components of hydrogen electrolyser simulator in OpenModelica

The following section describes the PEM electrolyser simulator developed in OpenModelica, which consists of 160 x 46 KW high pressure PEM electrolysers in series, a compressor and a storage unit. The simulator can be multiplied 24 times to represent the whole hydrogen plant. An overview of the parameters and variables for the OpenModelica model can be found in Table A-2 in the Appendix.

Electrolyser - Electrochemical model

The voltage model of the PEM cell is tripartite and consists of the open-circuit, activation and ohmic voltage [85, 86].

$$V_{cell,h} = V_{ocv,h} + V_{act,h} + V_{ohm,h} \tag{3-25}$$

The open circuit voltage can be described by using the Nernst equation [86]:

$$V_{ocv,h} = V_{rev,h} + \frac{R \cdot T_h}{2 \cdot F} \ln\left(\frac{pp_{H_2} \dot{pp}_{O_2}^{0.5}}{pp_{H_2O}}\right) \tag{3-26}$$

where $V_{ocv,h}$ is the open circuit voltage, $V_{rev,h}$ is the reversible voltage, R is the universal gas constant, T_h is the cell temperature, F is the Faraday constant, pp_{H_2}, pp_{O_2} and pp_{H_2O} are the partial pressures of H_2, O_2 and H_2O respectively. The reversible voltage is modeled using the following empirical equation [86]:

$$V_{rev,h} = V_{std,h} - 0.0009(T_h - T_{std}) \tag{3-27}$$

where V_{std} is the reversible voltage at standard conditions and T_{std} is the temperature at standard conditions which is 298.15 K.

The activation or kinetic voltage is the voltage required for the electrochemical reaction to start. The contribution from the anode is most important and has been modeled as follows [86]:

$$V_{act,h} = \frac{R \cdot T_h}{2 \cdot \alpha_{ano} \cdot F} \cdot asinh\left(\frac{j_{dens}}{2 \cdot j_{0,an}}\right) \tag{3-28}$$

where α_{ano} is an experimentally determined value, F is the Faraday constant, j_{dens} is the current density and $j_{0,an}$ is the exchange current density. The exchange current density is the current density in the absence of net electrolysis and at zero overpotential, and it is described as followed:

$$j_{0,an} = j_{0,an,std} \cdot exp \cdot \left(-\frac{E_{exc}}{R} \cdot \left(\frac{1}{T_h} - \frac{1}{T_{std}}\right)\right) \tag{3-29}$$

where, $j_{0,an,std}$ is the exchange current density at standard conditions and E_{exc} is the activation energy required for electron transport in the anode.

The ohmic voltage results from the resistance to ion flow in the PEM cell and can be described by [85, 86]:

$$V_{ohm,h} = R_{mem} \cdot j_{dens} \tag{3-30}$$

where, $V_{ohm,h}$ is the ohmic overpotential and R_{mem} is the cell membrane resistance. The membrane resistance can be described with the following formula:

$$R_{mem} = \frac{1}{\sigma_{mem}} \cdot \delta_{mem} \tag{3-31}$$

where, σ_{mem} is the membrane conductivity and δ_{mem} $[m]$ is the membrane thickness. The membrane conductivity describes the degree of permeability of ions through the membrane and it can be calculated with the following formula:

$$\sigma_{mem} = \sigma_{mem,std} \cdot exp\left(\frac{E_{pro}}{R}\left(\frac{1}{T_h} - \frac{1}{T_{std}}\right)\right) \tag{3-32}$$

where $\sigma_{mem,std}$ is the membrane conductivity at standard conditions and E_{pro} is the activation energy needed for proton transport in the membrane.

Electrolyser - Mass flow model

The production rates of hydrogen and oxygen is governed by Faraday's Law, and they can be modelled as followed [85, 86]:

$$\dot{N}_{H_2,h} = \frac{N_{cells,h} \cdot I_h}{2 \cdot F} \cdot \eta_f \tag{3-33}$$

$$\dot{N}_{O_2} = \frac{N_{cells,h} \cdot I_h}{4 \cdot F} \cdot \eta_f \tag{3-34}$$

$$\dot{N}_{H_2O} = \frac{N_{cells,h} \cdot I_h}{2 \cdot F} \cdot \eta_f \tag{3-35}$$

where $\dot{N}_{H_2,h}$, $\dot{N}_{O_2}$ and $\dot{N}_{H_2O}$ are the molar production rates of H_2 and O_2 respectively, $N_{cells,h}$ is the amount of cells in a 46 KW PEM electrolyser stack and η_f is the Faraday efficiency. The value of 2, 4 and 2 in the equations above indicate the number of electrons needed for the production of a mol of H_2, O_2 and H_2O.

Electrolyser - Pressure model

The water vapour exerts a pressure on the PEM cell which is calculated with the following equation [85, 86]:

$$pp_{H_2O} = 6.1078 \cdot 10^{-3} \cdot exp\left(17.2694 \cdot \frac{T_h - 273.15}{T_h - 34.85}\right) \tag{3-36}$$

where the pp_{H_2O} is the partial pressure of water vapour. Under the assumption of ideal gas behaviour, the partial pressures of H_2 and O_2 can be derived using Dalton's law of partial pressures [86]:

$$pp_{H_2} = p_{cat} - pp_{H_2O} \tag{3-37}$$

$$pp_{H_2} = p_{ano} - pp_{H_2O} \tag{3-38}$$

where pp_{H_2} and pp_{O_2} are the partial pressures of H_2 and O_2 respectively, and p_{cat} and p_{ano} are the partial pressures of H_2 and O_2 at the outlet respectively. A negative pressure gradient of 1 bar from cathode to anode is implemented in order to reduce stress on the membrane [86].

Electrolyser - Thermal model

The thermal model of the electrolyser can be described by an energy balance equation using a lumped capacitance model [85, 86]:

$$N_{s,h} \cdot C_{pt,h} \cdot \frac{dT_h}{dt} = N_{s,h} \cdot (\dot{Q}_{gen,h} + \dot{Q}_{pump,loss} - \dot{Q}_{cool} - \dot{Q}_{loss,h} - \sum_j \dot{n}_j \cdot \Delta h_j) \tag{3-39}$$

where $N_{s,h}$ is the amount of 46 KW PEM electrolysers in series, $C_{pt,h}$ is the lumped thermal capacity of the 46 KW PEM electrolyser system and T_h is the operating temperature of the electrolyser stack.

The electrolysis heat generation $\dot{Q}_{gen,h}$ is the heat generated due to operating at a potential above the thermoneutral potential [86]:

$$\dot{Q}_{gen,h} = (V_{cell,h} - V_{tn}) \cdot I_h \cdot N_{cells,h} \tag{3-40}$$

where $V_{cell,h}$ is the cell voltage, V_{tn} is the thermoneutral voltage, I_h is the current across the electrodes of the PEM electrolyser stack and $N_{cells,h}$ is the number of cells in a 46 KW PEM electrolyser stack.

In the study of [85] it was found that the pump that supplies the electrolyser with water was a source of heat. Therefore, $\dot{Q}_{pump,loss}$ is the heat flow from the pump towards the electrolyser.

$$\dot{Q}_{pump,loss} = \dot{Q}_{elec} \cdot \eta_{pump} \tag{3-41}$$

where, $\dot{Q}_{pump,loss}$ is the heat transferred to the electrolyser due to the pump operation, $\dot{Q}^{elec}$ is the electrical input to the water pump, and η_{pump} is the electrical efficiency of the pump.

$\dot{Q}_{cool}$ refers to the heat flow that is removed from the electrolyser from the cooling system. The modelling of the cooling system is outside the scope of this thesis and as in [86] it is assumed that $\dot{Q}_{cool}$ can attain a range of values.

The heat loss to the ambient $\dot{Q}_{loss,h}$ is due to the difference between the ambient temperature and operating temperature of the electrolyser [85, 86]:

$$\dot{Q}_{loss,h} = \frac{1}{R_{th,h}} \cdot (T_h - T_{amb}) \tag{3-42}$$

where $Q_{loss,h}$ is the heat loss to the environment, R_{th} is the thermal resistance of the electrolyser stack and T_{std} is the temperature at standard conditions.

The final term indicates the enthalply that is removed from the system due to the produced H_2 and O_2 that leaves the electrolyser [85, 86]:

$$\sum_j \dot{N}_j \cdot \Delta h_j = \dot{N}_{H_2,h} \cdot C_{p,m,H_2} \cdot (T_h - T_{amb}) + \dot{N}_{O_2} \cdot C_{p,m,O_2} \cdot (T_h - T_{amb}) \tag{3-43}$$

where, $\dot{N}_{H_2,h}$ and $\dot{N}_{O_2}$ refer to the molar production rate of H_2 and O_2 of a 46 KW PEM electrolyser.

The heat capacities of H_2 and O_2 depend on the operating temperature and can be described with two empirical formulas:

$$C_{p,m,H_2} = (29.11 - 1.92 \cdot 10^{-3} \cdot T_h + 4.0 \cdot 10^{-6} \cdot T_h^2 - 8.7 \cdot 10^{-10} \cdot T_h^3) \tag{3-44}$$

$$C_{p,m,O_2} = (25.48 + 1.52 \cdot 10^{-2} \cdot T_h - 7.16 \cdot 10^{-6} \cdot T_h^2 + 1.31 \cdot 10^{-9} \cdot T_h^3) \tag{3-45}$$

where C_{p,m,H_2} and C_{p,m,O_2} is the heat capacity of H_2 and O_2 gas respectively.

Compressor model

A single stage centrifugal compressor is used to increase the pressure of the hydrogen gas from 35 to 100 bar which is generally needed for large-scale above ground storage [87]. The compressor model equations used for the chlor-alkali plant have been applied in this section [22]:

$$W_{comp,h}^{th} = R \cdot T_{i,h} \frac{n_h}{n_h - 1} \cdot \left(\left[\frac{P_f}{P_i}^{\frac{n_h - 1}{n_h}} \right] - 1 \right) \tag{3-46}$$

$$W_{comp,h}^{elec} = \frac{W_{comp,h}^{th}}{\eta_{p,h}} \tag{3-47}$$

$$\eta_{p,h} = \frac{(k-1)/k}{(n_h - 1)/n_h} \tag{3-48}$$

$$k = \frac{C_p}{C_v} = 1.4 \tag{3-49}$$

where $W^{th}_{comp,h}$ is the theoretical energy required for the compression of a mol of produced hydrogen, $W^{elec}_{comp,h}$ is the actual energy required for the compression of a mol of H_2, R is the universal gas constant, $\eta_{p,h}$ is the polytropic efficiency and k and n_h are the polytropic and adiabatic exponent respectively.

Storage model

The storage model can be described by a simple mass balance using the following equation:

$$\frac{dM_{s,h}}{dt} = \dot{M}_{in,h} - \dot{M}_{out,h} \tag{3-50}$$

where $M_{s,h}$ is the total amount of moles of H_2 stored in the pressured tank, and $\dot{M}_{in,h}$ and $\dot{M}_{out,h}$ are the molar flow rates of H_2 in and out of the storage. A constant molar outflow is assumed, which is equal to the H_2 production at nominal conditions.

Validation

The hydrogen plant developed in OpenModelica in this thesis is validated with the experimental data found in ref. [85] and the dynamic model developed in [86] of the high pressure 46 KW PEM electrolyser. In the left graph of Figure 3-7, the polarization curve of the PEM electrolyser is shown which relates the cell voltage to the applied current density. A typical shape of the I-V curve can be seen and the experimental data of [85] coincides well with the model developed in OpenModelica. Furthermore, on the right plot the thermal response of the electrolyser developed in literature [86] and the OpenModelica model developed in this thesis to the application of a constant current of 400 A is shown. Following the procedure in [86], the temperature is allowed to rise from a cold start at 25 °C to 55.8 °C after which a cooling load of 6911 W per 46 KW electrolyser is applied. A good agreement between the temperature transient of the model in literature and the OpenModelica simulator can again be seen.

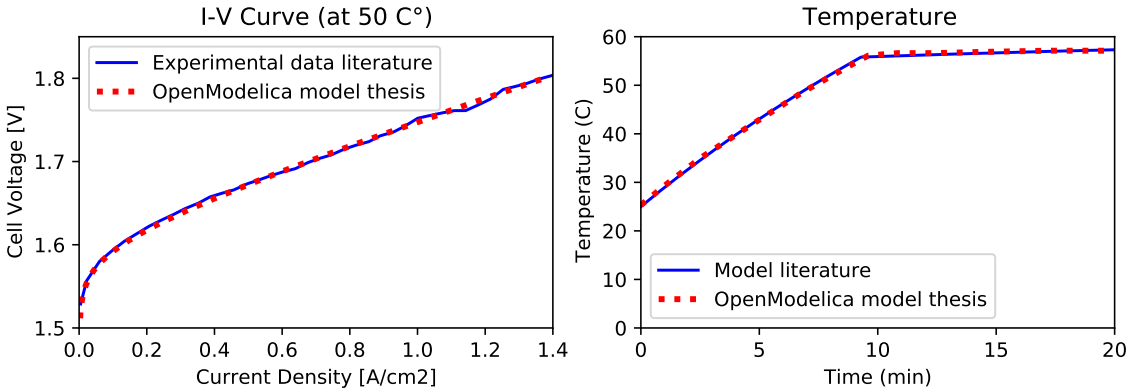

Figure 3-7: Responses of thesis and literature model to step increase of current density

At a current density of 1.6 $\frac{A}{cm^2}$, which is considered the rated current density in this thesis, and an electrolyser temperature of 55 °C, the power consumption of the hydrogen plant with its twenty-four hydrogen electrolysers is 193.4 MW. This closely represents the power consumption of the hydrogen plant that will be developed in the Port of Rotterdam by Shell of 200 MW. The rated power consumption per large-scale hydrogen electrolyser is then 8.08 MW. The compressor power of the plant is 0.91 MW which is only around 0.5% of the total plant's power consumption. For simplification, the power consumption of the compressor model has been omitted in the simulation study.

Chapter 4

Model Predictive Control for Imbalance Minimization

4-1 Virtual Power Plant operation

The daily operation of the Virtual Power Plant in this thesis consists of a Day-Ahead bidding phase and an Intraday redispatch phase during which imbalances are minimized (see Figure 4-1). The focus of this study is on the Intraday redispatch phase for which a Model Predictive Control (MPC) unit has been developed.

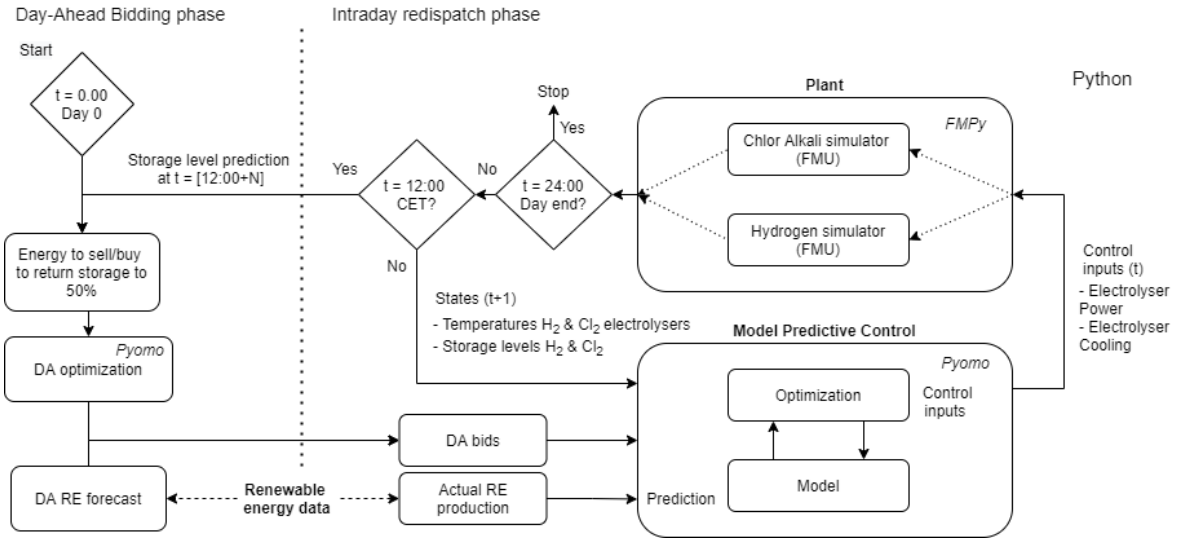

Figure 4-1: Energy Management System with a Day-Ahead and intraday redispatch phase

The operation of the Virtual Power Plant can be explained as follows, starting with the Intraday redispatch phase:

1. Each time step, the MPC integrates the current states of the plants, which are the cell temperature of the electrolysers and the hydrogen/chlorine storage levels, into the control model.

2. The MPC predicts the actual renewable energy production, $Q_{RE,act}$[t:t+N], by reading the time-series file developed in Chapter 3 and compares it to the Day-Ahead bids, $Q_{DA,bids}$[t:t+N], to generate the imbalance prediction, Q_{imb}[t:t+N], over the prediction horizon N.

3. The MPC performs an optimization to calculate the control inputs for the electrolysers which minimize the imbalances Q_{imb}[t:t+N] while respecting constraints of the unit. The control inputs of the first time step are sent to the industrial plants and consists of a power set-point and a cooling input for the electrolyser.

4. The simulators of the electrolysers developed in Chapter 4 implement the control inputs and simulate the time step, hence the time changes from t to t + 1. The output of the plant simulators consists of the temperatures of the hydrogen/chlor-alkali electrolysers and the hydrogen/chlorine storage levels at t + 1.

5. The cell temperatures simulated by the plant and predicted by the MPC are sent to a state estimator. The state estimator uses the error between the simulated and predicted temperature to calculate a new state vector that represents temperature in the MPC.

6. Finally, the state vectors that represent the cell temperature and the storage levels at t + 1 are sent to the MPC.

Every day at 12:00 CET, the MPC loop is interrupted for the Day-Ahead bidding phase in which the bids for the Day-Ahead market are generated. The bids are determined by the Day-Ahead forecast of renewable energy production and a correction term which is implemented to ensure the storage levels do not keep operating at their limits over time. The Day-Ahead bidding procedure consists of the following steps:

1. At 12:00 CET, the Virtual Power Plant records the expected position of the hydrogen and chlorine storage level at t = 12:00+N and calculates the total energy $\Delta Q_{stor,tot}$ that would need to be bought/sold in the Day-Ahead market to return the storage levels back to 50%.

2. A Day-Ahead optimization is performed to sell $\Delta Q_{stor,tot}$ during times of high prices in case there is a surplus of chemicals in the storage, and buy $\Delta Q_{stor,tot}$ during times of low prices if tanks are in a deficit compared to the midway level. The prices are historical Day-Ahead prices of 2020 in Belgium obtained from ENTSO-E Transparency and these can be found in Figure A-1 in the Appendix [88]. The additional energy bought or sold on the Day-Ahead market at each hour is $Q_{DA,stor}$[0.00:24.00].

3. A Day-Ahead forecast of the renewable energy portfolio, $Q_{RE,DA}$[0.00:24.00], is performed to which the $Q_{DA,stor}$[0.00:24.00] of the previous step is added/subtracted to produce the final $Q_{DA,bid}$[0.00:24.00]. This Day-Ahead forecast is read from the time-series file developed in Chapter 3.

4. These final Day-Ahead bids $Q_{DA,bid}$[0.00:24.00] are sent to the MPC and provide the reference trajectory of the next day.

This simulation loop has been developed in Python. To this purpose, the Day-Ahead forecast and actual renewable energy production time-series developed in Chapter 3 were imported using Pandas, a library for data analysis and manipulation. Furthermore, the MPC and Day-Ahead optimization were developed in Pyomo which is a Python package for formulating and analysing optimization problems. Finally to simulate the industrial plants, the OpenModelica simulators were converted to Functional Mock-up Units (FMU). These FMU's could be imported and simulated in Python using the FMPy library.

4-2 Model Predictive Control development

4-2-1 Control model development

MPC requires an internal model of the industrial plants, which is referred to in this thesis as a control model. The integration of process dynamics in the control model of chemical plants is crucial to avoid generating schedules that would violate process constraints [89]. Although detailed first principles models can be used, such as the OpenModelica simulators, these are highly nonlinear and contain a large amount of irrelevant variables for scheduling. Furthermore, the resulting nonlinear optimization problem (NLP) can be intractable within a scheduling slot or produce sub-optimal solutions [24].

4-2-2 Hammerstein-Wiener model for nonlinear dynamics

In Ref. [24, 90, 91], Hammerstein-Wiener models are proposed to describe nonlinear dynamics. A Hammerstein-Wiener model consists of a linear dynamic block sandwiched between a static nonlinear input and output block (see Figure 4-2). The sequential block structure of Hammerstein-Wiener models provides several benefits including the opportunity to use prior knowledge of the system, the high accuracy of the models and the ease of development which are convenient aspects for control purposes [92]. Hammerstein-Wiener models can be identified using input-output data of real plants, or simulators thereof. The nonlinear blocks can be described with various functions such as polynomials and piecewise linear equations. The benefit of piecewise linear functions is that it can allow the optimization problem to convert into a Mixed-Integer Linear Problem (MILP) which can be solved with less computational effort and towards a global optimum.

Constraints can be put on the 'inner' input and output variables, $v(t)$ and $w(t)$, rather than the 'real' input and output variables, $u(t)$ and $y(t)$, which can reduce computation time [24]. Furthermore, in case an input (or output) nonlinear block is monotonic, i.e. continuously increasing or decreasing, it is not part of an important equation in the optimization function and the input (or output) variable is bounded, i.e. $u(t) = [u_{min}, u_{max}]$, the non-linearity can be effectively removed from the optimization by bounding the 'inner' input (output) variable, i.e. $v(t) = [F(u_{min}), F(u_{max})]$ [24, 90]. This significantly reduces the optimization problem complexity and improves the computation time. Here, $F()$ refers to the piecewise linear

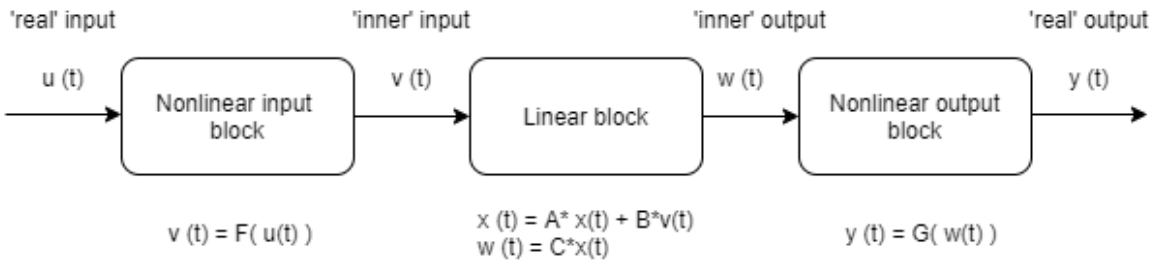

Figure 4-2: General structure of Hammerstein-Wiener model

function of an input nonlinear block. For a thorough explanation on the parameterization and replacement of 'real' and 'inner' variables in Hammerstein-Wiener models, the reader is recommended to read [91].

To avoid unnecessarily complicating the MPC, only a subset of the variables of the full-order model or the actual plant need to be integrated in the control model. These are process variables that: 1) are included in the objective function, and 2) can violate constraints during transitions, such as temperature for instance [24].

Chlor-Alkali - Cell Temperature & Current Density

The nonlinear dynamics of the chlor-alkali plant considered in this thesis are that of the electrolyser temperature and current density. The electrolyser temperature is an output which should remain between 85-90 °C and it depends on two inputs namely power consumption P_{Cl_2} and inlet temperature T_{in} [24]. The inlet temperature range in chlor-alkali plants is commonly between 70-80 °C [80]. The power input range at which the electrolyser operates could be determined by simulating the OpenModelica model using a current density input between 0.3-0.6 °C which is a regular operating range for membrane chlor alkali electrolysers [22]. This resulted in a power consumption between 3.81-8.50 MW per electrolyser, which is in good agreement with the power consumption range of the chlor-alkali model developed in [22].

With the range of the inputs and output known, an identification and validation set was created each consisting of 1445 step responses with a duration of 3.75 h which is enough time for electrolyser temperature to completely reach equilibrium. Random values for the input variable P_{Cl_2} and T_{in} within their respective range were chosen, but the combination always resulted in an electrolyser temperature, T_{Cl_2}, within 85-90 °C. A subset of the identification data-set is shown in Figure 4-7.

Matlab System Identification was used to identify the Hammerstein-Wiener models, as in [91, 24, 90], due to the lack of open-sources options. Piecewise functions were chosen to represent the nonlinear blocks such that the optimization problem turns into a Mixed Integer Linear Problem as in [90] whereas the linear block was represented by a transfer function which was converted to a state-space representation after the identification procedure. The standard transfer function setting in Matlab with 3 poles and 2 zeros was used as varying this setting did not improve the fit significantly. Some important remarks about the nonlinear blocks:

- P_{Cl_2} - the 'real' power input cannot be removed from the control model as it is necessary for calculating various equations such as the power balance [24]. Hence, the aim was to identify a nonlinear block with limited breakpoints to reduce the binary variables.
- T_{in} and T_{Cl_2} - The 'real' inlet temperature and cell temperature can be removed from the control model as they are not needed in another equation and therefore they can be replaced by bounds on the 'inner' variables only [91]. The number of break-points is not important since the piecewise function is not part of the control model, but to avoid the need for binary variables completely it was aimed to identify a monotonically increasing/decreasing piecewise function.

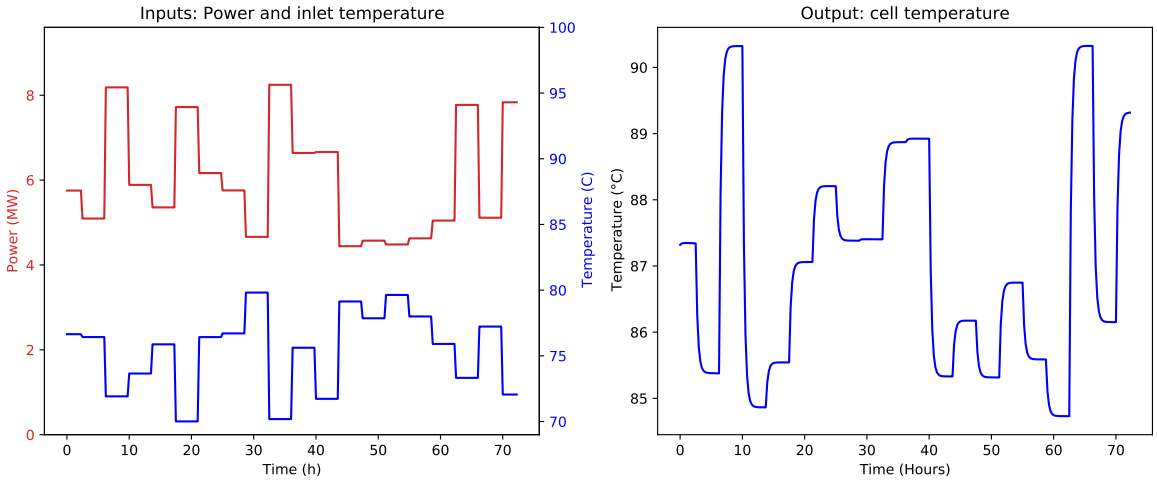

Figure 4-3: Sub-set of input-output data for the identification of the chlor-alkali temperature model

The final Hammerstein Wiener model is described below. For the input nonlinear block for $P_{Cl_2}(t)$, a piecewise linear function with a single breakpoint was identified:

$$v_{power,Cl_2}(t) = \begin{cases} 2.80 \cdot (P_{Cl_2}(t) - 3.52) - 82.97 & P_{Cl2}(t) \leq 6.18[MW] \\ 3.33 \cdot (P_{Cl_2}(t) - 6.18) - 75.5 & P_{Cl2}(t) \geq 6.18[MW] \end{cases} \tag{4-1}$$

where $v_{power,Cl_2}(t)$ is the 'inner' power input. A nonlinear input block for inlet temperature T_{in} was not necessary since this only marginally improved the fit.

The discrete linear state-space block comprises 6 state variables where it should be noted that the sampling time of the state space model, Δt, comprises an ISP (15 min):

$$\vec{x}_{Cl_2}(t+1) = A_{Cl_2} \cdot \vec{x}_{Cl_2}(t) + B_{Cl_2} \cdot \vec{u}_{Cl_2}(t) \tag{4-2}$$

$$w_{T,Cl_2}(t) = C_{Cl_2} \cdot \vec{x}_{Cl_2}(t) \tag{4-3}$$

where $\vec{x}_{Cl_2}(t)$ is the state vector consisting of $[x_{1_{Cl_2}}, x_{2_{Cl_2}}, x_{3_{Cl_2}}, x_{4_{Cl_2}}, x_{5_{Cl_2}}, x_{6_{Cl_2}}]^T$, $\vec{u}_{Cl_2}(t)$ is the input vector $[v_{power,Cl_2}(t), T_{in}(t)]$ which consists of the 'inner' control input for power

and the 'real' control input for inlet temperature, and $w_{T,Cl_2}(t)$ is the 'inner' output variable of electrolyser temperature. A_{Cl_2} is the state matrix, B_{Cl_2} is the input matrix, and C_{Cl_2} is the output matrix which are shown in Section A-3 in the Appendix.

The nonlinear output block for $T_{Cl_2}(t)$ could be described with a piecewise linear function with one break-point:

$$T_{Cl_2}(t) = \begin{cases} 0.22 \cdot w_{T,Cl2}(t) + 87.87 & w_{T,Cl2}(t) \leq 5.00 \\ 0.22 \cdot (w_{T,Cl2}(t) - 5.00) + 88.98 & w_{T,Cl2}(t) \geq 5.00 \end{cases} \tag{4-4}$$

This piecewise function is monotonic, hence the 'real' temperature can be ommitted from the control model and replaced with bounds on the 'inner' temperature without needing additional binary variables [24].

The left plot in Figure 4-7 shows the temperature response of the OpenModelica and Hammerstein Wiener model to the same inputs in the validation data-set. The identified Hammerstein-Wiener model is in good agreement with the validation data-set and according to Matlab System Identification Toolbox a fit of 97.2% to the identification data of the OpenModelica model was achieved. The right graph shows that the error between the OpenModelica and Hammerstein-Wiener model mostly lies within -0.1 and 0.1 °C.

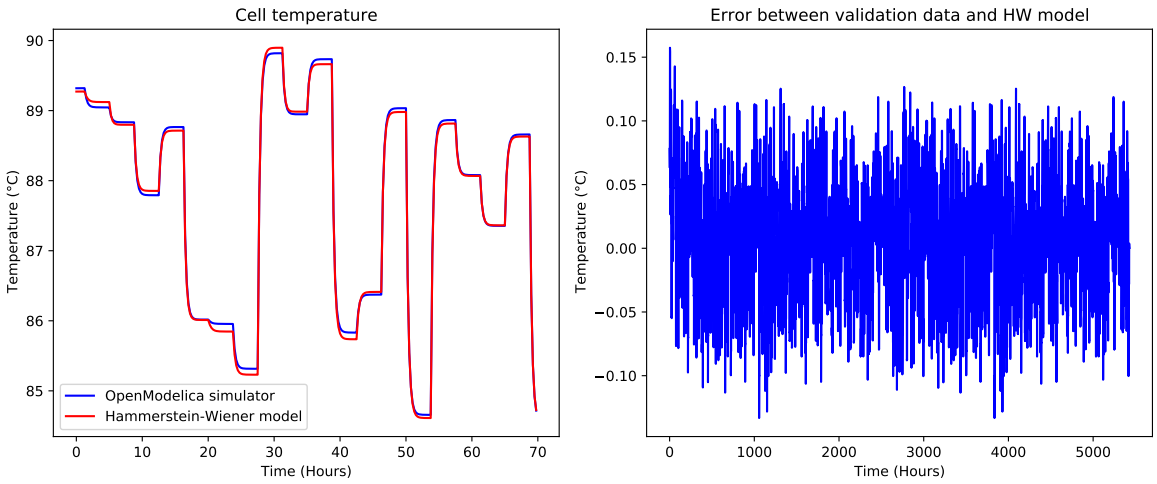

Figure 4-4: Step response of HW model compared to validation data (left) and error plot (right)

The current density j_{Cl_2} is a nonlinear function of power consumption P_{Cl_2} and cell temperature T_{Cl_2} [24] and the variable should remain within bounds of 0.3-0.6 A/cm^2 [22]. However, at the tight operating temperature range at which the cell operates (85-90 °C), the effect of cell temperature has a very limited influence on the current density, hence it is almost a linear function of P_{Cl_2} only. Based on a parametric plot with the identification data of variables j_{Cl_2} $[A/cm^2]$ and P_{Cl_2} $[MW]$ (left plot), a linear equation has been approximated which was compared to the validation data set (right plot) in Figure 4-8. Note that this equation is valid for a single chlor-alkali electrolyser.

$$j_{Cl_2}(t) = 0.0639932 \cdot (0.88 + P_{Cl_2}(t)) \tag{4-5}$$

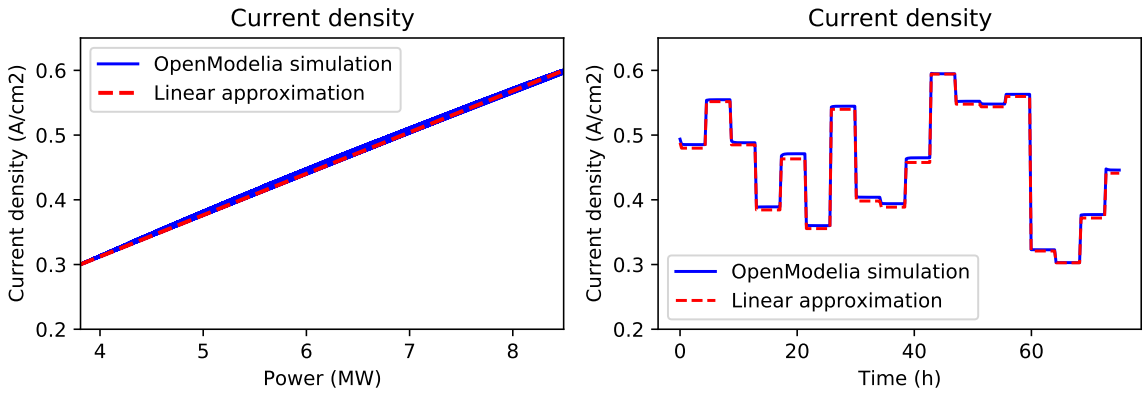

Figure 4-5: Linear approximation of current density vs power consumption of a chlor-alkali electrolyser (left) and comparison with identification data (right)

Hydrogen - Cell Temperature & Current Density

A similar approach was used to identify a Hammerstein-Wiener model for the temperature T_{H_2} of a hydrogen electrolyser which is based on inputs P_{H_2} and $\dot{Q}_{cool}$. An operating temperature range between 55-60 °C was assumed, because 60 °C is the maximum temperature of the PEM electrolyser [85] and operating close to the maximum temperature is favorable for the cell efficiency [93]. Furthermore, it was assumed that the PEM electrolyser operates at a current density of 1.0-1.6 A/cm^2 which is well within the current density range of state-of-the-art PEM electrolysers of 0.6-2.0 A/cm^2 [94]. After simulating the hydrogen electrolyser in OpenModelica with this current density and temperature range, the minimum and maximum power consumption could be identified as 4.8-8.0 MW. To be able to keep the temperature between 55-60 °C at this power consumption range, a cooling load, $\dot{Q}_{cool}$, was required between 0.69-1.44 MW.

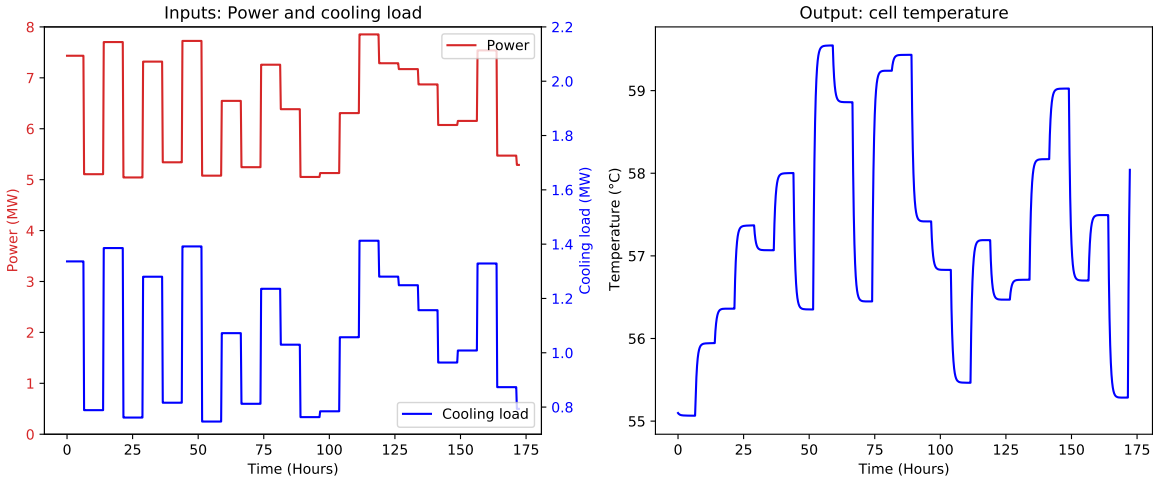

Figure 4-6: Sub-set of input-output data for the identification of the hydrogen temperature HW model

With the operating range of the electrolyser defined, an identification and validation data-set was developed with the OpenModelica model consisting of 1000 step responses that each last a time-period of 7.5 h to ensure that the electrolyser temperature had reached equilibrium. Values of the control inputs cooling load, $\dot{Q}_{cool}$, and power, P_{H_2} were randomly chosen within their bounds, however the combination always resulted in a cell temperature between 55-60 °C. A subset of the identification data is shown in Figure 4-6.

A Hammerstein-Wiener model was identified with a nonlinear input block, linear state-space block and a nonlinear output block. Since P_{H_2} will be required in the control model to calculate the energy balance and current density [91] it was attempted to limit the number of breakpoints of this nonlinear block. For the nonlinear input block of P_{H_2} a piecewise linear function with a single break point was identified:

$$v_{power,H_2}(t) = \begin{cases} 11.9 \cdot P_{in,H_2}(t) - 14.74 & P_{in,H_2}(t) \leq 6.50[MW] \\ 10.71 \cdot (P_{in,H_2}(t) - 6.5) + 62.69 & P_{in,H_2}(t) \geq 6.50[MW] \end{cases} \tag{4-6}$$

The input nonlinear block for $\dot{Q}_{cool}$ was described with a piecewise linear function with 6 breakpoints, again using the standard setting for identifying the linear model in Matlab:

$$v_{\dot{Q_{cool}},H_2}(t) = \begin{cases} -58.81 \cdot (\dot{Q}_{cool}(t) - 0.48) - 30.23 & \dot{Q}_{cool}(t) \leq 0.80[MW] \\ -55.39 \cdot (\dot{Q}_{cool}(t) - 0.80) - 49.27 & 0.80 \leq \dot{Q}_{cool}(t) \leq 0.94[MW] \\ -52.47 \cdot (\dot{Q}_{cool}(t) - 0.94) - 56.79 & 0.94 \leq \dot{Q}_{cool}(t) \leq 1.08[MW] \\ -45.36 \cdot (\dot{Q}_{cool}(t) - 1.08) - 64.00 & 1.08 \leq \dot{Q}_{cool}(t) \leq 1.20[MW] \\ -43.47 \cdot (\dot{Q}_{cool}(t) - 1.20) - 69.73 & 1.20 \leq \dot{Q}_{cool}(t) \leq 1.35[MW] \\ -41.71 \cdot (\dot{Q}_{cool}(t) - 1.35) - 76.14 & \dot{Q}_{cool}(t) \geq 1.35 \cdot 10^6[W] \end{cases} \tag{4-7}$$

where, $v_{\dot{Q}_{cool},H_2}(t)$ marks the inner variable for cooling. Since the real variable, $\dot{Q}_{cool}$, was not required in other equations in the control model and the piecewise function above is monotonic, it could be replaced with bounds on the inner variable $v_{\dot{Q}_{cool},H_2}(t)$ [24].

For the linear block, the standard setting with 3 poles and 2 zeros for the transfer function provided an accurate dynamic model which after conversion provided a state-space representation with 6 state variables:

$$\vec{x}_{H_2}(t+1) = A_{H_2} \cdot \vec{x}_{H_2}(t) + B_{H_2} \cdot \vec{u}_{H_2}(t) \tag{4-8}$$

$$w_{T,H_2}(t) = C_{H_2} \cdot \vec{x}_{H_2}(t) \tag{4-9}$$

where $\vec{x}_{H_2}(t)$ is the state variable vector of $[x_{1_{H_2}}(t), x_{2_{H_2}}(t), x_{3_{H_2}}(t), x_{4_{H_2}}(t), x_{5_{H_2}}(t), x_{6_{H_2}}(t)]^T$, $\vec{u}_{H_2}(t)$ is the input vector $[v_{power,H_2}(t), v_{\dot{Q},cool}(t)]$ consisting of the 'inner' input variables of power and cooling load, and $w_{T,H_2}(t)$ is the 'inner' output variable of cell temperature. A_{H_2} is the state matrix, B_{H_2} is the input matrix, and C_{H_2} is the output matrix which are shown in Section A-3 in the Appendix.

Finally, the nonlinear output block for cell temperature, $T_{H_2}(t)$, consists of a piecewise linear function with two breakpoints:

$$T_{H_2}(t) = \begin{cases} 0.08 \cdot (w_{T,H2}(t) - -30) + 327.56 & w_{T,H2}(t) \leq -21.07 \\ 0.22 \cdot (w_{T,H2}(t) - -21.07) + 328.25 & -21.07 \leq w_{T,H2}(t) \leq 64.67 \\ 0.27 \cdot (w_{T,H2}(t) - 64.67) + 347.69 & w_{T,H2}(t) \geq 64.67 \end{cases} \tag{4-10}$$

where, $T_{H_2}(t)$ is the real output variable of the electrolyser temperature and $w_{T,H2}(t)$ is the 'inner' temperature variable. The piecewise function is monotonic and the 'real' electrolyser temperature $T_{H_2(t)}$ is not needed in the control model for another function so the nonlinear block could be removed and replaced with bounds on the 'inner' output variable $w_{T,H2}(t)$ [91].

The identified Hammerstein-Wiener model is in good agreement with the validation data-set and a fit of 95.75% was achieved. Below the agreement between the Hammerstein-Wiener model and the validation data is shown, as well as an error plot for the whole validation data-set where it can be seen that the error generally lies within -0.3 and 0.25 °C.

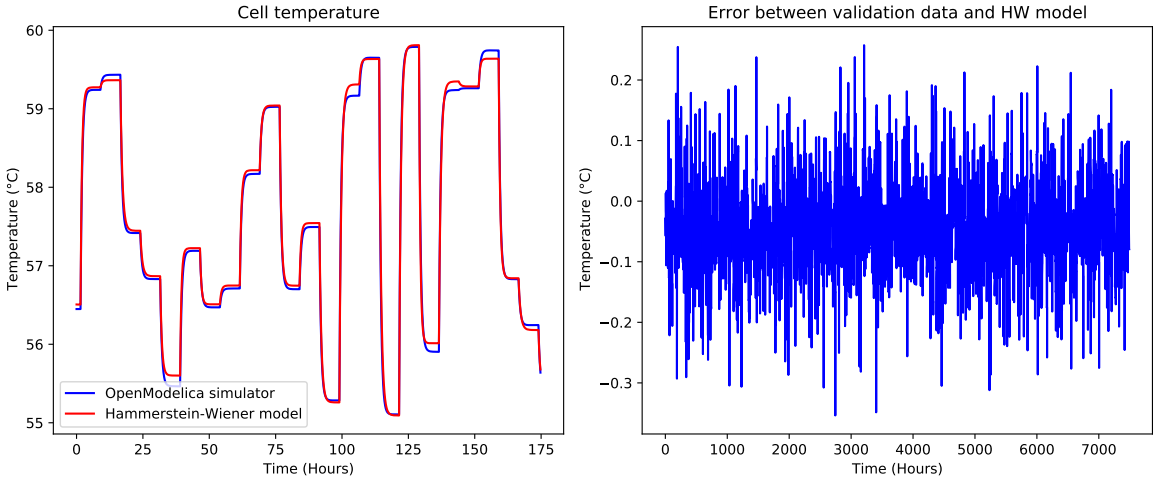

Figure 4-7: Step response of HW model for hydrogen electrolyser and validation data (left) and error plot (right)

Although the current density j_{H_2} is a nonlinear function of power consumption P_{Cl_2} and cell temperature T_{H_2}, at the tight operating temperature range at which the electrolyser operates (55-60 °C), the effect of electrolyser temperature on the current density was limited. Therefore the current density is almost a linear function of P_{H_2} only. Based on a parametric plot with j_{Cl_2} and P_{H_2}, a linear curve has been fitted which provides a good approximation (see Figure 4-8):

$$j_{i,H_2} = 0.1875 \cdot (0.533333 + P_{i,H_2}(t)) \tag{4-11}$$

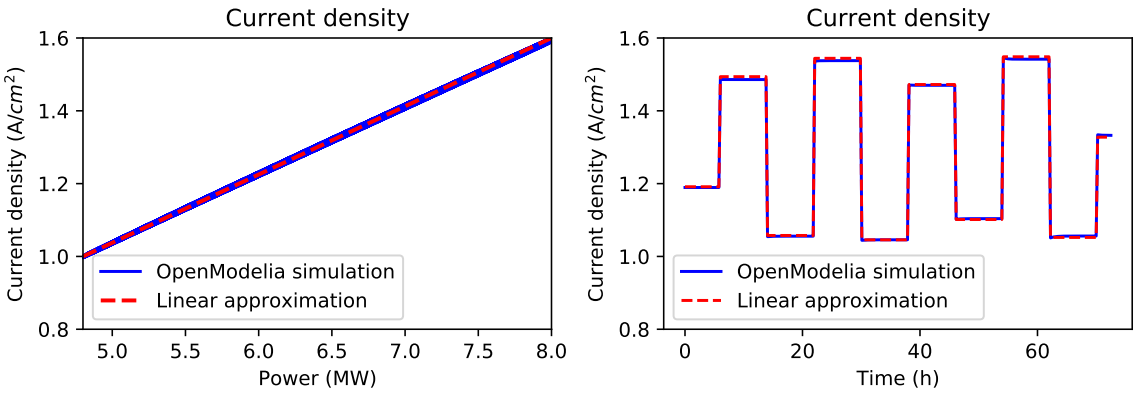

Figure 4-8: Linear approximation of current density vs power consumption of hydrogen electrolyser (left) and comparison with validation data (right)

4-3 MPC control problem formulation

This section describes the control problem formulation of the Model Predictive Controller implemented in Python using the Pyomo package.

4-3-1 Nomenclature

An overview of all parameters and variables of the MPC controller can be found in Table A-3, but to clarify the equations in the next sections some of the important terms are noted below:

- t = Time [15 min]
- N = Prediction horizon [-]
- G_{sub} = Number of electrolyser sub-groups in the chlor-alkali plant [-]
- K_{sub} = Number of electrolyser sub-groups in the hydrogen plant [-]
- g = Electrolyser sub-group number g in the chlor-alkali plant[-]
- k = Electrolyser sub-group number k in the hydrogen plant [-]
- $_{Cl_2}$ = Subscript for chlor-alkali [-]
- $_{H_2}$ = Subscript for hydrogen [-]

4-3-2 Objective Function

The objective function in this thesis is a minimization function of positive and negative imbalances, similar to ref. [13].

$$\begin{aligned} min \sum_{t=0}^{N} Q^{+}(t) + Q^{-}(t) + \sigma_1 \cdot (L_{norm,H_2}(t) - L_{norm,Cl_2}(t))^2 \\ +\sigma_2 \cdot (S_{Cl_2,low}(t) + S_{Cl_2,up}(t) + S_{H_2,low}(t) + S_{H_2,up}(t)) \end{aligned} \tag{4-12}$$

Where Q^+ and Q^- $[MWh]$ indicate the positive and negative imbalances respectively within an ISP and N is the prediction horizon. Furthermore, a penalty σ_1 is added on the difference between the normalized storage levels of the hydrogen and chlor-alkali plant $L_{norm,H_2}(t)$ and $L_{norm,Cl_2}(t)$. The constraint ensures that the storage levels remain close to one another thereby avoiding that one plant is forced to minimize imbalances by itself (for which it may not have a sufficient regulation capacity) because the other industrial plant is already operating at the storage limit. In addition, a penalty σ_2 is placed on exceeding the lower and upper limit of the chlorine and hydrogen tank using slack variables $S_{Cl_2,low}(t)$ and $S_{Cl_2,up}(t)$, and $S_{H_2,low}(t)$ and $S_{H_2,up}(t)$. The slack variables prevent infeasible solutions when the storage levels exceed the limits, which can occur if the predicted and simulated chemicals production are not completely aligned.

4-3-3 System Constraints

Imbalances

The predicted imbalances by the MPC are the difference between the Day-Ahead bids and the actual renewable energy production, which is implemented with the following constraint.

$$Q_{imb}(t) = Q_{act}(t) - Q_{DA,bid}(t) \qquad \forall t = 0, N \tag{4-13}$$

where $Q_{imb}(t)$ is the predicted imbalance to be minimized, $Q_{act}(t)$ is the forecast of the actual renewable energy production, and $Q_{DA,bid}(t)$ is the energy bid in the Day-Ahead market during an ISP. $Q_{act}(t)$ consists of the sum of the actual onshore wind and PV energy production data which was developed in Chapter 3.

The following energy balance equation ensures that the predicted imbalances by the MPC are equal to the demand response provided by the electrolysers of the industrial plants and the remaining imbalances in the Virtual Power Plant portfolio.

$$24 \cdot \sum_{g=1}^{G_{sub}} \frac{P_{g,dr,Cl_2}(t)}{G_{sub}} \cdot \frac{900}{3600} + 24 \cdot \sum_{k=1}^{K_{sub}} \frac{P_{k,dr,H_2}(t)}{K_{sub}} \cdot \frac{900}{3600} + Q^{+}(t) + Q^{-}(t) = Q_{imb}(t) \qquad \forall t = 0, N \tag{4-14}$$

where the factor 24 indicates the number of electrolysers per plant, $P_{g,dr}(t)$ and $P_{k,dr}(t)$ is the demand response provided by an electrolyser in sub-group g or k respectively and G_{sub} and

K_{sub} indicate the number of electrolyser sub-groups in the chlor-alkali plant and hydrogen plant. If for example, $G_{sub} = 1$ all 24 chlor-alkali electrolysers are gathered in a single group that operate with the same power consumption, whereas if $G_{sub} = 2$ the chlor-alkali electrolysers are divided in 2 sub-groups, each with 12 electrolysers, that can operate at a different power consumption level. $Q^+(t)$ and $Q^-(t)$ are the remaining positive or negative imbalances in the VPP portfolio, and $Q_{imb}(t)$ is the imbalance predicted by the MPC. The factor $\frac{900}{3600}$ converts power $[MW]$ to energy $[MWh]$.

The demand response provided by an electrolyser is equal to the difference between the actual power consumption, $P_{g,Cl_2}(t)$ and $P_{k,H_2}(t)$, and the nominal power consumption, P_{nom,Cl_2} and P_{nom,H_2}:

$$P_{g,dr,Cl_2}(t) = P_{g,Cl_2}(t) - P_{nom,Cl2} \qquad \forall t = 0, N, \forall g = 1, G_{sub} \tag{4-15}$$

$$P_{k,dr,H_2}(t) = P_{k,H_2}(t) - P_{nom,H_2} \qquad \forall t = 0, N, \forall k = 1, K_{sub} \tag{4-16}$$

Based on Ref. [15], constraints have been implemented that prevent the remaining imbalances $Q^+(t)$ and $Q^-(t)$ to be much higher or lower than the predicted imbalances:

$$0 \leq Q^+(t) \leq |Q_{imb}(t)| + Q_{res} \qquad \forall t = 0, N \tag{4-17}$$

$$-|Q_{imb}(t)| - Q_{res} \leq Q^-(t) \leq 0 \qquad \forall t = 0, N \tag{4-18}$$

An additional term has been included, Q_{res}, which is a small amount of reserve energy to ensure that if the storage limits is exceeded, due to a small mismatch between the predicted chemicals production by the MPC and simulated by the plants, the plants can return to the storage level limit. The value chosen for Q_{res} was 0.5 MWh/ISP which is a limited amount compared to the Day-Ahead forecast errors which have a standard deviation of 5.08 MWh/ISP. Various other values for Q_{res} were attempted which showed its influence on the imbalance results is very small and 0.5 MWh/ISP could be safely assumed.

Power consumption & current density

The relation between the power input and current density of a chlor-alkali electrolyser could be described with the identified empirical equation in Section 4-2-2:

$$j_{g,Cl_2}(t) = 0.0639932 \cdot (0.88 + P_{g,Cl_2}(t)) \qquad \forall t = 0, N, \forall g = 1, G_{sub} \tag{4-19}$$

where $j_{g,Cl_2}(t)$ is the current density and $P_{g,Cl_2}(t)$ is the power consumption per chlor-alkali electrolyser in sub-group g. The current density is limited between an upper and lower limit:

$$j_{Cl_2,min} \leq j_{g,Cl_2}(t) \leq j_{Cl_2,max} \qquad \forall t = 0, N, \forall g = 1, G_{sub} \tag{4-20}$$

where the lower limit is 0.3 A/cm^2 and the upper limit is 0.6 A/cm^2 for an industrial membrane chlor-alkali electrolyser, based on Ref. [22, 80].

The relation between the power input to the hydrogen electrolyser and the current density can be described with the empirical equation developed in Section 4-2-2:

$$j_{k,H_2}(t) = 0.1875 \cdot (0.533333 + P_{k,H_2}(t)) \qquad \forall t = 0, N, \forall k = 1, K_{sub} \tag{4-21}$$

where $j_{k,H_2}(t)$ is the current density and $P_{k,H_2}(t)$ is the power consumption per hydrogen electrolyser in sub-group g. The current density is limited between an upper and lower limit:

$$j_{H_2,min} \leq j_{k,H_2}(t) \leq j_{H_2,max} \qquad \forall t = 0, N, \forall k = 1, K_{sub} \tag{4-22}$$

As discussed in Section 4-2-2, the bounds on the hydrogen electrolyser current density are 1 A/cm^2 for the lower limit and 1.6 A/cm^2 for the upper limit, which is within the range of 0.6-2 A/cm^2 of state of the art PEM electrolysers.

Temperature

The Hammerstein-Wiener models developed in section 4-2-1 are included in the control model to describe the nonlinear cell temperature dynamics of the chlor-alkali and hydrogen electrolysers. Of the Hammerstein-Wiener models, only the nonlinear input blocks for power P_{Cl_2} and P_{H_2} and the linear blocks were necessary in the control model. The piecewise functions of their respective nonlinear blocks can be integrated efficiently in Pyomo with the *Piecewise* function. The other nonlinear blocks for the 'real' variables $\dot{Q}_{cool}$, T_{H_2} and T_{Cl_2} could be removed from the control model, and replaced with bounds on their 'inner' variables without additional binary variables. This is because their their piecewise functions are monotonic and the 'real' variables were not needed in another physical equation in the optimization, as was also discussed in Section 4-2-2 [91]. An overview of the Hammerstein-Wiener model parts inside and outside of the control model is shown below:

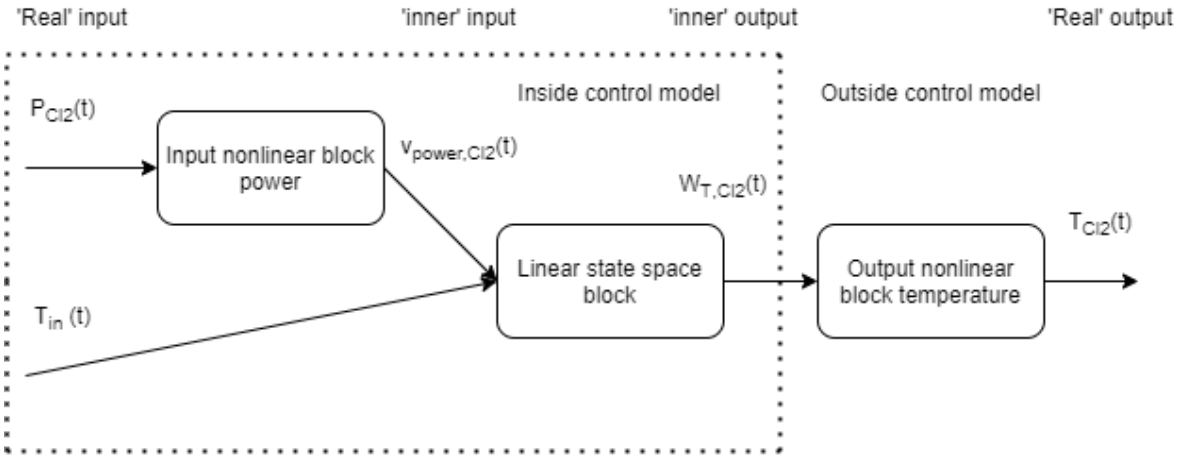

Figure 4-9: Parts of HW model inside and outside the control model (chlor-alkali

Below the temperature constraints of the control model for the chlor-alkali electrolysers are shown using Hammerstein-Wiener model found in 4-2-2. The nonlinear input block for power input, $P_{g,Cl2}$, to a chlor-alkali electrolyser was integrated with the following constraint:

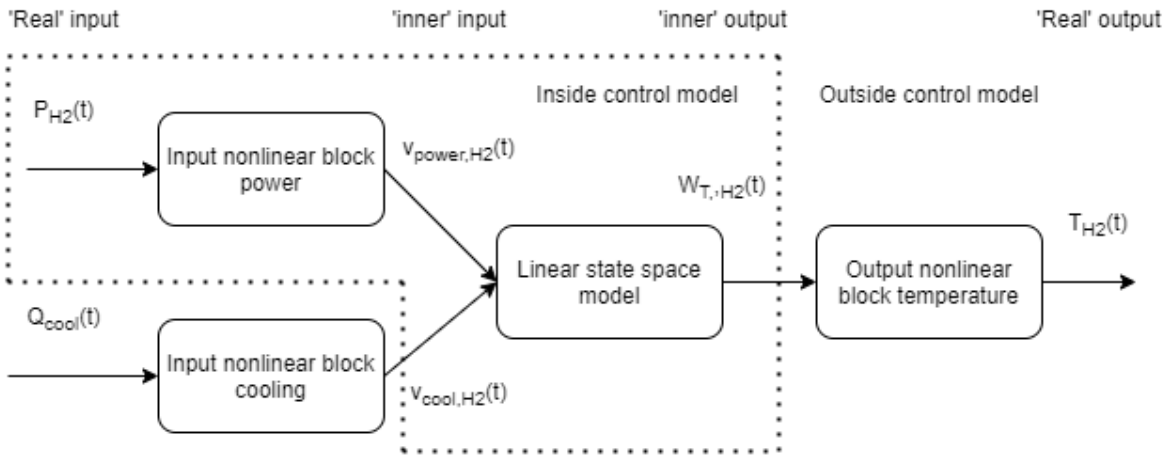

Figure 4-10: Parts of HW model inside and outside the control model (hydrogen)

$$v_{g,power,Cl_2}(t) = \begin{cases} 2.80 \cdot (P_{g,Cl2}(t) - 3.52) - 82.97 & P_{g,Cl2}(t) \leq 6.18[MW] \\ 3.33 \cdot (P_{g,Cl2}(t) - 6.18) - 75.5 & P_{g,Cl2}(t) \geq 6.18[MW] \\ & \forall t = 0, N, \forall g = 1, G_{sub} \end{cases} \tag{4-23}$$

where $v_{g,power,Cl_2}(t)$ is the 'inner' input variable and $P_{g,Cl2}(t)$ is the 'real' power consumption input per electrolyser in sub-group g.

The next constraint bounds the inlet temperature of the electrolyte, $T_{g,in}(t)$, that cools the chlor-alkali electrolyser:

$$T_{in,min} \leq T_{g,in}(t) \leq T_{in,max} \qquad \forall t = 0, N, \forall g = 1, G_{sub} \tag{4-24}$$

where, $T_{g,in}(t)$ is the electrolyte inlet temperature per chlor-alkali electrolyser in subgroup g which is bounded between 70-80 °C [80]

The following constraints integrate the linear state space model of the Hammerstein-Wiener model for the chlor-alkali electrolyser:

$$\vec{x}_{g,Cl_2}(t+1) = A_{Cl_2} \cdot \vec{x}_{g,Cl_2}(t) + B_{Cl_2} \cdot [v_{g,power,Cl_2}(t), T_{g,in}(t)] \qquad \forall t = 0, N, \forall g = 1, G_{sub} \tag{4-25}$$

$$w_{g,T,Cl_2}(t) = C_{Cl_2} \cdot \vec{x}_{g,Cl_2}(t), \qquad \forall t = 0, N, \forall g = 1, G_{sub} \tag{4-26}$$

where $\vec{x}_{g,Cl_2}$ is the state vector per chlor-alkali electrolyser in sub-group g, A_{Cl_2} and B_{Cl_2} are respectively the state and input matrices of the state-space model, $[v_{g,power,Cl_2}(t), T_{g,in}(t)]$ is the input vector with the 'inner' variable for power and the 'real' variable for inlet temperature per chlor-alkali electrolyser in sub-group g. w_{g,T,Cl_2} is the 'inner' temperature per electrolyser in sub-group g and C_{Cl_2} is the output matrix of a chlor-alkali elecrolyser.

With the next constraint, bounds are placed on the 'inner' temperature variable of the chlor-alkali electrolysers:

$$w_{T,Cl_2,min} \leq w_{g,T,Cl_2}(t) \leq w_{T,Cl_2,max}) \qquad \forall t = 0, N, \forall g = 1, G_{sub} \tag{4-27}$$

By inserting the 'real' temperature bounds in the piecewise linear equation 4-4, the bounds on the 'inner' temperature variable can be calculated. The operating temperature was set between 85+0.2 °C and 90-0.2 °C, where the small margin of 0.2 °C is used to avoid violating the operating temperature due to the minor plant-model mismatch, which results in a $w_{T,Cl_2,min}$ of -12 and a $w_{T,Cl_2,max}$ of 8.67. Since a Hammerstein-Wiener model is a black-box model, these values carry no physical meaning.

Below the temperature constraints for the hydrogen electrolysers in the control model are shown. The input nonlinear block that maps $P_{k,H_2}(t)$ to the 'inner' input variable $v_{k,power,H_2}(t)$ for power was described with a piecewise function as mentioned in Section 4-2-2 and was implemented as followed:

$$v_{k,power,H_2}(t) = \begin{cases} 11.91 \cdot P_{k,H_2}(t) - 14.74 & P_{k,H_2}(t) \leq 6.5[MW] \\ 10.71 \cdot (P_{k,H_2}(t) - 6.5) + 62.69 & P_{k,H_2}(t) \geq 6.5[MW] \end{cases} \qquad \forall t = 0, N, \forall k = 1, K_{sub} \tag{4-28}$$

where $P_{k,H_2}(t)$ and $v_{k,power,H_2}(t)$ is the respectively 'real' and 'inner' power input per hydrogen electrolyser in subgroup k.

The bounds on the 'inner' variable for the cooling load of the electrolyser could be described with the following constraint:

$$v_{\dot{Q},cool,min} \leq v_{k,\dot{Q},cool}(t) \leq v_{\dot{Q},cool,max} \qquad \forall t = 0, N, \forall k = 1, K_{sub} \tag{4-29}$$

where $v_{k,\dot{Q},cool}$ is the 'inner' cooling load input per hydrogen electrolyser in subgroup k. The bounds on the 'inner' cooling load have been calculated a priori by inserting the 'real' cooling load bounds (0.69-1.44 MW) that were defined in Section 4-2-2 into the piecewise linear equation 4-7 which results in a $v_{\dot{Q},cool,min}$ of -42.46 and a $v_{\dot{Q},cool,max}$ of -79.87.

The linear state-space model of the Hammerstein-Wiener model of a hydrogen electrolyser in subgroup k was integrated using the following constraint:

$$\vec{x}_{k,H_2}(t+1) = A_{H_2} \cdot \vec{x}_{k,H_2}(t) + B_{H_2} \cdot [v_{k,power,H_2}(t), v_{k,\dot{Q},cool}(t)] \qquad \forall t = 0, N, \forall k = 1, K_{sub} \tag{4-30}$$

$$w_{T_{k,H_2}}(t) = C_{H_2} \cdot \vec{x}_{k,H_2}(t) \qquad \forall t = 0, N, \forall k = 1, K_{sub} \tag{4-31}$$

where $\vec{x}_{k,H_2}(t)$ is the state vector per hydrogen electrolyser, A_{H_2} and B_{H_2} are the state and input matrix of the state space model, and $[v_{k,power,H_2}(t), v_{k,\dot{Q},cool}(t)]$ is the input vector where $v_{k,power,H_2}(t)$ is the 'inner' power input and $v_{k,\dot{Q},cool}(t)$ is the 'inner' cooling input.

Furthermore, $w_{T_{k,H_2}}(t)$ is the 'inner' output temperature and C_{H_2} is the output matrix of the state space model.

The 'inner' variable for temperature of a hydrogen electrolyser was bounded by integrating the following constraint:

$$w_{T,H_2,min} \leq w_{k,T,H_2}(t) \leq w_{T,H_2,max} \qquad \forall t = 0, N, \forall k = 1, K_{sub} \tag{4-32}$$

Rather than allowing the hydrogen electrolysers to operate freely within its operating range (55-60 °C), it was of interest to observe the ability of the MPC to keep the temperature of the hydrogen electrolysers at a set-point which was chosen at 57.5 °C. The 'inner' temperature bounds were calculated by inserting 57.5 °C into the piecewise linear function 4-10 which gave a value of -10.49 for both $w_{T,H_2,min}$ and $w_{T,H_2,max}$.

Since the nonlinear blocks of the 'real' variables $\dot{Q}_{cool}$, T_{H_2} and T_{Cl_2} were not part of the control model, after each optimization the piecewise equations 4-7, 4-4 and 4-10 were used respectively to convert the 'inner' variables calculated by the MPC to the 'real' values.

Ramp rates

The ramp rate up- and down of current density of the chlor-alkali electrolyser is restricted using the following formula:

$$\begin{aligned} -b_{g,Cl_2}(t) \cdot \Delta j_{Cl_2,down} \leq j_{g,Cl_2}(t+1) - j_{g,Cl_2}(t) \leq b_{g,Cl_2}(t) \cdot \Delta j_{Cl_2,up}, \\ \forall t = 0, N, \forall g = 1, G_{sub} \end{aligned} \tag{4-33}$$

where $\Delta j_{Cl_2,down}$ and $\Delta j_{Cl_2,up}$ are the maximum ramps in current density. Based on Ref. [80], membrane electrolysers could ramp with 0.15 A/cm^2 per 15 minutes however this may vary per plant. Therefore, a safe assumption was implemented that electrolysers can ramp with 0.075 A/cm^2 per ISP, which is half of 0.15 A/cm^2 [80].

Since hydrogen PEM electrolysers can ramp between the minimum and maximum load within seconds [70] which is well within the time-period of an ISP, there are no ramping limits integrated:

$$-b_{k,H_2}(t) \cdot \infty \leq j_{k,H_2}(t+1) - j_{k,H_2}(t) \leq b_{k,H_2}(t) \cdot \infty \qquad \forall t = 0, N, \forall k = 1, K_{sub} \tag{4-34}$$

As shown in the next section, the binary variables $b_{g,Cl_2}(t)$ and $b_{k,H_2}(t)$ have been integrated to control the ramping frequency of the electrolysers.

Ramp frequency & sub-unit operation

Durability of capital intensive equipment is of major importance in industry. Demand response requires dynamic operation of components which may lead to increased wear and tear, and therefore participants in demand response programs may want to limit the frequency at which their equipment is used [95]. Some works on degradation due to dynamic operation in

electrolysis have shown negative effects [96] and others neutral/positive effects on the PEM electrolyser performance from cycling PEM electrolysers [97]. Overall, the effect of intermittent operation on the degradation of PEM electrolysers is still limitedly understood [98, 99] with. Thus far no studies have been performed that analyse the effect of dynamic operation on the durability of chlor-alkali electrolysers.

A ramp frequency limitation is implemented in this thesis which can help avoid potential degradation and allow plant owners to decide how frequently the Virtual Power Plant can adjust the power consumption of their equipment. It will be activated during several simulation studies in the sensitivity section. A switching frequency constraint developed by [52] was modified and implemented:

$$\sum_{j=t-N}^{0} b_{g,Cl_2}(t) + \sum_{j=t}^{N} b_{g,Cl_2}(t) \leq b_{tot} \qquad \forall t = 0, N, \forall g = 1, G_{sub} \tag{4-35}$$

$$\sum_{j=t-N}^{0} b_{k,H_2}(t) + \sum_{j=t}^{N} b_{k,H_2}(t) \leq b_{tot} \qquad \forall t = 0, N, \forall k = 1, K_{sub} \tag{4-36}$$

where $b(t)$ is a binary variable which is 0 if the current density of the electrolysers remain constant, or 1 if the electrolysers switches to a different current density at a time step. The first section $\sum_{j=t-N}^{0} b(t)$ is the sum of ramps that have occurred up to N time-steps before the current time-step, and the second section $\sum_{j=t}^{N} b(t)$ is the sum of ramps up to N time-steps after the current time-step. The third section, b_{tot}, indicates the total number of ramps allowed within N time-steps. The ramp frequency limit constraint ensures that within a time period of N time steps the amount of current density changes, and therefore power changes, of an electrolyser sub-group is never allowed to exceed b_{tot}.

In literature, the electrolysers in a chlor-alkali plant are often assumed to operate at the same current density [22, 24, 62]. Under a ramp frequency limit, the operation as a single group could reduce the ability to minimize imbalances since the imbalances require energy consumption changes every time-step. Thus far, no study has considered organizing electrolysers in plants in sub-groups, where each sub-group can operate with a different power set-point. Since sub-groups could ramp one after another, this subdivision will help increase the ramping frequency of the whole plant while respecting the ramping limits on single electrolysers.

In the base-case simulation, the number of sub-groups, G_{sub} and K_{sub}, is 1 per plant and the ramp frequency is not limited. However, in the sensitivity analysis of this thesis, several simulations will be performed with a variation in the number of sub-groups and ramping frequency limits to observe their effect on the imbalance minimization ability of the industrial loads.

Production & storage of Cl_2 and H_2

The production of chlorine in a chlor-alkali electrolyser is described using Faraday's law with the following constraint:

$$\dot{N}_{g,Cl2}(t) = \frac{j_{g,Cl_2}(t) \cdot A_{e,Cl_2} \cdot N_{cells,Cl_2}}{2 \cdot F} \qquad \forall t = 0, N, \forall g = 1, G_{sub} \tag{4-37}$$

where $\dot{N}_{g,Cl_2}$ is the molar flow of chlorine per electrolyser in sub-group g, j_{g,Cl_2} is the current density per electrolyser in sub-group g and F is the Faraday constant. A_{e,Cl_2} is the surface area of a chlor-alkali cell which is equal to 2.7 m^2 and N_{cells,Cl_2} is the amount of cells which is equal to 160 [80].

The normalized level of the chlorine storage can be described using the following constraint:

$$L_{norm,Cl_2}(t+1) = L_{norm,Cl_2}(t) + 24 \cdot \sum_{g=1}^{G_{sub}} \frac{\dot{N}_{g,Cl_2}(t) \cdot 900}{G_{sub} \cdot L_{max,Cl2}} \qquad \forall t = 0, N \tag{4-38}$$

where L_{norm,Cl_2} is the normalized storage level of the chlorine tank, $\sum_{g=1}^{24} \dot{N}_{g,Cl_2}$ is the summed molar chlorine production of all twenty-four electrolysers, 900 is the amount of seconds in a time-step of 15 minutes and L_{max,Cl_2} is the maximum capacity of the chlorine storage. The maximum storage size has been chosen such that a full storage can an independently supply customers for six hours, following the study of [22]. The maximum storage size can be described with the following equation:

$$L_{max,Cl_2} = 24 \cdot \sum_{g=1}^{G_{sub}} \frac{j_{Cl_2,nom} \cdot A_{e,Cl_2} \cdot N_{cells,Cl_2}}{G_{sub} \cdot 2 \cdot F} \cdot 6 \cdot 3600 \tag{4-39}$$

where $j_{Cl_2,nom}$ indicates the nominal current density per electrolyser in sub-group g, and the $6 \cdot 3600$ corresponds to the amount of seconds in 6 hours.

Finally, the chlorine storage level is not allowed to exceed a lower and upper boundary which is achieved by implementing the following constraint

$$-S_{Cl_2,low}(t) + 0.2 \leq L_{norm,Cl_2}(t) \leq 0.8 + S_{Cl_2,up}(t) \qquad \forall t = 0, N \tag{4-40}$$

The slack variables $S_{Cl_2,low}(t)$ and $-S_{Cl_2,low}(t)$ are implemented to avoid infeasible solutions when storage limits are slightly exceeded which may occur when the simulated chlorine production slightly deviate from the predicted production of the MPC.

The constraints for the hydrogen electrolysers can be similarly implemented with the main difference that in equation 4-41 the 46 KW high-pressure electrolyser is put in series N_{series,H_2} times to represent a large-scale hydrogen electrolyser:

$$\dot{N}_{k,H_2}(t) = \frac{j_{k,H2_2}(t) \cdot A_{e,H_2} \cdot N_{cells,H_2} \cdot N_{series,H_2}}{2 \cdot F} \qquad \forall t = 0, N, \forall k = 1, K_{sub} \tag{4-41}$$

$$L_{norm,H_2}(t+1) = L_{norm,H_2}(t) + 24 \cdot \sum_{k=1}^{K_{sub}} \frac{\dot{N}_{k,H_2}(t) \cdot 900}{K_{sub} \cdot L_{max,H2}} \qquad \forall t = 0, N \tag{4-42}$$

$$L_{max,H_2} = 24 \cdot \sum_{k=1}^{K_{sub}} \frac{j_{H_2,nom} \cdot A_{e,H_2} \cdot N_{cells,H_2} \cdot N_{series,H_2}}{K_{sub} \cdot 2 \cdot F} \cdot 6 \cdot 3600 \tag{4-43}$$

$$-S_{H_2,low}(t) + 0.2 \leq L_{norm,H_2}(t) \leq 0.8 + S_{H_2,up}(t) \qquad \forall t = 0, N \tag{4-44}$$

Since there is no information available on the size of the hydrogen storage of the Shell plant, it is assumed that a full storage can independently supply customers for six hours similar to the chlor-alkali plant.

There is no constraint implemented at the end of the prediction horizon N that would force the storage levels to return to 50%. Such a constraint would strongly limit the ability to minimize imbalances, as it frequently occurs that the Day-Ahead errors are continuously positive/negative for a period longer than the prediction horizon. In those cases, the MPC cannot perform load shifting since there are no negative imbalances to compensate for the positive imbalances, and vice versa. This issue was present in the study of Ref. [13], where demand response in the form of load shifting was not possible during continuously positive or negative imbalances.

Therefore, in this thesis the hydrogen and chlorine storage levels are allowed to move freely within limits of 20%-80% without a constraint at the end of the prediction horizon that forces the storage levels to 50%. However, to ensure that the storage levels are not continuously operating at the limits which reduces the ability to provide demand response, the Day-Ahead market is used to sell/buy additional energy to guide the storage levels to the midway position. This Day-Ahead bid correction is explained in Section 4-5.

4-4 State estimation

A Luenberger observer is implemented to provide the MPC with feedback of the simulated cell temperature. Below the general structure of the Luenberger observer is shown:

$$\vec{x}(t+1) = A \cdot \vec{x}(t) + L \cdot (v_{T,mpc}(t) - v_{T,sim}(t)) + B \cdot \vec{u}(t) \tag{4-45}$$

where $\vec{x}(t)$ is the state vector of the state-space model in the MPC that predicts the temperature of an electrolyser, $v_{T,mpc}(t)$ is the 'inner' output value of temperature predicted by the MPC, $v_{T,sim}(t)$ is the 'inner' output value of temperature of the simulator. This is calculated after each optimization using the piecewise linear function that relates the 'real' output $T_{sim}(t)$ to the 'inner' output $v_{T,sim}(t)$), $\vec{u}(t)$ is the input vector, A is the state matrix, B is the input matrix and L is the Luenberger observer matrix. Adjusting the state-estimator matrix is an intensive task in control theory. It often requires modifying the observer matrices in such a way that a smooth feedback is achieved and a balance is found between the possible errors in the plant measurements and control model of the MPC. Such an intense tuning process is beyond the scope of this thesis; the following Luenberger observer matrices L_{Cl_2} and L_{H_2} were determined with a process of trial and error and provided a smooth feedback:

$$L_{H_2} = \begin{bmatrix} 0.624 \\ 14.5 \\ -933 \\ 85264 \\ 87990 \\ 1673 \end{bmatrix} \qquad L_{Cl_2} = \begin{bmatrix} -5866 \\ -5911 \\ -185 \\ -286 \\ -375 \\ 30.7 \end{bmatrix} \tag{4-46}$$

4-5 Day-Ahead bidding phase

At 12:00 CET, the Day-Ahead bidding takes place. The hourly bids on the Day-Ahead market, $Q_{DA,bid}$[0.00:24.00] consist of the Day-Ahead forecast of renewable energy $Q_{DA,RE}$[0.00:24.00] and a correction term called $Q_{DA,stor}$[0.00:24.00]. $Q_{DA,stor}$ is an additional amount of energy bought/sold on the Day-Ahead market to keep the storage levels returning to 50%.

The correction term $Q_{DA,stor}$[0.00:24.00] is calculated as followed. At 12:00 CET, the deviation between the midway position and the last storage level prediction of the MPC L_{norm}[12.00+N] is used to calculate the amount of energy that needs to be bought/sold such that storage levels return to 50%, which is called $\Delta Q_{stor,tot}$. The calculation of $\Delta Q_{stor,tot}$ is described in Section A-5 in the Appendix. Then, a Day-Ahead optimization is performed to sell (or buy) this energy on the Day-Ahead market during times of high (or low) prices which provides $Q_{DA,stor}$[0.00:24.00]. If the energy is bought/sold, then $Q_{DA,stor}$[0.00:24.00] is subtracted from/add to the Day-Ahead forecasts, $Q_{DA,RE}$[0.00:24.00], to comprise the final Day-Ahead bids, $Q_{DA,bid}$[0.00:24.00]. The next two sections explain the Day-Ahead optimization. All variables and parameters of the Day-Ahead optimization can be found in Figure A-4 in the Appendix.

4-5-1 Objective function

If $\Delta Q_{stor,tot}$ is positive this means that the storage levels needs to be reduced, which can be achieved by selling $\Delta Q_{stor,tot}$ on the Day Ahead market. The objective of the Day-Ahead optimization then becomes a maximization function:

$$max \sum_{t=0}^{24} Q_{DA,stor}(t) \cdot Price_{DA}(t) \tag{4-47}$$

If $\Delta Q_{stor,tot}$ is negative, storage levels needs to be increased, which can be achieved by buying $\Delta Q_{stor,tot}$ on the Day-Ahead market. The objective of the Day-Ahead optimization then becomes a minimization function:

$$min \sum_{t=0}^{24} Q_{DA,stor}(t) \cdot Price_{DA}(t) \tag{4-48}$$

Day-Ahead prices of 2020 in Belgium are obtained from Elia, the Belgium Transmission System Operator [88]. Since the economic analysis is not a core part of this study, it is assumed that the Virtual Power Plant has a perfect forecast of the Day-Ahead energy prices.

4-5-2 Constraints

An equality constraint is implemented such that the sum of the energy bought/sold at each hour of the next day is equal to the total energy needed $\Delta Q_{stor,tot}$:

$$\sum_{t=0}^{24} Q_{DA,stor}(t) = \Delta Q_{stor,tot} \tag{4-49}$$

Constraints on the maximum energy bought/sold per hour are implemented to avoid that the industrial plants are required to operate far from their nominal energy consumption and theres is no regulation capacity available to correct the Day-Ahead forecast errors:

$$0 \leq Q_{DA,stor}(t) \leq Q_{max} \qquad \forall t = 0, 24 \tag{4-50}$$

To return both storage levels from the limit to the midway position 628.1 MWh is required, hence the maximum energy bought/sold should be at least 25.88 MWh per hour. In this thesis, Q_{max} is set at 31.44 MWh per hour which gives the Virtual Power Plant some more opportunity to buy/sell at low/high prices to make a profit from the correction method. Since the additional energy bought/sold will create artificial errors which compound on the regular Day-Ahead forecast errors, it is important that the industrial plants have enough regulation capacity to eliminate the sum of both errors. As will be discussed in Section 4-6-1, together the chlor-alkali and hydrogen plant have a regulation capacity of +21.75 MWh/ISP and -25.83 MWh/ISP. In Figure 4-11, it can be seen that even if this regulation capacity of the plants is reduced by Q_{max}, which is 7.86 MWh/ISP, the regulation capacity will remain sufficient for minimizing most of the Day-Ahead forecast errors.

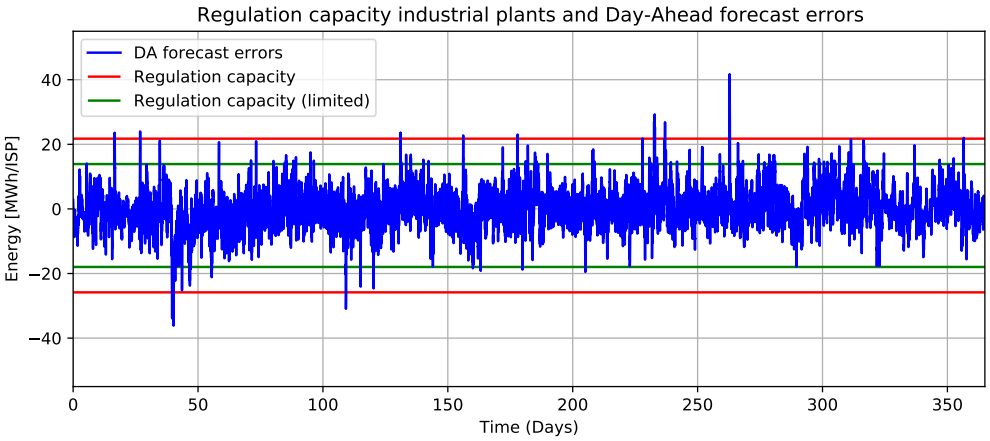

Figure 4-11: Regulation capacity industrial plants and annual Day-Ahead forecast errors

Finally after the Day-Ahead optimization, the Day-Ahead bids can be calculated using $Q_{DA,stor}[0.00{:}24.00]$. The Day-Ahead bids will be lowered with $Q_{DA,stor}$ if there was a storage deficit predicted and additional energy had to be bought in the Day-Ahead market:

$$Q_{DA,bid}(t) = Q_{DA,RE}(t) - Q_{DA,stor}(t) \qquad \forall t = 0, 24 \tag{4-51}$$

Day-Ahead bids will be increased with $Q_{DA,stor}$ if there was a surplus predicted and additional energy was sold in the Day-Ahead market:

$$Q_{DA,bid}(t) = Q_{DA,RE}(t) + Q_{DA,stor}(t) \qquad \forall t = 0, 24 \tag{4-52}$$

4-6 Simulation setup

This section describes the main parameters for the simulation of the base case and the sensitivity analysis. The simulations were performed on a MSI GP60 laptop with a Intel Core i5-4200 MHZ and 8 GB memory using the solver of Gurobi for Mixed Integer Linear Optimization problems (MILP).

4-6-1 Base-case

The main parameters for the Virtual Power Plant and MPC in the base-case are shown in Table 4-1. The time-steps of the Model Predictive Control unit are 15 minutes which is the length of an Imbalance Settlement Period and a prediction horizon of 3 hours is chosen similar to that in Ref. [100].

Parameters	Value
PV capacity	300 MW
Wind capacity	300 MW
Time-step Δt	15 min
Prediction horizon N	3 hours
Simulation period	1-30 October

Table 4-1: Virtual Power Plant and MPC parameters of base-case

The parameters of the chlor-alkali and hydrogen plant in the base-case are shown in Table 4-2. The chlor-alkali electrolysers can flexibly operate between a current density of 0.3-0.6 A/cm^2 in accordance with [22], and the hydrogen PEM electrolysers can flexibly vary the current density between 1-1.6 A/cm^2 which is well within the 0.6-2 A/cm^2 range of state-of-the-art PEM electrolysers [94]. This consequently results in an energy consumption range of 22.85-50.88 MWh/ISP and 28.8-48.35 MWh/ISP of the chlor-alkali and hydrogen plant respectively. In the base-case, it is assumed that there is no limit on the ramp frequency and there is 1 sub-group per plant. This means the 24 electrolysers in the chlor-alkali operate with the same current density and the same goes for the 24 electrolysers in the hydrogen plant. The utilization rate of the chlor-alkali plant is 80% following the average utilization rate of the chlor-alkali industry in 2020 [81]. This utilization rate has been applied to the hydrogen plant as well. This results in a nominal current density of 0.48 A/cm^2 and 1.28 A/cm^2 for the chlor-alkali and hydrogen plant respectively. The storage size is 6 hours of chlorine production at nominal production as in Ref. [22, 24] which has been implemented in the hydrogen plant as well.

Parameters	Chlor-Alkali plant (Nouryon)	Hydrogen plant (Shell)
N electrolysers	24 electrolysers	24 electrolysers
P rated	203.5 MW	193.4 MW
E range	22.85-50.88 MWh/ISP	28.8-48.35 MWh/ISP
j nominal	0.48 A/cm2	1.28 A/cm2
j range	0.3-0.6 A/cm2	1-1.6 A/cm2
Δj Ramp rate	0.075 A/cm2 p. electrolyser	∞ p. electrolyser
T electrolyser	85-90 °C	55-60 °C
Ramp frequency	Not restricted	Not restricted
Nr. of sub-groups	1 x 24 electrolysers	1 x 24 electrolysers
Utilization rate	80%	80%
Storage size	6 hr of nom production	6 hr of nom production
Storage bounds	20-80%	20-80%

Table 4-2: Plant parameters base-case

The base-case was simulated in October. Since the energy production and forecast errors change throughout the year, three other time-periods are simulated as well (January, April and July) to observe if there are significant differences in the performance.

Reference

The simulation results need to be compared to a reference in order to assess the ability to minimize imbalances. In the reference, the Virtual Power Plant does not apply industrial demand response to minimize imbalances, hence the plants will operate at their nominal consumption level and the imbalances will be exactly equal to the Day-Ahead forecast errors.

4-6-2 Sensitivity analysis

Next to the base-case, additional simulations will be performed using different values of parameters to assess their impact on ability of the chlor-alkali and hydrogen plant to minimize imbalances. The following parameters will be studied:

- Storage capacity - It is important to assess the effect of the storage size of the chlor-alkali and hydrogen plant as the storage size of Nouryon and Shell plant have been based on literature whereas the actual capacity could be different. To assess the effect of the storage capacity, simulations have been performed with the capacity of the chlor-alkali and hydrogen plant down-scaled to 3 hours of nominal consumption, as in [62], and up-scaled to 12 hours of nominal consumption as was assumed in [101].
- Utilization rates - Operating at utilization rates above 80% is common in the chemical industry in general and in the chlor-alkali industry specifically [16]. At higher utilization rates, the ability of industrial loads to increase load consumption above the nominal level will be impaired which can limit the minimization of positive imbalances. For this reason, simulations are performed with utilization rates of 85%, 90% and 95% for both the chlor-alkali and hydrogen plant.

- Day-Ahead bid correction - To generate the Day-Ahead bids, the Day-Ahead forecast of renewable energy has been decreased/increased with an energy quantity that guides the storage levels to the midway position as described in Section 4-5. In order to assess the effect of this method, a simulation is performed without the Day-Ahead bid correction.

- Prediction horizon - Increasing the prediction horizon length could improve the decision making of the MPC which can lead to lower imbalances, however it may also have limited to no effect other than increasing the computation time of the optimization. To assess the affect of prediction horizon length, two simulations are performed with a shorter prediction horizon (1.5 hour) and longer prediction horizon (6 hours).

- Imperfect forecast - In the base-case, it is assumed that the MPC has a perfect forecast of the actual power production of the renewable energy resources over the prediction horizon. Therefore, there are no errors assumed in the forecast of the imbalances. As a comparison, the impact of imperfect forecast on the MPC is assessed by using the approach of Ref. [102] to generate the imperfect forecast time series.

- Ramp frequency & Sub-groups - Reducing the ramp frequency of the electrolysers could reduce wear and tear cost and allow plant owners to choose how often the Virtual Power Plant can modulate their equipment. However, lowering the ramp frequency can also decrease the ability of the hydrogen and chlor-alkali plant to minimize imbalances, as the imbalances require a ramp at each time-step. To overcome this issue, the electrolysers in the industrial plants can be divided in sub-groups that can operate with a different power consumption, such as 1x24, 2x12, 3x8 electrolysers per plant. In total 9 simulations will be performed, in which ramping of electrolysers is allowed 12, 6, and 3 times per period of twelve time-steps. The amount of electrolyser sub-groups will be varied between 1, 2 and 3 in each plant.

4-6-3 Overview of simulation studies

An overview of the simulation studies performed in this thesis are shown in Table 4-3 with the parameters that will be varied. The remainder of the parameters of the simulations can be found in Table A-3 and Table A-4 in the Appendix. Note that the storage capacity is described in the amount of hours at the nominal production rate.

For the simulation studies with the varying ramp frequency limits and numbers of sub-groups, a single week in October has been simulated (9-16 October) rather than the whole month. The integration of the ramp frequency limit resulted in a higher computation time per time step due to the addition of binary variables, hence it was decided to reduce the simulation time-period to a week. The results of this section will therefore not be compared with the base-case, but these simulation results will be compared amongst each other. Finally, it is important to mention that the value noted in the ramp frequency column indicates the number of ramps that are allowed per 12 time-steps.

Simulation study	Storage capacities	Utilization rate	DA bid correction	Prediction horizon	Forecast accuracy	Ramp freq.	Sub-groups	Time period
Reference	-	-	-	-	-	-	-	1-30 Oct
Base-case	6 h	80%	Yes	12	Perfect	-	1	1-30 Oct
Time-period - Jan	6 h	80%	Yes	12	Perfect	-	1	1-30 Jan
Time-period - Apr	6 h	80%	Yes	12	Perfect	-	1	1-30 Apr
Time-period - July	6 h	80%	Yes	12	Perfect	-	1	1-30 July
Storage - low	3 h	80%	Yes	12	Perfect	-	1	1-30 Oct
Storage - high	12 h	80%	Yes	12	Perfect	-	1	1-30 Oct
Utilization rate # 1	6 h	85%	Yes	12	Perfect	-	1	1-30 Oct
Utilization rate # 2	6 h	90%	Yes	12	Perfect	-	1	1-30 Oct
Utilization rate # 3	6 h	95%	Yes	12	Perfect	-	1	1-30 Oct
Day-Ahead Bid correction - No	6 h	80%	No	12	Perfect	-	1	1-30 Oct
Prediction horizon - low	6 h	80%	Yes	6	Perfect	-	1	1-30 Oct
Prediction horizon - high	6 h	80%	Yes	24	Perfect	-	1	1-30 Oct
Forecast accuracy - imperfect	6 h	80%	Yes	12	Imperfect	-	1	1-30 Oct
Ramp freq. vs. sub-groups #1	6 h	80%	Yes	12	Perfect	12	1	9-16 Oct
Ramp freq. vs. sub-groups #2	6 h	80%	Yes	12	Perfect	12	2	9-16 Oct
Ramp freq. vs. sub-groups #3	6 h	80%	Yes	12	Perfect	12	3	9-16 Oct
Ramp freq. vs. sub-groups #4	6 h	80%	Yes	12	Perfect	6	1	9-16 Oct
Ramp freq. vs. sub-groups #5	6 h	80%	Yes	12	Perfect	6	2	9-16 Oct
Ramp freq. vs. sub-groups #6	6 h	80%	Yes	12	Perfect	6	3	9-16 Oct
Ramp freq. vs. sub-groups #7	6 h	80%	Yes	12	Perfect	3	1	9-16 Oct
Ramp freq. vs. sub-groups #8	6 h	80%	Yes	12	Perfect	3	2	9-16 Oct
Ramp freq. vs. sub-groups #9	6 h	80%	Yes	12	Perfect	3	3	9-16 Oct

Table 4-3: Overview of simulation studies performed in this thesis

Chapter 5

Results and Discussion

5-1 Reference imbalances

Figure 5-1 shows the Day-Ahead forecast errors in the month of October. The mean value of the Day-Ahead forecast errors is 3.98 MWh/ISP which indicates that the renewable energy production is generally under-predicted during the Day-Ahead bidding phase. Furthermore, the standard deviation is 5.08 MWh/ISP and the minimum and maximum Day-Ahead forecast error is -17.49 and 16.92 MWh/ISP.

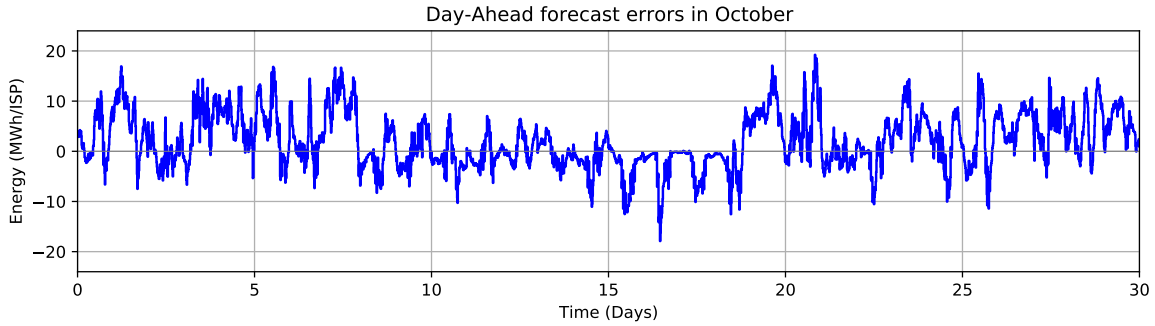

Figure 5-1: Day-Ahead forecast errors in October

In the reference no demand response is applied and the industrial plants operate at their nominal capacity. Hence the Day-Ahead forecast errors are not corrected and they will directly result in imbalances for the Virtual Power Plant. The imbalances are shown in Figure 5-2. The total amount of reference imbalances is 12947 MWh which consists of 3471 MWh negative and 9476 MWh positive imbalances. These reference imbalances provide a benchmark for assessing the ability of the industrial plants to minimize imbalances by providing demand response.

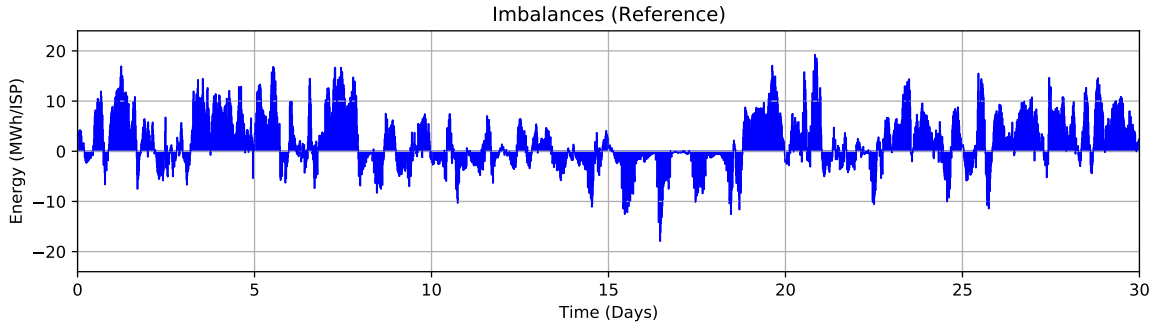

Figure 5-2: Reference imbalances in October

5-2 Base-case

In this section, first the operation of the MPC will be explained by zooming in on the simulation results of the first two days of October. Then, the amount of imbalances and the causes for the imbalances are described for the month of October, followed by a comparison to the imbalance minimization in the months of January, April and July.

5-2-1 Model Predictive Control operation

Figure 5-3 shows the error between the Day-Ahead bids and actual renewable energy production in the Virtual Power Plant Portfolio for the first two days of October. At each time-step, the MPC will forecast these errors after which it calculates the control inputs for the hydrogen and chlor-alkali electrolysers to minimize the errors. Note that the MPC is assumed to have a perfect forecast of these errors in the base-case and the results provide a maximum performance of the MPC. In the sensitivity analysis in Section 5-3, the perfect forecast results will be compared with simulations using an imperfect forecast.

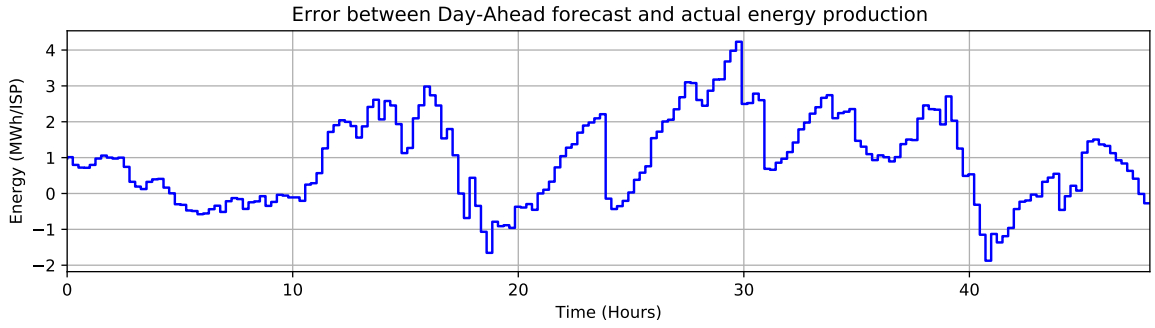

Figure 5-3: Error between Day-Ahead bids and actual renewable energy production first two days of October

In Figure 5-4 and 5-5 the energy consumption of the chlor-alkali and hydrogen plant are shown. The nominal energy consumption is indicated with the 'no demand response' line in red. For explaining the results, the term 'positive demand response' will be used to indicate

that the plants operate above the nominal consumption and 'negative demand response' indicates that the plants operate below the nominal consumption. It can be observed that the energy consumption of the plants follow the pattern of the errors between the Day-Ahead bids and actual renewable energy production that was shown in Figure 5-3. For example, during hours 12-17 the errors are positive which means that more energy is produced than the Day-Ahead bid. Therefore, the chlor-alkali and hydrogen plant are requested to increase their energy consumption above the nominal energy consumption (hence providing positive demand response) such that imbalances in the Virtual Power Plant are avoided.

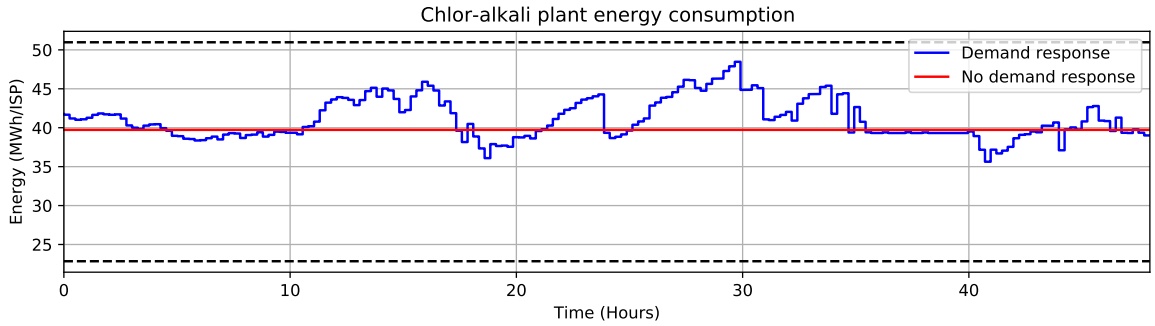

Figure 5-4: Chlor-Alkali plant energy consumption in the first two days of October

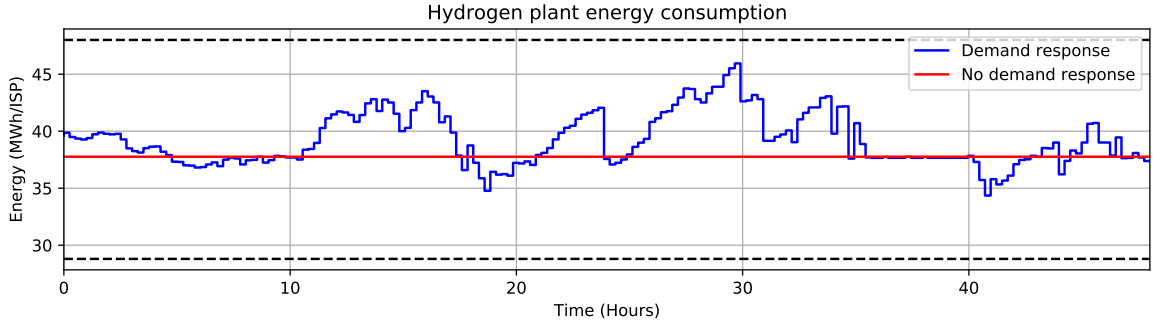

Figure 5-5: Hydrogen plant energy consumption in the first two days of October

Figure 5-6 shows the storage level for the first two days of October. It can be observed that the storage levels increase when the plants operate above their nominal energy consumption (for example between hours 12-17), and decrease when the plants operate below the nominal energy consumption (for example in hours 40-43). This is because when the plant operates at the nominal consumption the storage level remains constant since the production of chemicals equals the consumption of chemicals from the storages. The storage levels of the chlor-alkali and hydrogen plant almost completely overlap throughout the simulation which indicates that the penalty on the deviation between the storage levels is successfully implemented. On hours 35-40, the storage levels reach the maximum limit which means that the plants cannot operate above their nominal capacity during this time-period to provide positive demand response as can be seen in Figures 5-4 and 5-5. Hence, the positive errors during hours 35-40 that can shown in Figure 5-3 cannot be corrected and will cause imbalances in the Virtual Power Plant

portfolio. In Figure 5-7 the imbalances are shown that occur in the first two days of October. It can be observed that positive imbalances are indeed present when the storage levels are at their maximum.

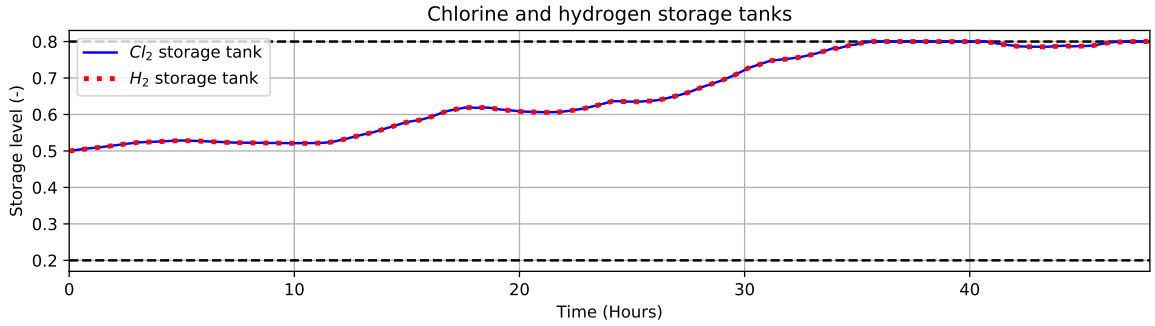

Figure 5-6: Storage level hydrogen and chlor-alkali plant in the first two days of October

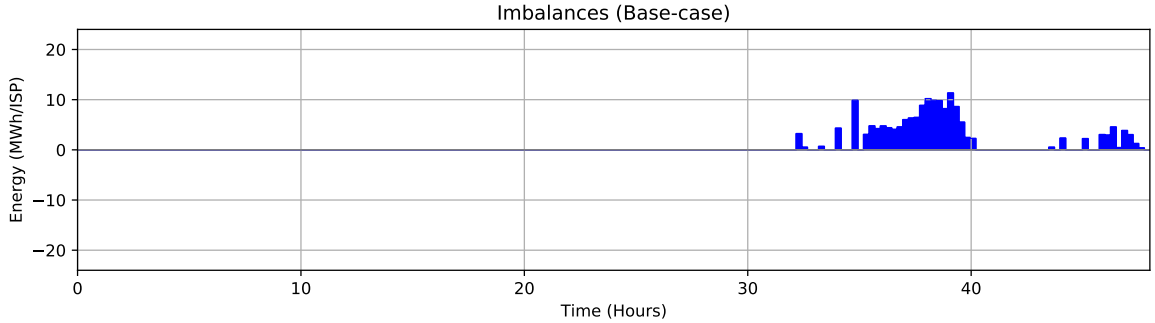

Figure 5-7: Remaining imbalances in the first two days of October

Finally, the effect of providing demand response on the production of chlorine and hydrogen can be seen in Figures 5-8 and 5-9. As can be seen the chlorine production and hydrogen production follow the shape of the power consumption shown in Figure 5-4 and 5-5 since the chemicals production via electrolysis is linearly related to the current density of the electrolysers through Faraday's law. The current density in its turn is approximately a linear function of power consumption as was established in Section 4-2-2. Furthermore, it can be noted that at the nominal production, which is equal to the nominal consumption shown in the Figure 5-8, around 18.32 kg/s of chlorine is produced. This corresponds to a production of 576 kt/year which is close to the annual production of the actual factory of Nouryon of 640 kt/year in 2016 [60]. The deviation can likely be explained by a slight difference in the nominal current density assumed in this thesis and used in the actual factory. The nominal hydrogen production in kg/s seems lower than that of chlorine, however when looking at this in mol/s, the hydrogen production is actually higher with 0.44 mol/s compared to that of chlorine of 0.25 mol/s.

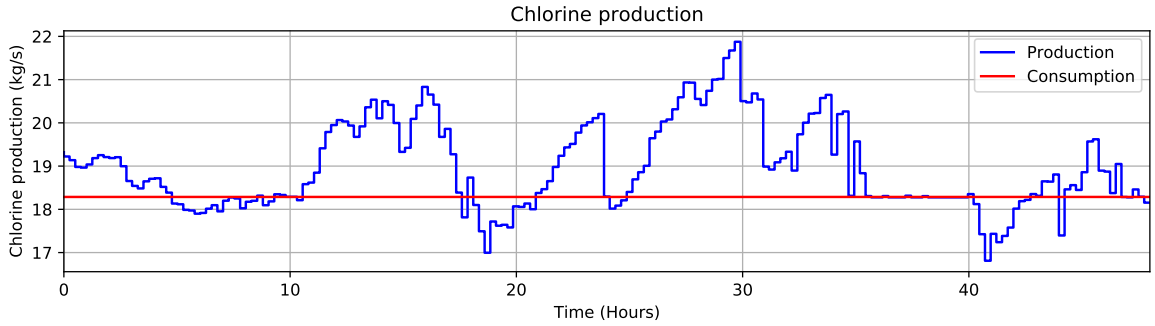

Figure 5-8: Chlorine production during the first two days of October

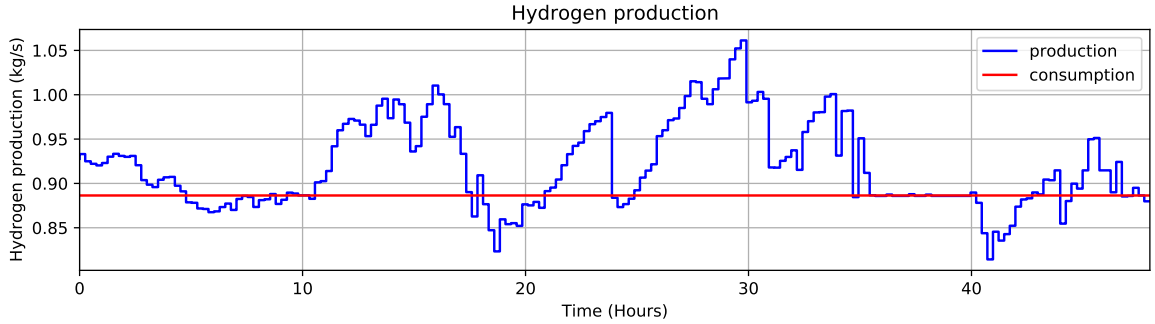

Figure 5-9: Hydrogen production during the first two days of October

Temperature & current density control

The purpose of the MPC is to control the electrolysers of the plants such that constraints on process variables are not violated. In Figure 5-10 the inputs inlet temperature and power to one of the chlor-alkali electrolysers in the plant are shown, as well as the output cell temperature predicted by the MPC and simulated by the plants. It can be seen that the MPC kan keep the cell temperature of the chlor-alkali electrolysers between 85-90 °C by varying the inlet temperature at different inputs of power consumption. The effect of increasing the power input on the electrolyser cell temperature can be observed between hours 26-29. During this period, power is increased whilst the inlet temperature remains constant which results in a rise in the cell temperature from 85.2 to nearly 87 °C. Increasing the inlet temperature on the other hand increases cooling of the electrolyser which can thereby lower the cell temperature. This cooling effect can be observed during hours 2-6, when the power consumption is decreased whereas inlet temperature is increased which leads to a constant cell temperature near 85 °C. It can be observed in the bottom graph of 5-10 that the plots of the cell temperature predicted by the MPC and simulated by the plants nearly overlap. Firstly, this results from the good agreement between the dynamic Hammerstein-Wiener model in the MPC and the simulators of the plant. Secondly, in each time step the Luenberger observer updates the states that describe cell temperature in MPC by using the simulated temperature as feedback. In Figure A-2 in the Appendix, it can be observed that the MPC could maintain the cell temperature in the range of 85-90 °C for the whole month of October by varying the inlet temperature

between 70-80 °C which is a normal operating range for industrial chlor-alkali electrolysers [80]. These results indicate that the developed MPC is suitable for rescheduling the chlor-alkali electrolysers while ensuring cell temperatures remain within bounds.

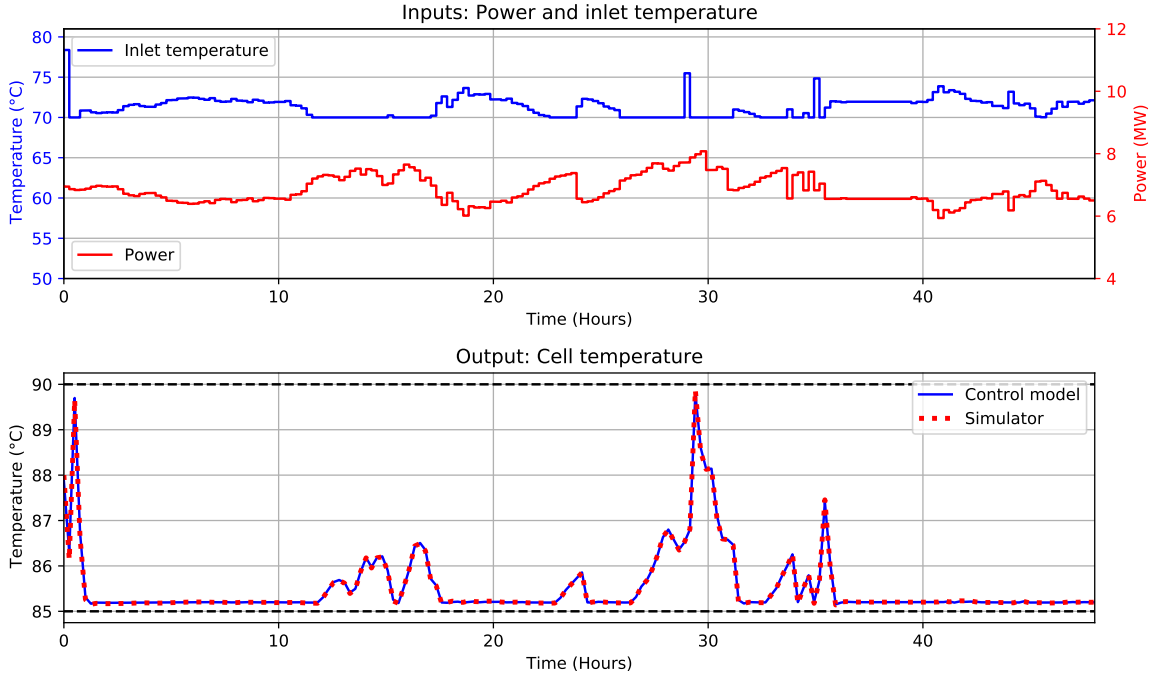

Figure 5-10: Inputs and output of a single chlor-alkali electrolyser in the first two days of October

In Figure 5-11, the inputs power and cooling load to a single hydrogen electrolyser is shown as well as the output cell temperature. To assess the ability of the MPC to keep an electrolyser at a constant operating temperature, rather than a range as shown in Figure 5-10, a cell temperature set point of 57.5 °C was introduced. In the top plot, it can be seen that the power and cooling load show similar shapes. This can be explained by the fact that increasing (or decreasing) power would result in a rise (or drop) in cell temperature, hence an increase (or decrease) in the cooling load would be necessary to maintain the cell at the desired operating temperature. In the bottom graph, it can be shown that the temperature predicted by the Hammerstein-Wiener model in the MPC and simulated by the plants have a good agreement. This again results from the fit between the Hammerstein-Wiener model that was identified and the high-fidelity OpenModelica model as well as the operation of the Luenberger observer that can integrate the simulated temperature as feedback to update the internal states of the MPC. In Figure A-3 in the Appendix, it can be observed that the MPC can maintain the operating temperature of an electrolyser near 57.5 °C for the whole simulation period by controlling the cooling input to the electrolyser.

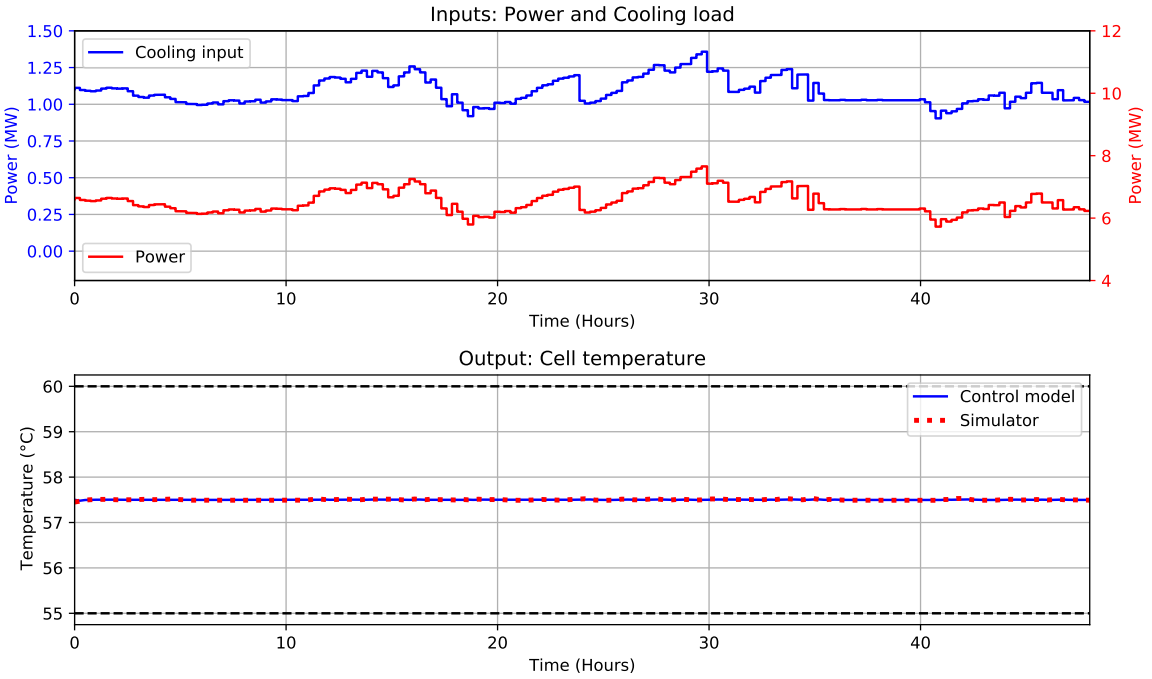

Figure 5-11: Inputs and output of a single hydrogen electrolyser in the first two days of October

Another requirement is that the current density of the electrolysers remain within the bounds. Although the current density is affected by both the power consumption and cell temperature of the electrolyser, it was shown in Section 4-2-2 that within the tight temperature operating range of the electrolysers, a linear approximation based on only the power input could be sufficient for the control model. Figure 5-12 shows the current density predicted by the MPC and simulated by the plants of a single chlor-alkali and hydrogen electrolyser. The graphs show that the linear approximation of the control model is in close agreement with the simulators. Furthermore, in Figure A-4 in the Appendix it is shown that the current density remains within the respective bounds of 0.3-0.6 A/cm2 and 1.0-1.6 A/cm2 of the chlor-alkali and hydrogen electrolyser during the whole month of October. It should be noted that the linear approximations are suitable for describing the current density in the control model in the operating cell temperature of 85-90 °C for the chlor-alkali electrolyser and 55-60 °C for the hydrogen electrolyser. However, when the temperature would be allowed to vary more widely, the electrolyser temperature will affect the voltage more significantly and thereby the current density. The consequential reduction in the control model accuracy can be solved by replacing the linear approximation with a Hammerstein-Wiener model using both power and cell temperature as inputs and the current density as the output, as was shown in Ref. [24].

Although the use of Hammerstein-Wiener models has shown suitable for describing nonlinear process dynamics, there are also challenges with the application of Hammerstein-Wiener models. Firstly, the Hammerstein-Wiener model is a generally a black-box model in which the inner variables and equations have no physical representation. For Virtual Power Plant operators this can make it more difficult to localize problems with the control model or establish the causes for infeasible solutions [103]. On the other hand, Hammerstein-Wiener

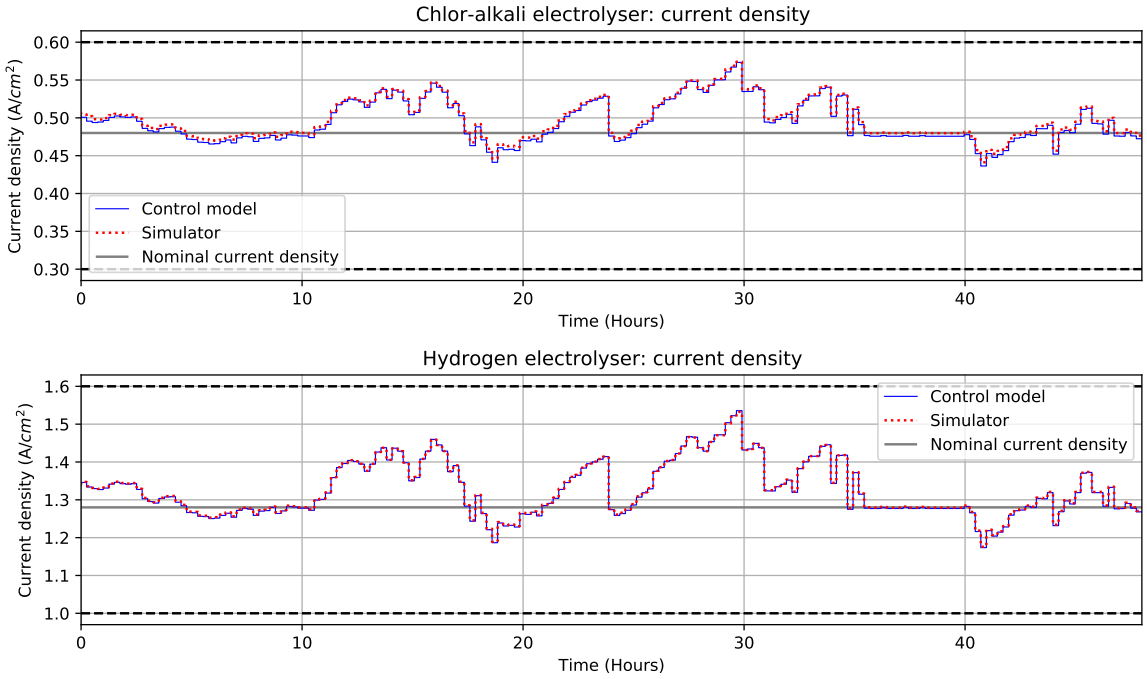

Figure 5-12: Current density of a single chlor-alkali and hydrogen electrolyser in the first two days of October

models can be used as a grey-box model that captures actual physical phenomena in the non-linear and linear blocks thereby increasing the physical meaning of the model [104]. Secondly, the Hammerstein-Wiener models are developed for a specific operating region and should be updated regularly to take into account changes in the behaviour of the plant, such as a degradation of the plant performance or a change of operating conditions. This can be solved by using MPC structures that continuously update the control model based on plant measurements (adaptive MPC) [105] and applying MPC approaches that switch between control models depending on the operating region (gain-scheduled MPC) [106].

5-2-2 Imbalance minimization

Figure 5-13 shows the imbalances remaining after the simulation of the base-case for a time-period of 30 days in October. In total there are 1277 MWh imbalances remaining in the base-case of which 1277 MWh are positive imbalances and 0 MWh are negative imbalances. This is a significant reduction of -90.1% compared to the reference imbalances of 12947 MWh that are shown Figure 5-13 .

The cause for the imbalances can be revealed by looking the storage level of the hydrogen and chlor-alkali plant in Figure 5-14. The time-periods at which the imbalances occur coincide with the periods at which the storage levels reach the maximum limit. When the storage levels have reached their maximum limit, the plants cannot operate above their nominal capacity to provide positive demand response and thereby minimize the positive errors. Another cause for imbalances could be the limited regulation capacity of the plants, which refers to the minimum

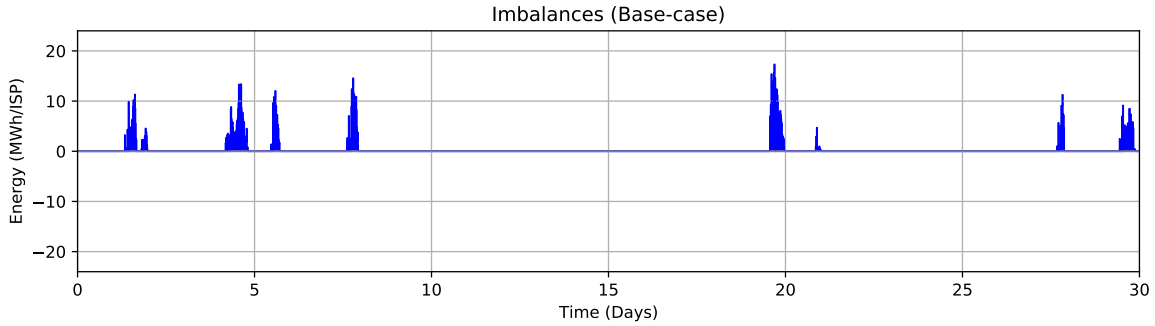

Figure 5-13: Imbalances in the base-case during October

and maximum demand response that the plants can provide, expressed in MWh/ISP. In Figure 5-15, the sum of the energy consumption of the chlor-alkali and hydrogen plant is shown over the simulation period. It can be seen that the plants did not have to operate at their minimum/maximum energy consumption, and hence the regulation capacity limits are not a cause for the imbalances during the simulation period. Also, limits on the ramp-up/down rate of the electrolysers could be a source of imbalances. During the simulation, the maximum ramp that was required to minimize an imbalance was 9.69 MWh/ISP which is well within the ramp rate ability of both plants combined which is -/+ 34.6 MWh/ISP. This high ramp rate is made possible predominantly by the hydrogen plant with the PEM electrolysers, which is capable of ramping down/up with -/+ 27.65 MWh/ISP, whereas the chlor-alkali plant can reach ramp with -/+ 6.91 MWh/ISP. If the ramp rate would form the only limiting factor, the renewable energy portfolio could be increased over 3 times the current capacity (34.6 / 9.69 $>$ 3) before the ramp-rate starts to become a limiting factor. However in practise, such an upscale will result in a high amount of imbalances firstly due to the limited storage and secondly due to the limit on the regulation capacity.

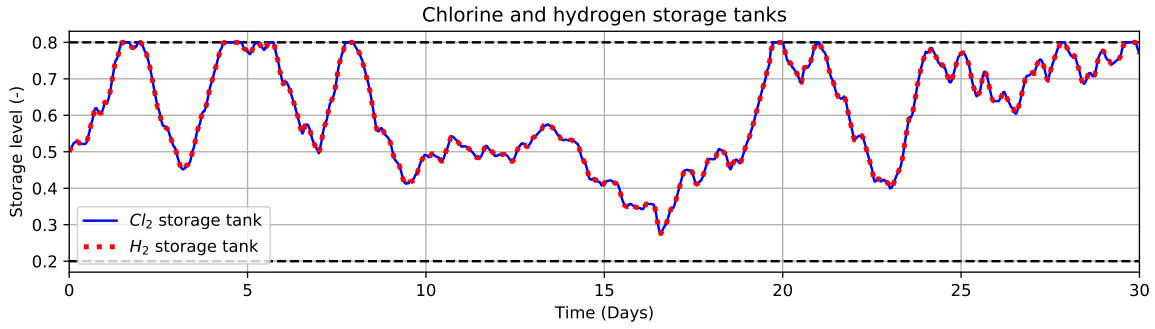

Figure 5-14: Chlor-alkali and hydrogen storage level in base-case during October

From these results, it can be seen that applying industrial demand response can reduce imbalances significantly compared to the reference in which demand response is not used to correct imbalances (-90.1%). The imbalances can be explained by the limited storage capacity of the industrial plants. The regulation capacity of the plants on the other hand is sufficient as maximum and minimum energy consumption limits are not reached. Finally, the ramp-rate does not impact the imbalance minimization by the chlor-alkali and hydrogen production

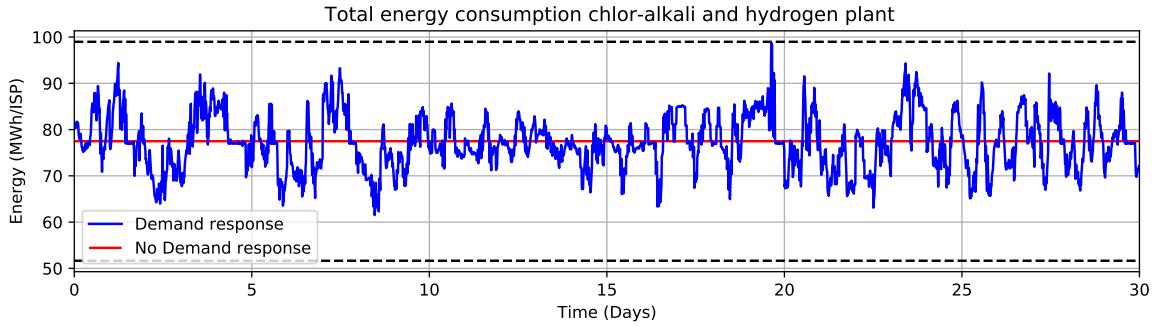

Figure 5-15: Total energy consumption of hydrogen and chlor-alkali plants in base-case during October

process since the ramping capability of the plants exceeds the maximum demand response ramp required.

As a final remark, in this thesis a lower limit of 1 A/cm^2 was assumed for the hydrogen electrolysers, whereas literature indicates that the lower limit of PEM electrolysis could also be lower such as 0.6 A/cm^2 for example [94]. In the base-case simulation study, the assumption of either 0.6 or 1 A/cm^2 would not have affected the imbalance minimization results since the lower energy consumption limit and therefore the lower current density limit of 1 A/cm^2 is never required to minimize negative imbalances, as is also visible in Figure 5-15. However, if a minimum current density of 0.6 A/cm^2 had been implemented, it would have increased the load shedding capability of the hydrogen plant which would be visible by a large regulation capacity in Figure 5-15. This would have highlighted that a significant amount of load shedding capability would remain mostly unused by the Virtual Power Plant since already at 1 A/cm^2 the ability to minimize negative imbalances is sufficient. This feature could be addressed in more detail in future studies, which could include an analysis to determine if the hydrogen plant can participate in load shedding regimes next to the minimization of imbalances for the Virtual Power Plant.

Comparison with different time-periods

To observe how the MPC performs at different time-periods than October, performance in the months of January, April and July have also been simulated. Figure 5-16 and Table 5-1 shows the simulation results of each month. As mentioned, the reference refers to the imbalances that would occur if the Virtual Power Plant does not use demand response to correct the Day-Ahead forecast errors. It can be observed that the minimization of imbalances using the MPC is fairly similar and the reduction is within the range of -89.5 to -99.3%, being lowest in July and highest in January.

Month	**January**	**April**	**July**	**October (base-case)**
Reference	9809 MWh	9301 MWh	10240 MWh	129747 MWh
Imbalances remaining	65 MWh	311 MWh	1077 MWh	1277 MWh
Reduction	-99.3%	-96.7%	-89.5%	-90.1%

Table 5-1: Imbalance minimization in several months of 2020

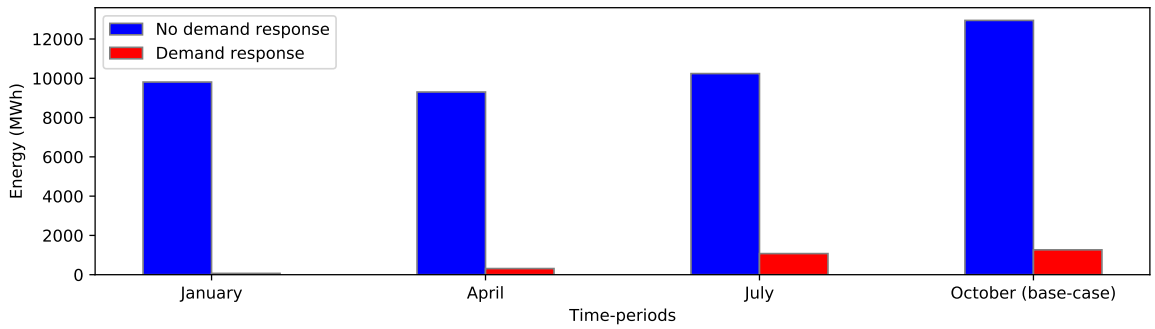

Figure 5-16: Simulation of different months in the year

The reason for the limited remaining imbalances during January is the fact that storage limits were reached only once whilst the regulation capacity of the industrial plants was sufficient throughout the simulation. In April, imbalances resulted from a period of highly negative forecast errors which caused the industrial plants to reach their lowest energy consumption point and to operate at the lower storage level for a period of time. Finally in July, there were multiple time periods in which the storage limits were reached resulting in an inability to minimize imbalances.

Computation-time

The computation time of the MPC is very suitable for minimizing imbalances as on average less than 0.25 seconds was necessary for an optimization with 12 time-steps which is well within the 15 minutes of an ISP. The fast computation time can be attributed to the limited number of time-steps and the removal of most binary variables from the optimization as described in Section 4-2-2. Eventually only 2 constraints with binary variables were necessary in the optimization, whereas all other constraints were linear. The fast computational performance shows that the MPC in this thesis is tractable and scale-able, i.e. could be extended with additional components such as flexible loads and storage units, while it is still able to describe nonlinear process dynamics. Given the fast computational performance future studies could consider reformulating the MPC to include stochastic or robust optimization thereby incorporating the effect of uncertainty in the renewable energy production.

5-3 Sensitivity Analysis

5-3-1 Storage capacity

To observe the effect of the storage capacity on the imbalance minimization, simulation studies have been performed with half the size and double the size of the hydrogen/chlorine storage. The imbalances at the different storage capacities are shown in Figure 5-17. Reducing the storage capacity to 3 hours of nominal production leads to 4149 MWh imbalances which is an increase of 225% compared to the base-case. Note that the imbalances in the base-case amount to 1277 MWh. On the other hand, raising the storage capacity to 12 hours of

nominal production results in 18 MWh imbalances which is a reduction of -99% compared to the base-case.

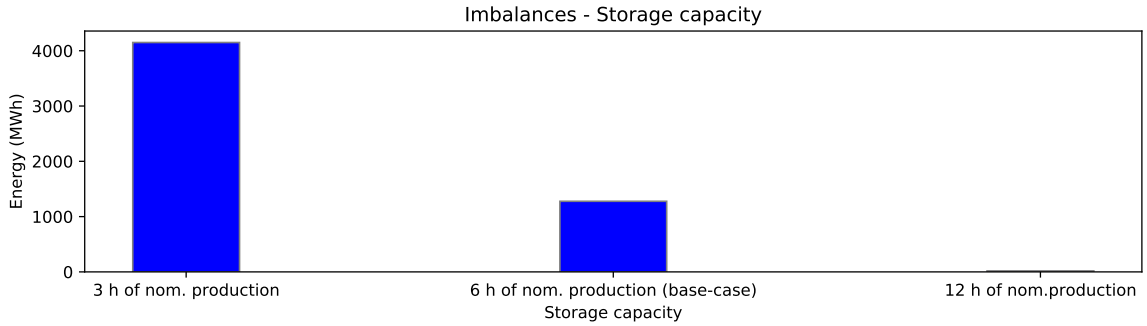

Figure 5-17: Imbalances at with different storage levels

The reasons for the large effect of the storage capacity on the imbalance minimization can be explained with Figures 5-18 and 5-19. As can be seen in Figure 5-18, the limits of the storage at a capacity of 3 hours of nominal production are frequently reached and during these periods demand response cannot be provided, hence resulting in a higher amount of imbalances than in the base-case. In Figure 5-19, on the other hand, it can be observed that at a capacity of 12 hours of nominal production the storage level limits are never reached. In this case, the capability to provide demand response is no longer impeded by the storage level limits and the imbalances can be eliminated almost completely.

It should be noted that during the simulation with the storage size doubled, the amount of energy that could be bought per hour on the Day-Ahead market was also increased to 62.88 MWh/hour (which is 15.72 MWh/ISP) such that always enough energy could be bought to return the storage levels to the midway level even if the storage limit was reached. However, the artificial forecast errors of 15.72 MWh/ISP will compound on the regular Day-Ahead forecast potentially leading to imbalances. Upon checking, the regulation capacity of the industrial plants was reached several times in this simulation period, however this only lead to a very limited amount of additional imbalances of 18 MWh.

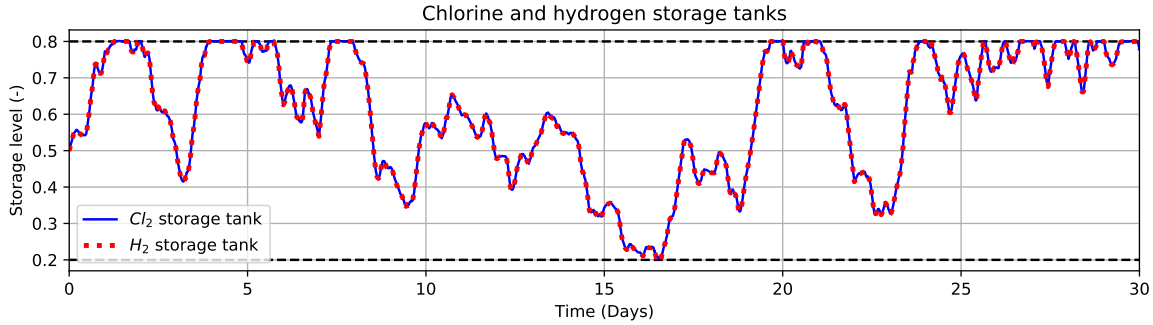

Figure 5-18: Storage levels at capacity of 3 h. of nominal consumption

Based on the results it can be shown that the ability to minimize imbalances is strongly dependent on the storage capacity of the chlor-alkali and hydrogen plant. At half the storage

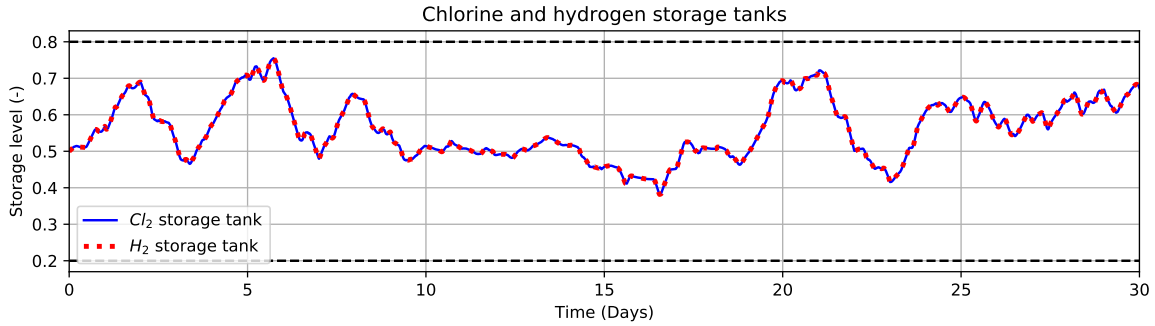

Figure 5-19: Storage levels at capacity of 12 h. of nominal consumption

capacity, the storage level limits are more frequently reached resulting in a higher amount of imbalances (4149 MWh) than the base-case (1277 MWh), whereas at double the storage capacity imbalances can be almost eliminated (18 MWh).

5-3-2 Utilization rate

Since chemical plants often operate with higher utilization rates than the 80% assumed in the base-case [16], the imbalance minimization has also been simulated at utilization rates of 85%, 90% and 95%. Figure 5-20 shows the imbalances at the different utilization rates. The effect of the utilization rate is limited at 85% and 90% as the imbalances are 1150 MWh and 1121 MWh respectively which is close to the imbalance minimization at 80%. However, a significant increase in imbalances can be observed at 95% to 2891 MWh (+126%).

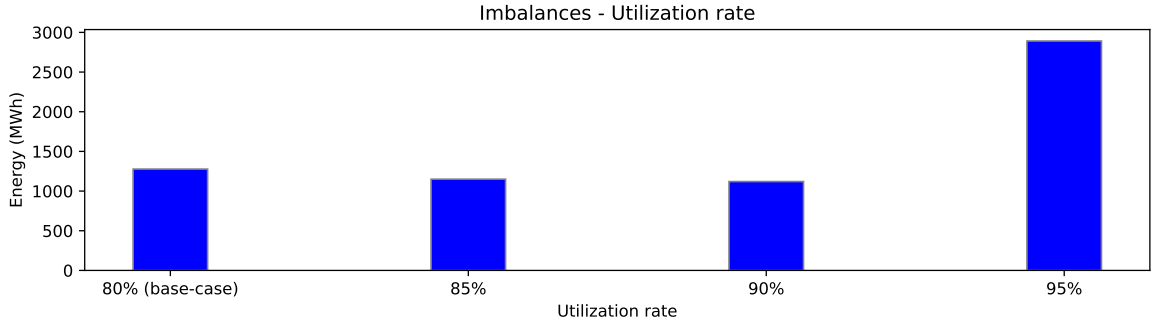

Figure 5-20: Imbalances at different utilization rates

The increase of imbalances at 95% can be explained with Figures 5-21 and 5-22. The figures show the error between the Day-Ahead bids and actual renewable energy production that needs to be eliminated by applying demand response (blue line) and the minimum/maximum demand response that the plants can provide per ISP, known as the regulation capacity (dashed black line). By increasing the utilization rate from 80% to 95% the demand response that can be provided by increasing the energy production above the nominal decreases from -21.75 MWh/ISP (top dashed black lines in Figure 5-21) to 5.37 MWh/ISP (top dashed black lines in Figure 5-22). The positive errors exceed the maximum of 5.37 MWh/ISP more

frequently than -21.75 MWh/ISP. Hence, at 95% the plants often cannot sufficiently increase their energy consumption above the nominal consumption to minimize the errors.

Being able to vary the utilization rate between 80-90% without impacting the imbalances raises the question whether the renewable energy portfolio is sized too small compared to the size of the industrial plants. However, with the current renewable energy portfolio size, the storage capacity is already the main limiting factor and it would restricts further up-sizing. It can also be noted in Figure 5-22 that at the utilization rate of 95% the demand response energy quantity that can be provided by load shedding remains largely unused. This unused potential would increase even further if the PEM electrolysers of the hydrogen plant could operate as low as 0.6 A/cm^2 rather than the 1 A/cm^2 assumed in this study. As mentioned, it would be interesting for future studies to assess whether this load shedding potential can be offered in additional energy markets, without impacting the ability to minimize imbalances in the Virtual Power Plant.

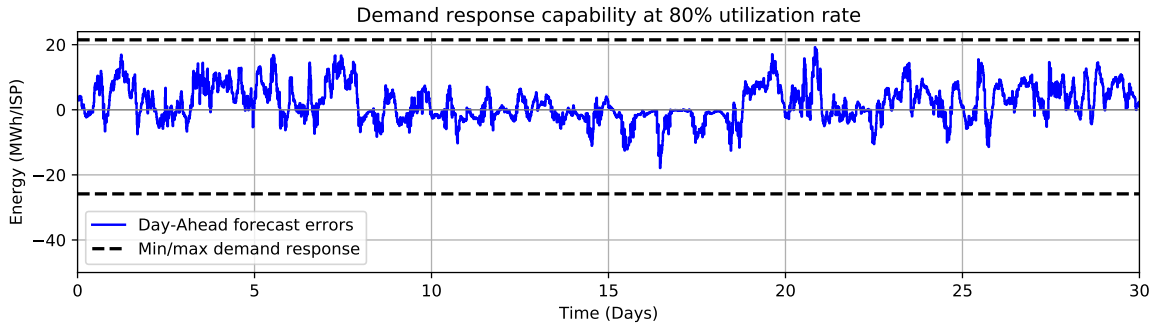

Figure 5-21: Day-Ahead errors and demand response capability of plants at 80% utilization rate

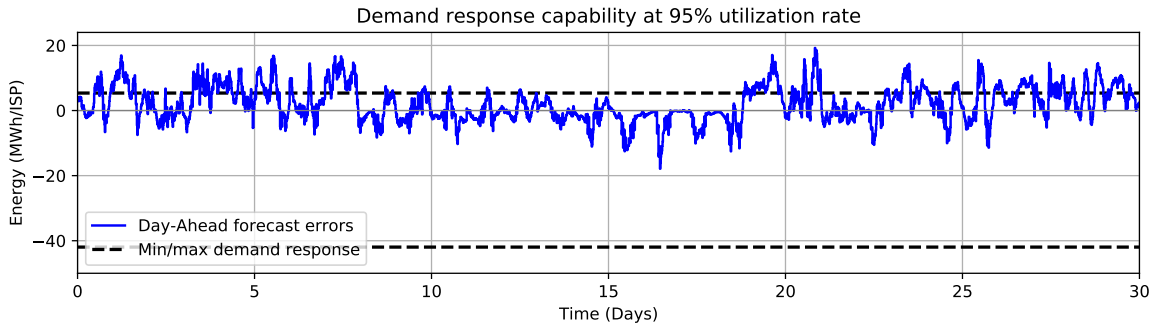

Figure 5-22: Day-Ahead errors and demand response capability of plants at 95 % utilization rate

Based on these results, it can be argued that the chemical plants could be operated at utilization rates between 80-90% without significantly impacting the ability to minimize imbalances. However at 95% the utilization rate becomes an significant impairment to minimize imbalances.

5-3-3 Day-Ahead bid correction

A simulation was performed without the Day-Ahead bid correction described in Section 4-5 and it was compared to the base-case simulation (see Figure 5-23). Without the Day-Ahead correction the amount of imbalances is 6643 MWh which is an increase of 420% compared to the base-case (1277 MWh) and a decrease of -49% compared to the reference imbalances (12947 MWh). The reason for the higher number of imbalances without the Day-Ahead correction is because the storage limits are reached more frequently due to prolonged periods of positive or negative Day-Ahead forecast errors. This can be observed in Figure 5-24 which presents the Day-Ahead bids and the average storage level for the first 7 days of October with (red line) and without the bid correction (blue line). The green dots in the bottom plot indicate the moments in time the Day Ahead ahead bidding is performed and therefore when the MPC is providing the last storage level prediction of t = 12:00+N to determine how much energy needs to be bought/sold in the Day-Ahead market.

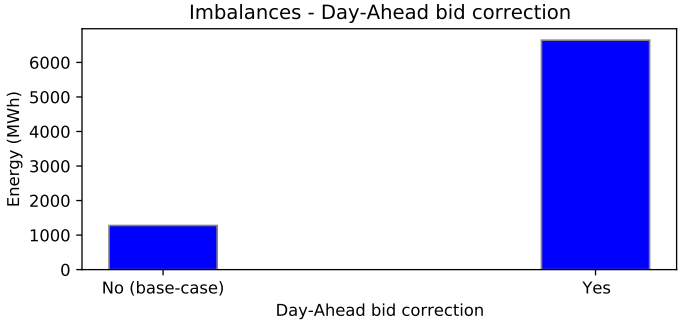

Figure 5-23: Day-Ahead bids with and without correction for the storage level

The effect of the Day-Ahead correction on the storage level can be seen most clearly between Day 1-3. On Day 1-2, the storage level (red line) reaches the maximum limit and to sell this abundance of hydrogen/chlorine and reduce the storage levels, the Day-Ahead bids on Day 2-3 are therefore significantly increased. By increasing the Day-Ahead bids, the chlor-alkali and hydrogen plant need shed more load on Day 2-3 which results in a steeper drop of the storage levels towards the midway position. Without the correction (blue line), however, the storage level remains close to the maximum limit which reduces the ability of the plants to provide demand response and minimize positive imbalances.

The benefit of the Day-Ahead bid correction is the ability to sell a surplus of chemicals on the Day-Ahead market at hours of high prices or replenish the chemicals at hours with low prices during a deficit. In addition, the storage tanks are continuously guided towards the midway position and the plants maintain the ability to provide demand response to minimize imbalances. There are also some challenges with the Day-Ahead bid correction. Firstly, the last storage level prediction is of t = 12:00 + N which is multiple hours before the actual energy exchange on the Day-Ahead market starts and in the meantime the storage tanks may have changed considerably. This can lead to an over/underestimation of the energy that needs to be bought/sold in order return the storage tanks back to 50%. The problem would be corrected by increasing the prediction horizon of the MPC at t = 12.00 up to 12 hours ahead, however it should be studied whether the accuracy of the storage level prediction this

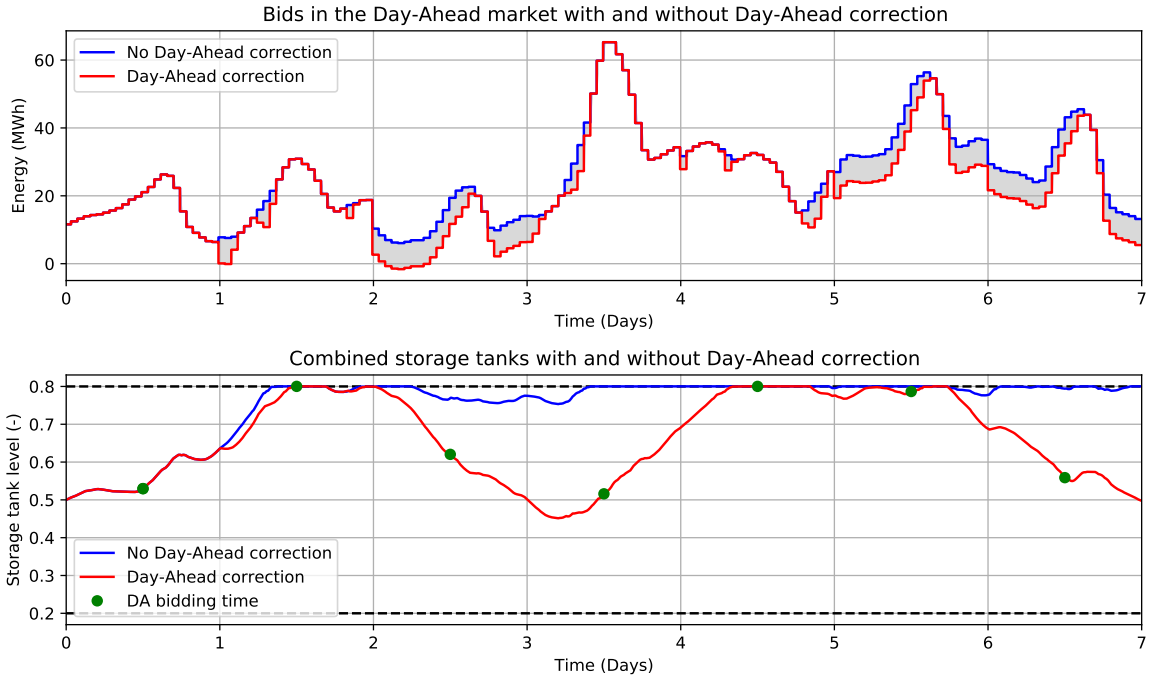

Figure 5-24: Day-Ahead bids with and without correction for the storage level

far ahead would remain accurate. Secondly, by placing bids that deviate from the Day-Ahead forecast of renewable energy, this method introduces artificial forecast errors. These artificial errors compound on the Day-Ahead forecast errors and require sufficient regulation capacity of the plants to the minimize both the Day-ahead forecast and artificial error. This method is therefore particularly useful for industrial processes that have abundant regulation capacity, but are limited by other parameters (i.e. storage, ramp-rate), such as the hydrogen and chlor-alkali plant in this thesis. In addition, future work could focus on optimizing the constraint of the maximum energy bought/sold per hour in the Day-Ahead market based on the regulation capacity of the plants which can enhance the financial benefits of this method. Thirdly, the storage level correction may act too late if for instance the additional energy is sold/bought mostly, or in part, by the end of the next day rather than at the beginning. One of the solutions here could be to investigate the use of the intraday market in the optimization to partially buy/sell the energy on the same day rather than on the next day.

5-3-4 Prediction horizon MPC

The prediction horizon determines how far in the future imbalances can be predicted by the MPC. In this thesis, the effect of the prediction horizon on the imbalance minimization has been assessed by comparing the horizon of 3 hours (base-case) to 1.5 hours and 6 hours. Figure 5-26 shows the imbalances at different prediction horizons. As can be seen, increasing the prediction horizon has reduced the amount of imbalances compared to the base-case namely at 1.5 h the imbalances are 1538 MWh (+20%) whereas at 6 h the imbalances are 1070 MWh (-16%). The reason for the reducing trend of imbalances with a growing prediction horizon is the more accurate forecast of the amount of energy that needs to be bought/sold on the

Day-Ahead market to return the storages to the midway level. With a longer prediction horizon, the storage level prediction at 12:00 CET, $L_{norm}[t = 12.00 + N]$, is closer to the actual storage level at 0:00 AM of the next day. This means a more accurate amount of energy will be bought/sold in the Day-Ahead market.

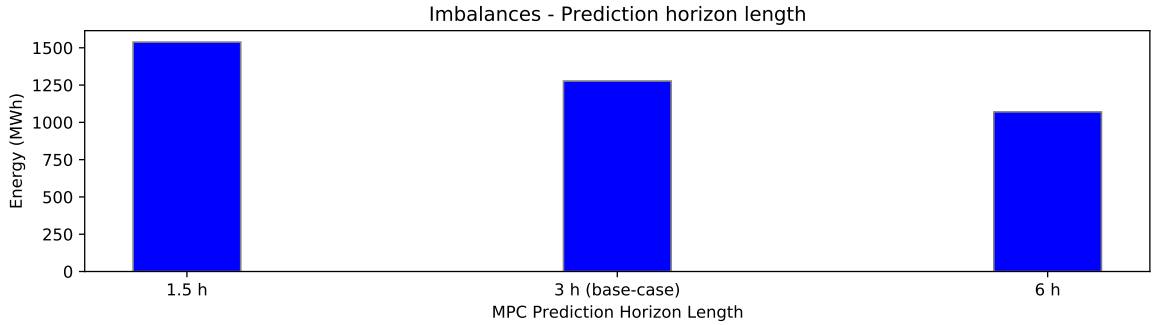

Figure 5-25: Effect of prediction horizon length on the minimization of imbalances

However, varying the prediction horizon does not affect the imbalance minimization performance of the MPC during the intraday redispatch phase. This can be shown by simulating the month of October without the Day-Ahead correction 5-3-3 such that the errors between the Day-Ahead bids and the actual renewable energy production are exactly the same in each of the simulations. In Figure 5-26, it can be seen that the ability of the MPC to minimize imbalances is not affected by varying the prediction horizon and all imbalances are equal to 6643 MWh. The fact the MPC performance is the same, independent of the prediction horizon length was also described in Ref. [107] and can be explained by the high ramp rate ability of the plants. The maximum ramp rate required to minimize an imbalance during the simulation is 9.69 MWh/ISP which is well within the ramping ability of the chlor-alkali and hydrogen plant of -/+34.6 MWh/ISP, as mentioned in Section 5-2-2. With this ramp rate, the plants can reach a desired energy consumption set-point within one time step and thus only an accurate one step ahead prediction is important. As indicated in Ref. [107], reducing the ramp-rate of the plants would eventually make the prediction horizon length a factor of importance. Yet, the aim of this thesis is to implement realistic parameters for the industrial processes involved and the reduction of the ramp-rates would yield an unrealistic chlor-alkali and hydrogen plant operation. The prediction horizon would also become important if the MPC is used for economic objectives (Economic MPC) rather than minimizing imbalance volumes. For example, if the goal is to minimize operational cost of the plants and they are exposed to time-varying prices such as in Ref. [23], it is important to be able to predict prices further into the future such that the MPC can make more informed decisions on when to buy/sell energy. However, this study is a technical analysis and therefore including economic factors in the MPC such as predictions of balancing prices is outside of its scope.

These results show that the prediction horizon length does not affect the performance of the MPC to minimize imbalances. However, increasing the prediction horizon does allow more accurate buying/selling of energy on the Day-Ahead market to return the storage levels to the midway level. This lowers the imbalances as the amount of times that the storage levels operates at the limits is reduced. It is noteworthy that despite the fact that the prediction horizon does not affect the performance of the MPC, the application of the MPC

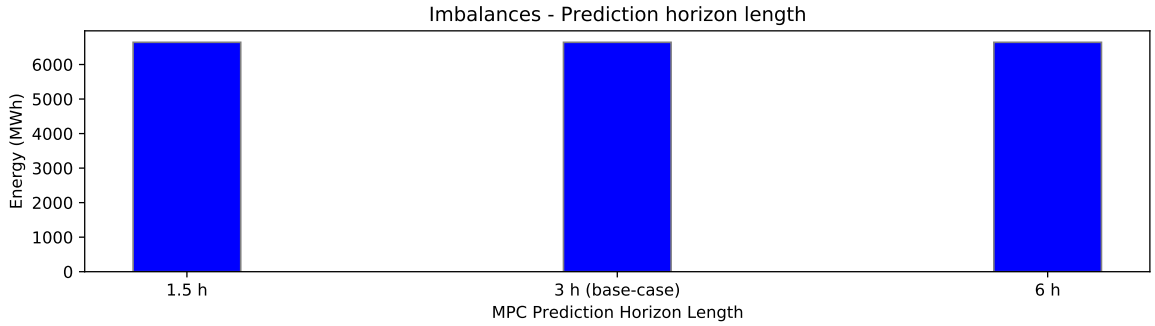

Figure 5-26: Minimization of imbalances without Day-Ahead correction

remains important even at a prediction horizon of one time-step. The point is that the MPC integrates a dynamic model of the cell temperatures amongst other and which ensures that the rescheduling of the electrolysers while ensuring that temperature bounds are not violated.

5-3-5 Imperfect forecast MPC

In the base-case, the forecast of the MPC on the actual renewable energy production was considered perfect, hence the MPC could also perfectly forecast the imbalances. In reality, the actual renewable energy forecast will be affected by uncertainty and hence the imbalance prediction will also be imperfect. To assess the effect of the forecast accuracy, a simulation with an imperfect forecast of the MPC is performed using the approach of [102]. In this approach, the forecast of the actual renewable energy production by the MPC progressively degrades over the prediction horizon and it gets closer to the Day-Ahead forecast.

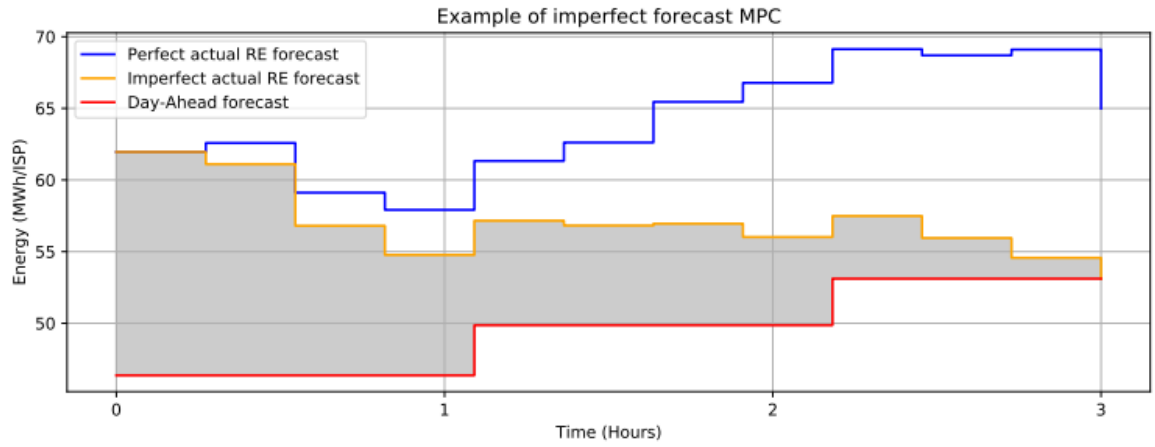

Figure 5-27: Imperfect forecast of actual renewable energy production by MPC

Figure 5-27 shows an example of the perfect and imperfect forecast of the MPC using this approach. It can be seen that the imperfect forecast of the MPC accurately predicts the actual renewable energy at t = 0, however it deteriorates along the prediction horizon until it becomes equal to the Day-Ahead forecast at t = 3 hours. The grey area shows the Day-Ahead

forecast errors, which are correctly predicted by the MPC at t = 0 yet increasingly become less accurate along the prediction horizon. This approach takes into account the fact that the MPC forecasts are more accurate at the beginning of the prediction horizon compared to the end.

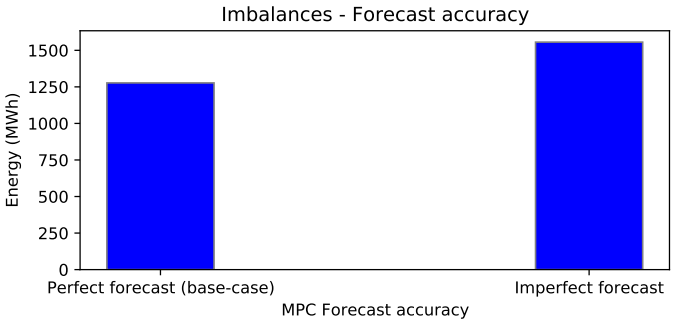

Figure 5-28: Imbalances with perfect and imperfect forecast

The simulation results of the imperfect forecast are compared with the base-case in which a perfect forecast was assumed (see Figure 5-28). As can be seen the imbalances with the imperfect forecast are higher compared to the perfect forecast, namely they are 1556 MWh which is an increase of +22% compared to the base-case of 1277 MWh. This can be explained similarly to the previous section on prediction horizon length. During the Day-Ahead bidding phase, the storage prediction by the MPC during the Day-Ahead bidding phase, L_{norm}[12.00:N], is less accurate when using the imperfect forecast compared to the perfect forecast. Therefore, the amount of energy that is bought on the Day-Ahead market to return the storage tanks back to the midway level is also less accurate and the storage levels will operate more frequently at the boundaries.

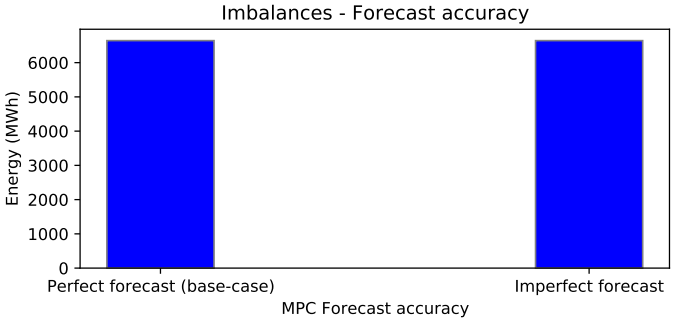

Figure 5-29: Imbalances using perfect and imperfect forecast without the Day-Ahead storage correction

As in the previous section on the prediction horizon length, additional simulations were performed in which the Day-Ahead correction for the storage levels was omitted. The results are shown in Figure 5-29 and indicate that the perfect and imperfect forecast both yield the same amount of imbalances, namely 6643 MWh. The imperfect forecast does not affect the imbalance minimization of the MPC due to the high ramp rate of the chlor-alkali and hydrogen plants. As long as the imbalance forecast of the first time-step is correct, which is assumed

to be the case following the approach of [102], the predictions after the first time-step do not affect the minimization of imbalances.

5-3-6 Ramp frequency & Number of sub-groups

In the base-case scenario, it was assumed the chlor-alkali and hydrogen electrolysers could change energy consumption every time-step. However, frequent modulation of electrolysers may result in unwanted wear/tear cost and, furthermore, industrial plant operators may wish to negotiate with the Virtual Power Plant operator how often their equipment can be modulated. To study the effect of reducing the number of ramps, a limit on the ramping frequency was set to 12, 6 and 3 ramps within a time-period of 12 steps. The time period of 12 steps was chosen since this is equal to the prediction horizon. These ramping limits mean that on average respectively 4, 2 and 1 ramp(s) per hour are allowed to occur per electrolyser. Note that imbalances change each 15 minutes which means the industrial plants should be able to ramp 4 times per hour in order to eliminate all imbalances. To overcome the ramp limit frequency, the electrolysers in the plants have been divided in sub-groups of which the energy consumption can be separately controlled.

Since limiting the ramp rate frequency of electrolysers requires the introduction of binary variables, as explained in Section 4-3-3, this comes at the cost of an increased computation time per time-step. To reduce simulation time, a single week in October (9-16 October) was simulated and Figure 5-30 shows the Day-Ahead forecast errors during this week. Unless these Day-Ahead forecast errors are corrected using industrial demand response the imbalances would be 1786 MWh.

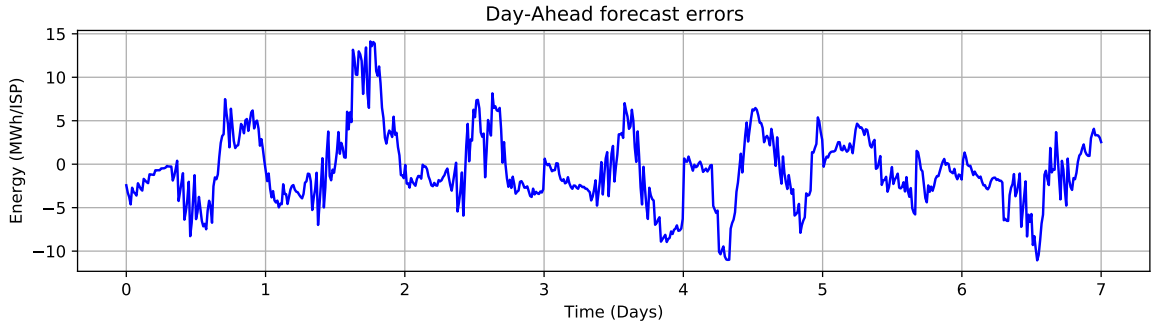

Figure 5-30: Day-Ahead forecast errors between 9-16 October

The results of simulating this week with the varying ramp frequency limits and number of subgroups per plant are shown in Table 5-2. It can be observed that at a ramping limit of 12 times, which is on average 4 times per hour, all the imbalances are eliminated independent of the amount of sub-groups. Firstly, the low amount of imbalances is because the storage levels are not reached during this period and the regulation capacity of the plants is sufficient. Secondly, a ramping limit of 12 in a time period of 12 steps allows each of the electrolysers to ramp at every time-step which therefore does not restrict the ramping ability. Therefore, the results with a ramp frequency of 12 steps can be seen as the maximum reduction in imbalances possible. When setting the ramping limit of the electrolysers to 6 ramps, which is on average

2 ramps per hour per electrolyser, some imbalances are observed but they still remain very limited (0-13 MWh). This is because even at 1 sub-group per plant, the chlor-alkali and hydrogen plant can ramp interchangeably and thereby combined they can reach a ramping frequency of 4 times per hour. Finally however, at a limit of 3 ramps, which is on average 1 ramp per hour per electrolyser, the effect of ramp limits on the imbalance minimization becomes important. At 1 subgroup, the imbalances result in 227 MWh and this high number of imbalances occurs because the chlor-alkali and hydrogen plant can only ramp 2 times per hour on average whilst the imbalances require a ramp frequency of 4 times per hour. In this case the MPC has to make the decision when ramping of the sub-groups is most optimal for minimizing imbalances. When the electrolysers per plant are sub-divided into 3 groups per plant on the other hand the imbalances reduce significantly to 13.8 MWh. This is because there are 3 sub-groups in the hydrogen plant and in the chlor-alkali plant respectively, hence 6 individually operable sub-groups in total, which can ramp after another and therefore allow a ramping rate of 4 times per hour.

Ramp frequency per 12 time-steps	12 ramps			6 ramps			3 ramps		
Nr. of sub-groups per plant	1	2	3	1	2	3	1	2	3
Imbalances (MWh)	0	0	0	13	0	9.1	227.0	30.8	13.8

Table 5-2: Imbalances during 9-16 October with varying ramp-frequencies and subgroups

The operation of the Virtual Power Plant with a ramp frequency of 3 per twelve time-steps and with 3 sub-groups can be explained in more detail with Figures 5-31, 5-32 and 5-33. In Figures 5-31 and 5-32 the energy consumption is shown of hydrogen sub-group #1 with 8 electrolysers and chlor-alkali sub-group #1 with 8 electrolysers. It can be seen that the ramp frequency in these sub-groups is significantly lower than required for the rapidly changing Day-Ahead forecast errors as shown in 5-30. However, by aggregating the energy consumption provided by all different electrolyser sub-groups (3x8 of the hydrogen plant and 3x8 of the chlor-alkali plant) as shown in Figure 5-33 it can be seen the industrial plants combined can provide the Virtual Power Plant demand response with the same granularity as the Day-Ahead forecast errors. For this simulation, the MPC optimizes the ramping moments and ramp height of the individual subgroups which results in an elimination of nearly all imbalances from 1786 MWh to 9.1 MWh (-99.5%).

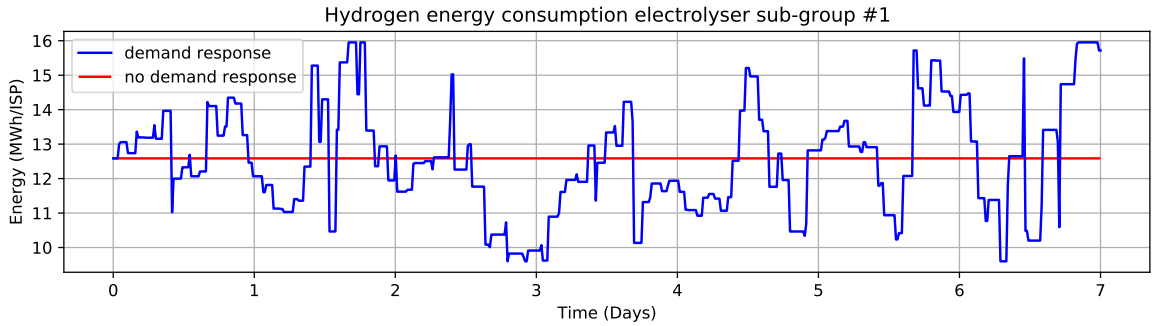

Figure 5-31: Hydrogen sub-group #1 with 3 ramps and 3 sub-groups

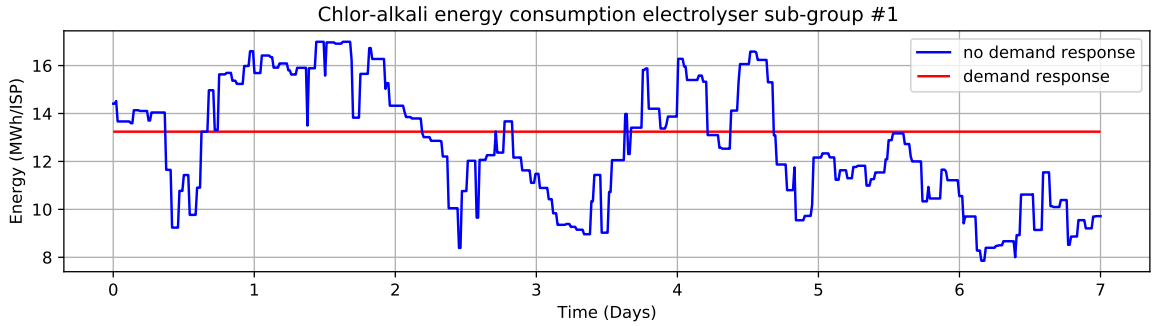

Figure 5-32: Chlor-alkali sub-group #1 with 3 ramps and 3 sub-groups

The results above show that a reduction of the ramping frequency of electrolysers does not have to affect the imbalance minimization ability if the number of independently operating sub-groups is increased. With the proposed method, Virtual Power Plants can offer industrial consumers the option to choose a frequency at which their equipment can be modulated which can be beneficial for reducing potential wear/tear cost. However, it should be noted that the computation time significantly increased by implementing a ramp frequency especially with a growing number of subgroups. At 3 sub-groups and 3 ramps per electrolyser the computation time per solution often exceeded 20 seconds, which was the maximum solution time allowed this thesis in order to restrict the simulation time. The rise in the computation time can be explained by the growing number of binary variables caused by the increasing number of sub-groups that each have a ramping frequency constraint. Given this observation, increasing the number of sub-groups and implementing ramping limits could quickly lead to tractability issues. Solutions to counter the tractability problem are to limit the maximum computation time of the solver as was performed in this study, granted that a feasible solution can always be found and the results are remain satisfactory. Furthermore, the optimality gap of the solver could be increased.

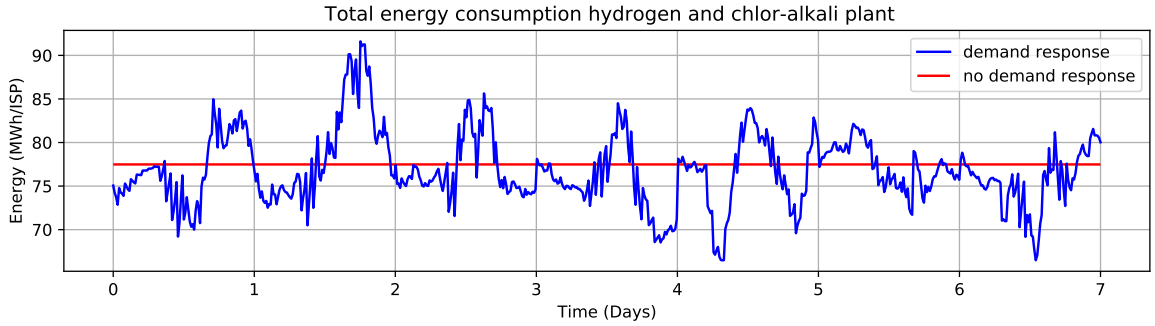

Figure 5-33: Total energy consumption of plants with 3 ramps and 3 sub-groups

Chapter 6

Conclusion

Virtual Power Plants can integrate and redispatch distributed renewable energy resources to gain revenue in the Day-Ahead market, however as a Balancing Responsible Party it can risk high imbalance costs due to errors between the Day-Ahead forecast and actual energy production. Several industrial processes have the capability to flexibly adjust their energy consumption which could assist in the reduction of imbalances in a Virtual Power Plant portfolio. In this thesis a technical analysis was performed to assess the ability of industrial processes to minimize imbalances in Virtual Power Plants due to Day-Ahead forecast errors.

For the first research question, literature on industrial demand response was reviewed to outline the advantages and disadvantages of major industrial processes for minimizing imbalances by operating as a flexible load in a short-term redispatch scheme. Suitable processes included refrigerated warehouses, chlor-alkali plants, hydrogen plants and aluminum production plants, which presented advantages such as a high ramp-rate, low process complexity, fast response time and ability to shift load consumption in time. On the other hand, less suitable processes were the steel-making, cement production and paper & pulp industry due to common disadvantages such as inefficiencies at partial load, significant inter-dependencies of processes, high utilization rates and low ramping capabilities.

For the second research question, an analysis was performed to assess the capability of the chlor-alkali and hydrogen industry to minimize imbalances in Virtual Power Plants due to errors in the Day-Ahead forecast of renewable energy. A Virtual Power Plant was developed in Python consisting of onshore wind (300 MW) and PV (300 MW), a chlor-alkali (203.5 MW) and hydrogen plant (193.4 MW), and a Model Predictive Control (MPC) unit. High fidelity models for the industrial plants were constructed in OpenModelica which could be simulated as Functional Mock-up Units in Python and historical data was used to represent Day-Ahead forecast errors in the renewable energy portfolio. The MPC developed in this thesis integrated nonlinear dynamics of the industrial plants by using data-driven Hammerstein-Wiener models. The objective of the MPC was to minimize imbalances by adjusting the energy consumption of the industrial plants while respecting process constraints. A simulation study of a base-case in the month of October showed that the chlor-alkali and hydrogen plant could minimize imbalances significantly from 12947 MWh to 1277 MWh which is a reduction of

-90.1%. Simulations during the months of January, April and July showed similar high imbalance reduction percentages between -89% and -99%. The ability to minimize imbalances is mostly impaired by the limited storage capacity of the industrial plants. The utilization rate and limited regulation capacity marginally contribute to the imbalances that remained. Furthermore, the chlor-alkali and the hydrogen plant could ramp up and down significantly within a time-step hence imbalances due to high ramps between imbalances were not present.

For the third research question, the effect of several parameters of the MPC and the industrial plants on the imbalance minimization was evaluated. Halving the storage capacity of the hydrogen and chlor-alkali tanks increased the imbalances significantly to 4149 MWh (+225%) whereas doubling the storage capacity could almost completely eliminate the imbalances 18 MWh (-99%). Increasing the storage capacity significantly reduces imbalances since the storage level boundaries are reached less often and therefore the industrial plants maintain the ability to operate below/above the nominal energy consumption to provide demand response. Varying the utilization rates between 80-90% limitedly affected the imbalances whilst at 95% the imbalances increased significantly to 2891 MWh (+126%) since the ability to operate above the nominal capacity was impaired which lead to positive imbalances. Omitting the Day-Ahead bid correction that guides the storage levels to 50% majorly increased imbalances to 6643 MWh (+420%) since continuously negative/positive imbalances keep the storage levels operating at their limits for prolonged periods of time. The prediction horizon and forecast accuracy of the MPC had limited to no influence on the imbalance minimization owing to the favorably high ramping capability of the chlor-alkali and hydrogen plant. In fact, as long as this first step-ahead forecast is accurate, the plants are able to reach the set-point and minimize the imbalance completely owing to their high ramping ability. Finally, it was shown that the imbalance minimization ability of the industrial plants can be maintained under a limit on the ramping frequency of individual electrolysers by organizing the electrolysers into separately controllable sub-groups in the industrial plants.

Chapter 7

Recommendations

Based on the research several recommendations for future study can be provided.

- In this study, the parameters of the industrial plants were based on literature. In future work, actual data of the chlor-alkali and hydrogen plants in the Port of Rotterdam could be used which would strongly increase the applicability of the research. This data can consist of actual storage sizes, utilization rates, chemical consumption by consumption as well as data on the electrolysers such as the operating temperature, inlet temperature range, ramp-rate and nr. of electrolysers in the plant.
- In this thesis, the chlor-alkali and hydrogen plant was chosen to be integrated in the Virtual Power Plant owing to their favorable characteristics for short-term dispatch and their location in the Port of Rotterdam. However, future work could focus on assessing the ability of the aluminum production and refrigerated warehouse industry to minimize imbalances. These processes both show similar favorable characteristics and their ability to minimize imbalances in Virtual Power Plants has not been assessed.
- The PEM electrolysers in the plant of this thesis operate with a minimum current density of 1 A/cm^2. However, research indicates that PEM electrolysers could operate as low as 0.6 A/cm^2, which would strongly increase the ability to shed loads. In this thesis, changing the lower limit from 1 to 0.6 A/cm^2 would have a limited effect on the imbalance minimization since the minimum current density of the electrolysers are not reached during the simulation. However, future work could focus on implementing a lower minimum current density for the PEM electrolysers and study whether it is profitable to offer the additional load shedding capability in energy markets.
- The control model of the MPC in this thesis provides the ability to control the cell temperature of the chlor-alkali and hydrogen electrolysers at different inputs of power. Future work could consider focusing on expanding the control model to make it include more process variables of the plant. Additional variables that can be included in the control model by means of Hammerstein-Wiener models could be the concentration of $NaOH(aq)$ and $NaCl_2(aq)$ in the chlor-alkali electrolyser cell and the volumetric

flow-rate of electrolyte into the cells. Expanding the control model of the MPC with additional relevant process variables would increase the applicability of the controller for a real hydrogen and chlor-alkali plant.

- The MPC in this thesis can integrate dynamics at the process time-frame in the scheduling time-frame at which energy markets operate. Therefore it provides a good foundation to be used for economic analyses in future study. The MPC can be included in a study on maximizing profits for Virtual Power Plants that integrate industrial processes in their portfolio to provide demand response in multiple energy markets or in studies on minimizing imbalance cost rather than imbalance volumes of Virtual Power Plants.
- In this study, the Day-Ahead market was used to buy/sell additional energy which allowed the storage levels to operate around the 50% level. The Day-Ahead optimization that was implemented to this purpose can be improved in future work by tuning the parameters, amongst others, of the maximum/minimum amount of energy that can be bought per hour during the Day-Ahead optimization and the maximum ramp on the hourly bids. Additionally, future work could consider incorporating the intraday market to avoid the delay between the time that the additional energy is bought/sold and that the energy becomes available to the industrial plants.

Appendix A

Guiding tables and figures

A-1 Parameters and variables of OpenModelica plants

A-1-1 Chlor-Alkali plant

Symbol	Description	Value	Ref.
α	Multiplication factor [−]	0.5	[22]
$A_{e,c}$	Cell membrane area $[m^2]$	2.7	[22, 80]
C_{Cl}^{ano}	Concentration chloride ions in anode $[\frac{mol}{m^3}]$		
C_{NaCl}^{ano}	Concentration of sodium chloride in outlet flow rate $[\frac{mol}{m^3}]$		
C_{NaOH}^{cat}	Concentration of sodium hydroxide in outlet flow rate $[\frac{mol}{m^3}]$		
C_{OH}^{cat}	Concentration chloride ions in cathode $[\frac{mol}{m^3}]$		
$C_{NaCl}^{ano,in}$	Concentration of sodium chloride in inlet flow $[\frac{mol}{m^3}]$		
$C_{NaOH}^{cat,in}$	Concentration of sodium hydroxide in inlet flow rate $[\frac{mol}{m^3}]$		
$C_{p,OH}$	Heat capacity of chlorine $[\frac{J}{mol \cdot K}]$	75	[22]
$C_{p,Cl}$	Heat capacity of hydroxide $[\frac{J}{mol \cdot K}]$	60	[22]
C_{p,H_2O}	Heat capacity of water $[\frac{J}{mol \cdot K}]$	50	[22]
$C_{pt,c}$	Lumped heat capacity of cell $[\frac{J}{mol \cdot K}]$		
$C_{pt,c}^{in}$	Lumped heat capacity of inlet flow rate $[\frac{J}{mol \cdot K}]$		
D_{H_2O}	Membrane diffusivity $[\frac{m^2}{s}]$	$2 \cdot 10^{-10}$	[22, 84]
F	Faraday constant $[\frac{C}{mol}]$	96485	[22]
ΔH_{rxn}	Heat consumed by the chlor-alkali reaction per mol $[\frac{J}{mol}]$	$447 \cdot 10^3$	[22]
ΔH_{vap}	Heat consumed by evaporation of one mol of water $[\frac{J}{mol}]$	$41 \cdot 10^3$	[22]
I_c	Current in electrolyser $[A]$		
k	Adiabatic exponent [−]	1.4	[22]
$M_{s,c}$	Amount of chloride in storage $[mol]$		
$\dot{M}_{in,c}$	Molar flow rate of chloride into storage $[\frac{mol}{s}]$		
$\dot{M}_{out,c}$	Molar flow rate of chloride out of storage $[\frac{mol}{s}]$		
n_c	Polytropic exponent [−]	1.45	[22]
$n_{H_2O}^{ano}$	Amount of moles of water in anolyte $[mol]$		
$n_{H_2O}^{cat}$	Amount of moles of water in catholyte $[mol]$		
$\dot{n}_{Cl_2}^{ano,out}$	Molar production of chlorine gas by cell $[\frac{mol}{s}]$		
$\dot{N}_{Cl_2}^{ano,out}$	Molar production of chlorine gas by stack $[\frac{mol}{s}]$		
$\dot{N}_{H_2,c}^{cat,out}$	Molar production of hydrogen gas by stack $[\frac{mol}{s}]$		
$\dot{n}_t^{in}$	Total molar inflow rate in cell $[\frac{mol}{s}]$		

$\dot{n}_t^{out}$	Total molar outflow rate in cell $[\frac{mol}{s}]$		
$N_{cells,c}$	Number of cells in a chlor-alkali electrolyser $[-]$	160	[22, 80]
n_{cl}^{ano}	Amount of moles of chloride ions in anolyte $[mol]$		
$n_{H_2O}^{cat}$	Amount of moles of water in catholyte $[mol]$		
n_{OH}^{cat}	Amount of moles of hydroxide in catholyte $[mol]$		
n_t	Total amount of moles in electrolyser cell $[mol]$		
η_{pc}	Polytropic efficiency $[-]$		
$P_{Cl_2}^{ano}$	Pressure anode chamber $[bar]$	1.213	[22]
$P_{f,c}$	Pressure of chlorine gas after compression $[bar]$	3.04	[22]
$P_{i,c}$	Pressure of chlorine gas before compression $[bar]$	1.013	[22]
P_c	Power consumed by electrolyser $[watt]$		
$\dot{Q}_{evp}$	Heat flow from evaporation $[watt]$		
$\dot{Q}_{gen,c}$	Heat generation from electrolysis $[watt]$		
$\dot{Q}_{loss,c}$	Heat loss to environment $[watt]$		
$\dot{Q}_{rxn}$	Heat flow from chemical reactions $[watt]$		
R	Universal gas constant $[\frac{J}{molK}]$	8.314	[22]
$R_{th,c}$	Thermal resistance of electrolyser $[\frac{C}{watt}]$	0.167	[22]
T_{amb}	Ambient temperature $[K]$	298.15	[22]
$T_{f,c}$	Temperature of chlorine gas after compression $[K]$		
$T_{i,c}$	Temperature of chlorine gas before compression $[K]$	286.15	[22]
$T_{in,c}$	Temperature of inlet flow $[K]$		
T_c	Temperature of electrolyser cell $[K]$		
$V_{act,c}$	Activation voltage $[V]$		
$V_{cell,c}$	Cell voltage $[V]$		
$V_{equ,c}$	Equilibrium voltage $[V]$		
$V_{ohm,c}$	Ohmic voltage $[V]$		
$V_{rev,c}$	Reversible voltage $[V]$	1.4	[22]
V	Cell volume $[m^3]$	0.2	[22]
δV	Membrane thickness $[m]$	$2.5 \cdot 10^{-4}$	[22]
$\dot{V}$	Outlet flow rate $[\frac{m^3}{s}]$		
$\dot{V}^{in}$	Inlet flow rate $[\frac{m^3}{s}]$		
$W_{comp,c}^{elec}$	Actual compression energy for a mole of chlorine $[\frac{J}{mol}]$		
$W_{comp,c}^{th}$	Theoretical compression energy for a mole of chlorine $[\frac{watt}{mol}]$		
x_i	Mole fraction of species i $[-]$		

Table A-1: Parameters and variables of chlor-alkali OpenModelica model

A-1-2 Hydrogen plant

Symbol	Description	Value	Ref.
α_{ano}	Experimental constant $[-]$	0.7353	[85, 86]
C_{p,m,H_2}	Heat capacity of hydrogen $[J/(mol \cdot K)]$		
C_{p,m,O_2}	Heat capacity of oxygen $[J/(mol \cdot K)]$		
$C_{pt,h}$	Heat capacity of a 46 KW PEM electrolyser $[J/K]$	162116	[85, 86]
δ_{mem}	Membrane thickness $[m]$	$178 \cdot 10^{-6}$	[85, 86]
E_{exc}	Activation energy for electron transport in anode $[J]$	52994	[85, 86]
E_{pro}	Activation energy for proton transport $[J]$	10536	[85, 86]
F	Faraday constant $[C/mol]$	96485	[85, 86]
Δh_j	Enthaply of species j $[J/mol]$		
I_h	Current in electrolyser $[A]$		
$j_{0,an}$	Exchange current density $[A/cm^2]$	$1.08 \cdot 10^{-4}$	[85, 86]
j_{dens}	Current density $[A/cm^2]$		
k	Adiabatic exponent $[-]$	1.4	[85, 86]
n	Polytropic exponent $[-]$	1.609	[108]
$M_{s,h}$	Amount of hydrogen in storage $[mol]$		
$\dot{M}_{in,h}$	Molar flow rate of hydrogen into storage $[mol/s]$		

$\dot{M}_{out,h}$	Molar flow rate of hydrogen out of storage $[mol/s]$		
$\dot{n}_j$	Moles of species j $[mol]$		
$N_{cells,h}$	Nr. of cells in a 46 KW PEM electrolyser $[-]$	60	[85, 86]
$N_{s,h}$	Nr. of 46 KW PEM electrolysers in series $[-]$	160	
$\dot{N}_{H_2,h}$	Molar production rate of hydrogen $[mol/s]$		
$\dot{N}_{H_2O}$	Molar consumption rate of water $[mol/s]$		
$\dot{N}_{O_2}$	Molar production rate of oxygen $[mol/s]$		
η_{pc}	Polytropic efficiency $[-]$		
η_{pump}	Electric efficiency of water pump $[-]$	0.75	[85, 86]
$\sigma_{mem,std}$	Membrane conductivity at standard conditions $[S/m]$	10.31	[85, 86]
σ_{mem}	Membrane conductivity $[S/m]$		
p_{ano}	Pressure in the anode $[Pa]$	$29 \cdot 10^5$	[85, 86]
p_{cat}	Pressure in the cathode $[Pa]$	$30 \cdot 10^5$	[85, 86]
P_f	Pressure of hydrogen after compression $[bar]$	100	[87]
P_i	Pressure of hydrogen before compression $[bar]$	30	[85, 86]
pp_{H_2}	Partial pressure of hydrogen $[bar]$		
pp_{H_2O}	Partial pressure of water $[bar]$		
pp_{O_2}	Partial pressure of oxygen $[bar]$		
$\dot{Q}_{cool}$	Heat removal by cooling system $[J/s]$		
$\dot{Q}_{elec}$	Power consumption of water pump $[J/s]$	1100	[85, 86]
$\dot{Q}_{gen,h}$	Heat generation from electrolysis $[J/s]$		
$\dot{Q}_{loss,h}$	Heat loss to ambient $[J/s]$		
$\dot{Q}_{pump,loss}$	Heat generation from water pump $[J/s]$		
R	Gas constant $[J/(mol \cdot K)]$	8.14	[85, 86]
R_{mem}	Membrane resistance $[\Omega \cdot m^2]$		
$R_{th,h}$	Thermal resistance of 46 KW PEM electrolyser $[K/(J \cdot s)]$	0.0668	[85, 86]
$T_{i,h}$	Temperature of hydrogen before compression $[K]$	298.15	[109]
T_{std}	Temperature at standard conditions $[K]$	298.15	[85, 86]
T_h	Temperature of electrolyser $[K]$		
$V_{act,h}$	Activation voltage $[V]$		
$V_{cell,h}$	Cell voltage $[V]$		
$V_{ocv,h}$	Open-circuit voltage $[V]$		
$V_{ohm,h}$	Ohmic voltage $[V]$		
$V_{rev,h}$	Reversible voltage $[V]$		
$V_{std,h}$	Voltage at standard conditions $[V]$	1.23	[85, 86]
V_{tn}	Thermo-neutral voltage $[V]$	1.48	[85, 86]
$W^{elec}_{comp,h}$	Actual compression energy for mole of hydrogen $[J/mol]$		
$W^{th}_{comp,h}$	Theoretical compression energy for mole of hydrogen $[J/mol]$		

Table A-2: Parameters and variables of hydrogen OpenModelica model

A-2 Day-Ahead electricity prices Belgium of 2020

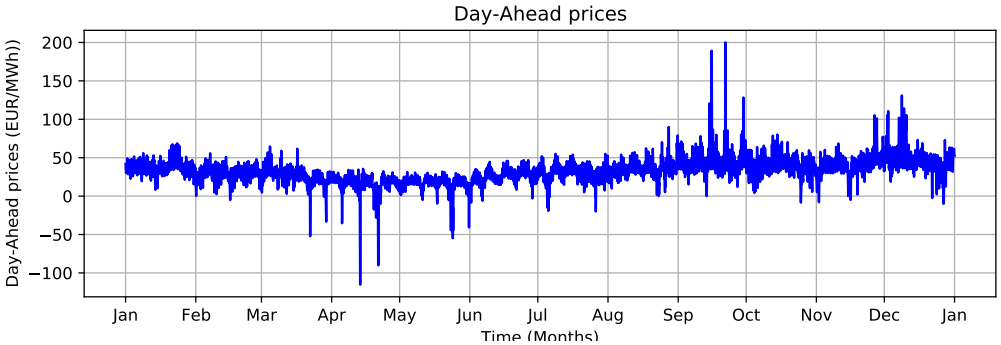

Figure A-1: Day-Ahead prices of 2020 in Belgium

A-3 Matrices of state-space models

$$A_{Cl_2} = \begin{bmatrix} 2.68 & -1.71 & 0.09 & 0 & 0 & 0 \\ 2.29 & -1.30 & 0.07 & 0 & 0 & 0 \\ 0.05 & -0.02 & 0.0012 & 0 & 0 & 0 \\ 0 & 0 & 0 & 2.80 & -1.81 & 0.16 \\ 0 & 0 & 0 & 2.36 & -1.36 & 0.12 \\ 0 & 0 & 0 & 0.11 & -0.05 & 0.004 \end{bmatrix} \quad B_{Cl_2} = \begin{bmatrix} 5.03 & 0 \\ 2.74 & 0 \\ 0.03125 & 0 \\ 0 & 5.12 \\ 0 & 2.77 \\ ,0 & 0.0625 \end{bmatrix} \tag{A-1}$$

$$C_{Cl_2} = \begin{bmatrix} 1 & -0.98 & 0 & 1 & -1 & 0 \end{bmatrix} \tag{A-2}$$

$$A_{H_2} = \begin{bmatrix} 1.65 & -0.66 & -0.01 & 0 & 0 & 0 \\ 1 & 0 & 0 & 0 & 0 & 0 \\ 0 & 0.008 & 0 & 0 & 0 & 0 \\ 0 & 0 & 0 & 1.63 & 0.64 & -0.009 \\ 0 & 0 & 0 & 1 & 0 & 0 \\ 0 & 0 & 0 & 0 & -0.008 & 0 \end{bmatrix} \quad B_{H_2} = \begin{bmatrix} 4 & 0 \\ 0 & 0 \\ 0 & 0 \\ 0 & 4 \\ 0 & 0 \\ ,0 & 0 \end{bmatrix} \tag{A-3}$$

$$C_{H_2} = \begin{bmatrix} 0.64 & -0.64 & 1.04 & 1 & 0.64 & 0.624 & 1.01 \end{bmatrix} \tag{A-4}$$

A-4 Parameters and variables of MPC and Day-ahead optimization

A-4-1 Model Predictive Controller

Symbol	Description	Value	Ref.
A_{Cl_2}	State matrix of linear model for Cl_2 electrolyser		
A_{e,Cl_2}	Cl_2 electrolyser cell area $[m^2]$	2.7	[80]
A_{e,H_2}	H_2 electrolyser cell area $[m^2]$	0.29	[85, 86]
A_{H_2}	State matrix of linear model for H_2 electrolyser		
B_{Cl_2}	Input matrix of linear model for Cl_2 electrolyser		
$b_{g,Cl_2}(t)$	Binary variable on ramping of Cl_2 electrolyser in group g $[-]$		
B_{H_2}	Input matrix of linear model for H_2 electrolyser		
$b_{k,H_2}(t)$	Binary variable on ramping of H_2 electrolyser in group k $[-]$		
b_{tot}	Maximum nr. ramps per N time steps $[-]$		

C_{Cl_2}	Output matrix of linear model for Cl_2 electrolyser		
C_{H_2}	Output matrix of linear model for H_2 electrolyser		
F	Faraday constant $[C/mol]$	94865	[22]
g	Cl_2 electrolyser sub-group number g $[-]$		
G_{sub}	Number of sub-groups in Cl_2 plant $[-]$		
$j_{Cl_2,max}$	Max. current density of Cl_2 electrolyser $[A/cm^2]$	0.6	[22]
$j_{Cl_2,min}$	Min. current density of Cl_2 electrolyser $[A/cm^2]$	0.3	[22]
$j_{Cl_2,nom}$	Nominal current density of Cl_2 electrolyser $[A/cm^2]$		
$j_{g,Cl_2}(t)$	Current density of Cl_2 elec. in sub-group g at time t $[A/cm^2]$		
$j_{H_2,max}$	Max. current density of H_2 electrolyser $[A/cm^2]$	1.6	[110]
$j_{H_2,min}$	Min. current density of H_2 electrolyser $[A/cm^2]$	1	
$j_{H_2,nom}$	Nominal current density of H_2 electrolyser $[A/cm^2]$		
$j_{k,H_2}(t)$	Current density of H_2 elec. in sub-group k at time t $[A/cm^2]$		
$\Delta j_{Cl_2,down}$	Ramp-down of current density of Cl_2 electrolysers $[A/cm^2]$	0.075	[80]
$\Delta j_{Cl_2,up}$	Ramp-up of current density of Cl_2 electrolysers $[A/cm^2]$	0.075	[80]
k	H_2 electrolyser sub-group number g $[-]$		
K_{sub}	Number of sub-groups in H_2 plant		
L_{max,Cl_2}	Max Cl_2 storage capacity $[mol]$		
L_{max,H_2}	Max H_2 storage capacity $[mol]$		
$L_{norm,Cl_2}(t)$	Normalized storage level of Cl_2 at time t $[-]$		
$L_{norm,H_2}(t)$	Normalized storage level of H_2 at time t $[-]$		
N	Prediction horizon $[15min]$	12	[100]
N_{cells,Cl_2}	Amount of cells in Cl_2 electrolyser stack $[-]$	160	[22]
N_{cells,H_2}	Amount of cells in H_2 electrolyser stack $[-]$	60	[85, 86]
N_{series,H_2}	Amount of 46 KW PEM electrolysers in series $[-]$	160	
$\dot{N}_{g,Cl2}(t)$	Production of Cl_2 per elec. in sub-group g at time t $[mol/s]$		
$\dot{N}_{k,H_2}(t)$	Production of H_2 per elec. in sub-group k at time t $[mol/s]$		
σ_1	Penalty on the storage level deviation $[-]$	1000	
σ_2	Penalty on the slack variables $[-]$	1000000	
$P_{g,Cl_2}(t)$	Power cons. per Cl_2 electrolyser in sub-group g at time t $[MW]$		
$P_{g,dr,Cl_2}(t)$	Demand response per Cl_2 elec. in sub-group g at time t $[MW]$		
$P_{k,dr,H_2}(t)$	Demand response per H_2 elec. in sub-group k at time t $[MW]$		
$P_{k,H_2}(t)$	Power cons. per H_2 electrolyser in sub-group k at time t $[MW]$		
$P_{nom,Cl2}$	Nominal power cons. of Cl_2 electrolyser $[MW]$		
P_{nom,H_2}	Nominal power cons. of H_2 electrolyser $[MW]$		
$Q^-(t)$	Negative imbalance at time t $[MWh/ISP]$		
$Q^+(t)$	Positive imbalance at time t $[MWh/ISP]$		
$Q_{act}(t)$	Actual renewable energy production at time t $[MWh/ISP]$		
$Q_{DA,bid}(t)$	Energy bid in the Day-Ahead market at time t $[MWh/ISP]$		
$Q_{imb}(t)$	Imbalance forecast at time t $[MWh/ISP]$		
Q_{res}	Energy reserve [MWh]	0.5	
$\dot{Q}_{cool,max}$	Maximum cooling load of H_2 electrolyser $[MW]$	1.44	
$\dot{Q}_{cool,min}$	Minimum cooling load of H_2 electrolyser $[MW]$	0.69	
$\dot{Q}_{k,cool}(t)$	Cooling load per H_2 electrolyser of sub-group k at time t $[MW]$		
$S_{Cl_2,up}(t)$	Upper slack variable on chlorine storage level at time t $[-]$		
$S_{Cl_2,low}(t)$	Lower slack variable on chlorine storage level at time t $[-]$		
$S_{H_2,up}(t)$	Upper slack variable on hydrogen storage level at time t $[-]$		
$S_{H_2,low}(t)$	Lower slack variable on hydrogen storage level at time t $[-]$		
t	Time $[15min]$		
Δt	Time-step $[min]$	15	
$T_{g,in}(t)$	Inlet temp. per Cl_2 elec. in sub-group g at time t $[^\circ C]$		
$T_{in,max}$	Max inlet temperature to Cl_2 electrolyser $[^\circ C]$	80	[82, 80]
$T_{in,min}$	Min inlet temperature to Cl_2 electrolyser $[^\circ C]$	70	[80]
$T_{g,Cl_2}(t)$	Temperature per Cl_2 electrolyser in sub-group g at time t		
T_{max,Cl_2}	Max temperature of Cl_2 electrolyser $[^\circ C]$	90	[82, 80]
T_{min,Cl_2}	Min temperature of Cl_2 electrolyser $[^\circ C]$	85	[82, 80]
$T_{k,H_2}(t)$	Temperature per H_2 electrolyser in sub-group g at time t		

T_{max,H_2}	Max temperature of H_2 electrolyser [$^\circ C$]	60	[85, 86]
T_{min,H_2}	Min temperature of H_2 electrolyser [$^\circ C$]	55	
$v_{\dot{Q},cool,max}$	Max 'inner' cooling input per H_2 electrolyser [−]	−79.87	
$v_{\dot{Q},cool,min}$	Min 'inner' cooling input per H_2 electrolyser [−]	−42.46	
$v_{g,power,Cl_2}(t)$	Inner' power input per Cl_2 elec. in sub-group g at time t [−]		
$v_{k,\dot{Q},cool}(t)$	Inner' cooling input per H_2 elec. in sub-group k at time t [−]		
$v_{k,power,H_2}(t)$	Inner' power input per H_2 elect. in sub-group k at time t [−]		
$w_{g,T,Cl_2}(t)$	Inner' temperature per Cl_2 elec. In sub-group g at time t [−]		
$w_{k,T,H_2}(t)$	Inner' temperature per H_2 elec. in sub-group k at time t [−]		
$w_{T,Cl_2,max}$	Max 'inner' temperature of Cl_2 electrolyser [−]	8.6	
$w_{T,Cl_2,min}$	Min 'inner' temperature of Cl_2 electrolyser [−]	−12	
$w_{T,H_2,max}$	Max 'inner' temperature of H_2 electrolyser [−]	−10.49	
$w_{T,H_2,min}$	Min 'inner' temperature of H_2 electrolyser [−]	−10.49	
$\vec{x}_{g,Cl_2}(t)$	inner' state vector per Cl_2 electrolyser in sub-group g [−]		
$\vec{x}_{k,H_2}(t)$	inner' state vector per H_2 electrolyser in sub-group k [−]		

Table A-3: Parameters and variables of Model Predictive Controller

A-4-2 Day-Ahead optimization

Symbol	Description	Value
$Q_{DA,bid}(t)$	Energy bid in Day-Ahead market [MWh/h]	
$Q_{DA,RE}(t)$	Actual renewable energy production [MWh/h]	
$Q_{DA,stor}(t)$	Energy bought/sold to return storage levels to 50% [MWh/h]	
$Price_{DA}(t)$	Day-Ahead energy price [EUR/MWh]	
ΔQ_{stor}	Total energy surplus/deficit to return storage levels to 50% [MWh]	
Q_{max}	Maximum energy bid in Day-Ahead market [MWh/h]	7.7
ΔQ_{max}	Maximum ramp of energy bids in Day-Ahead market [MWh/h]	3.85

Table A-4: Parameters and variables of Day-Ahead optimization

A-5 Energy calculation to return storage levels to midway level

The calculation of the energy needed to return the storage levels back to the midway level is described below, using the chlorine storage tank as an example. First, the last prediction by the MPC of the chlorine storage level $L_{norm,H_2}[12.00+\text{N}]$ is used to determine the deviation of the storage levels from the midway level.

$$\Delta L_{norm,Cl_2}[12.00+N] = L_{norm,Cl_2}[12.00+N] - 0.5 \tag{A-5}$$

Then, re-arranging Faraday's law the average current density at which the chlor-alkali electrolysers should operate during the next day to return the storage levels to the original levels is:

$$\Delta j_{Cl_2} = -\frac{\Delta L_{norm,H_2}[12.00+N] \cdot L_{max,Cl_2}}{0.5 \cdot A_{e,c} \cdot N_{cells,c} \cdot N_{s,c} \cdot 3600 \cdot 24} \cdot F \tag{A-6}$$

$$j_{avg,Cl_2} = \Delta j_{Cl_2} + j_{Cl_2,nom} \tag{A-7}$$

where j_{avg,Cl_2} is the average current density at which the chlor-alkali plant should operate for a day to return the storage to the midway level, $j_{Cl_2,nom}$ is the nominal current density, Δj_{Cl_2} is the average current density above/below the nominal current density, $A_{e,c}$ is the surface area of a single chlor-alkali cell, N_c is the amount of cells per electrolyser, $N_{s,c}$ is the amount of electrolyser stacks in the plant, $3600 \cdot 24$ is the amount of seconds per day, and F is the Faraday constant.

The average power consumption, $P_{avg,Cl_2}(t)$, at which the electrolysers need to operate to return the storage back to the midway level can be calculated by rewriting the empirical relationship between power and current density.

$$P_{avg,Cl_2}(t) = \frac{j_{avg,Cl_2}(t)}{0.0639932} - 0.88 \tag{A-8}$$

After this, the average power consumption of the chlor-alkali electrolyser above/below the nominal power production can be calculated:

$$\Delta P_{avg,Cl_2}(t) = N_{cells,c} \cdot (P_{avg,Cl_2}(t) - P_{nom,Cl_2}) \tag{A-9}$$

where $\Delta P_{avg,Cl_2}$ is the difference between the nominal power consumption and the actual power profile needed to return the chlorine storage back to the midway position.

Using $\Delta P_{avg,Cl_2}$, the total energy that needs to be bought/sold to return the chlorine storage to the midway position can be calculated:

$$\Delta Q_{stor,Cl_2} = \frac{\Delta P_{avg,Cl_2} \cdot 24 \cdot 3600}{3600} \tag{A-10}$$

where $\Delta Q_{stor,Cl_2}$ indicates the amount of energy that needs to be bought/sold in the Day-Ahead market to return the storage back to the midway position, the $24 \cdot 3600$ term indicates the amount of seconds in a day, and the division by 3600 is used to convert MJ to MWh.

A-6 Simulation results

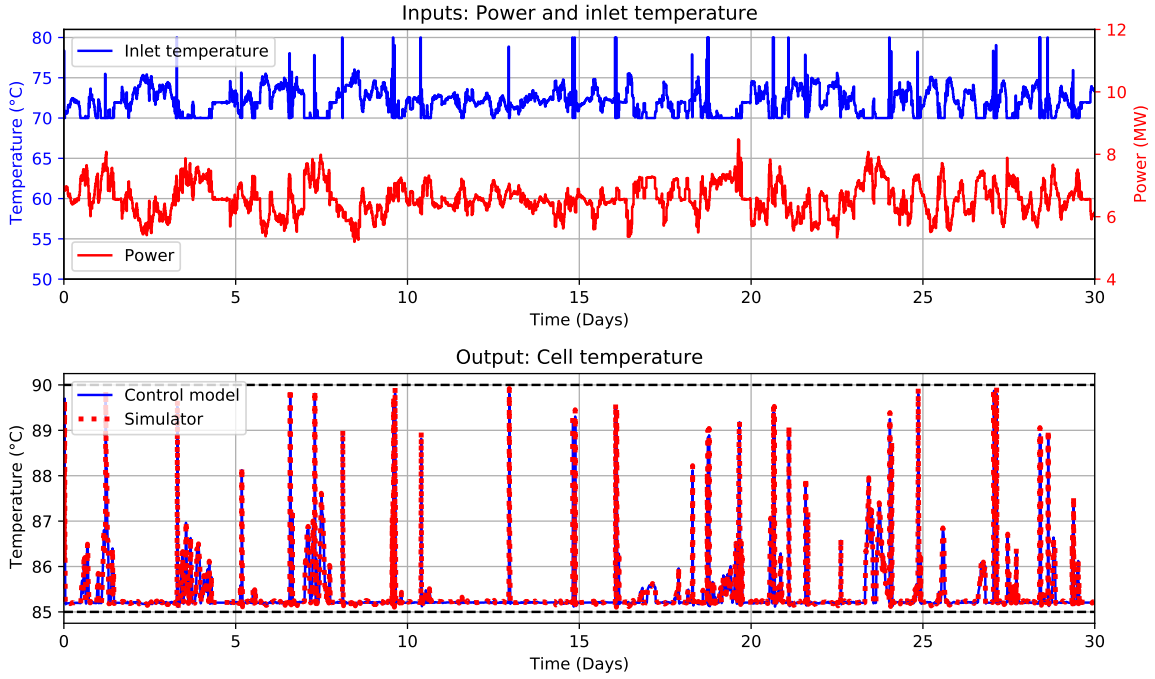

Figure A-2: Input and output of chlor-alkali electrolyser during October

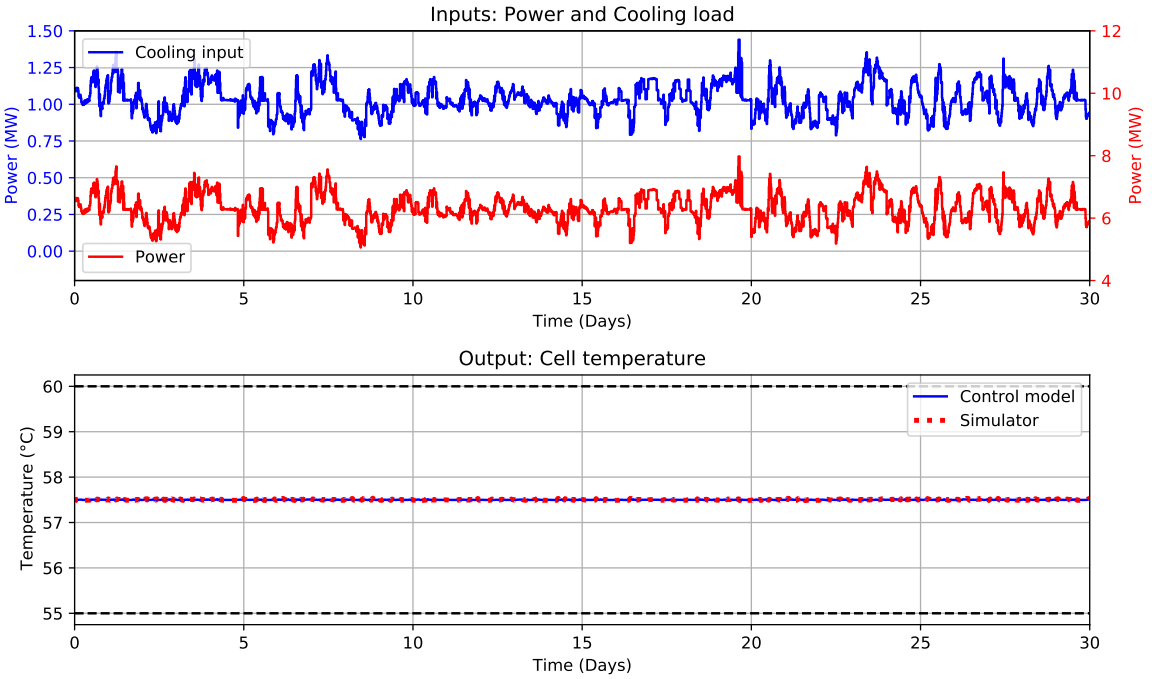

Figure A-3: Input and output of a hydrogen electrolyser during October

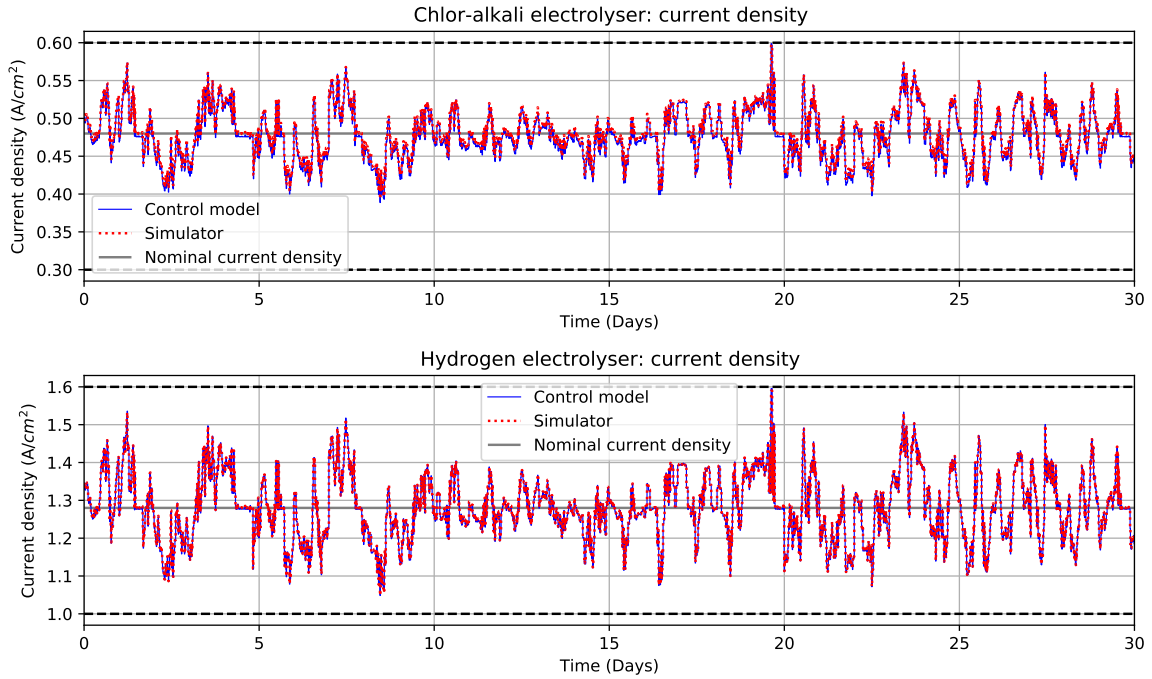

Figure A-4: Current density predicted and simulated of electrolysers during October

Bibliography

[1] J. Rogelj, M. Den Elzen, N. Höhne, T. Fransen, H. Fekete, H. Winkler, R. Schaeffer, F. Sha, K. Riahi, and M. Meinshausen, "Paris agreement climate proposals need a boost to keep warming well below 2 c," *Nature*, vol. 534, no. 7609, pp. 631–639, 2016.

[2] S. R. Sinsel, R. L. Riemke, and V. H. Hoffmann, "Challenges and solution technologies for the integration of variable renewable energy sources—a review," *renewable energy*, vol. 145, pp. 2271–2285, 2020.

[3] A. Zahedi, "A review of drivers, benefits, and challenges in integrating renewable energy sources into electricity grid," *Renewable and Sustainable Energy Reviews*, vol. 15, no. 9, pp. 4775–4779, 2011.

[4] K. Oureilidis, K.-N. Malamaki, K. Gallos, A. Tsitsimelis, C. Dikaiakos, S. Gkavanoudis, M. Cvetkovic, J. M. Mauricio, J. M. Maza Ortega, J. L. M. Ramos, *et al.*, "Ancillary services market design in distribution networks: review and identification of barriers," *Energies*, vol. 13, no. 4, p. 917, 2020.

[5] M. F. Akorede, H. Hizam, and E. Pouresmaeil, "Distributed energy resources and benefits to the environment," *Renewable and sustainable energy reviews*, vol. 14, no. 2, pp. 724–734, 2010.

[6] S. M. Nosratabadi, R.-A. Hooshmand, and E. Gholipour, "A comprehensive review on microgrid and virtual power plant concepts employed for distributed energy resources scheduling in power systems," *Renewable and Sustainable Energy Reviews*, vol. 67, pp. 341–363, 2017.

[7] D. Pudjianto, C. Ramsay, and G. Strbac, "Virtual power plant and system integration of distributed energy resources," *IET Renewable power generation*, vol. 1, no. 1, pp. 10–16, 2007.

[8] H. Saboori, M. Mohammadi, and R. Taghe, "Virtual power plant (vpp), definition, concept, components and types," in *2011 Asia-Pacific Power and Energy Engineering Conference*, pp. 1–4, IEEE, 2011.

[9] H. Pandžić, I. Kuzle, and T. Capuder, "Virtual power plant mid-term dispatch optimization," *Applied Energy*, vol. 101, pp. 134–141, 2013.

[10] F. Tanrisever, K. Derinkuyu, and G. Jongen, "Organization and functioning of liberalized electricity markets: An overview of the dutch market," *Renewable and Sustainable Energy Reviews*, vol. 51, pp. 1363–1374, 2015.

[11] E. G. Kardakos, C. K. Simoglou, and A. G. Bakirtzis, "Optimal offering strategy of a virtual power plant: A stochastic bi-level approach," *IEEE Transactions on Smart Grid*, vol. 7, no. 2, pp. 794–806, 2015.

[12] A. H. Elgamal, G. Kocher-Oberlehner, V. Robu, and M. Andoni, "Optimization of a multiple-scale renewable energy-based virtual power plant in the uk," *Applied Energy*, vol. 256, p. 113973, 2019.

[13] Ö. Okur, N. Voulis, P. Heijnen, and Z. Lukszo, "Aggregator-mediated demand response: Minimizing imbalances caused by uncertainty of solar generation," *Applied Energy*, vol. 247, pp. 426–437, 2019.

[14] A. Jamali, J. Aghaei, M. Esmaili, A. Nikoobakht, T. Niknam, M. Shafie-khah, and J. P. Catalão, "Self-scheduling approach to coordinating wind power producers with energy storage and demand response," *IEEE Transactions on Sustainable Energy*, vol. 11, no. 3, pp. 1210–1219, 2019.

[15] J. Zapata, J. Vandewalle, and W. D'haeseleer, "A comparative study of imbalance reduction strategies for virtual power plant operation," *Applied Thermal Engineering*, vol. 71, no. 2, pp. 847–857, 2014.

[16] M. Paulus and F. Borggrefe, "The potential of demand-side management in energy-intensive industries for electricity markets in germany," *Applied Energy*, vol. 88, no. 2, pp. 432–441, 2011.

[17] M. H. Shoreh, P. Siano, M. Shafie-khah, V. Loia, and J. P. Catalão, "A survey of industrial applications of demand response," *Electric Power Systems Research*, vol. 141, pp. 31–49, 2016.

[18] S. M. Nosratabadi, R.-A. Hooshmand, and E. Gholipour, "Stochastic profit-based scheduling of industrial virtual power plant using the best demand response strategy," *Applied energy*, vol. 164, pp. 590–606, 2016.

[19] R.-A. Hooshmand, S. M. Nosratabadi, and E. Gholipour, "Event-based scheduling of industrial technical virtual power plant considering wind and market prices stochastic behaviors-a case study in iran," *Journal of cleaner production*, vol. 172, pp. 1748–1764, 2018.

[20] S. M. Nosratabadi and R.-A. Hooshmand, "Stochastic electrical energy management of industrial virtual power plant considering time-based and incentive-based demand response programs option in contingency condition," *International Journal of Emerging Electric Power Systems*, vol. 1, no. ahead-of-print, 2020.

[21] R. C. Pattison, C. R. Touretzky, I. Harjunkoski, and M. Baldea, "Moving horizon closed-loop production scheduling using dynamic process models," *AIChE Journal*, vol. 63, no. 2, pp. 639–651, 2017.

[22] J. I. Otashu and M. Baldea, "Demand response-oriented dynamic modeling and operational optimization of membrane-based chlor-alkali plants," *Computers & Chemical Engineering*, vol. 121, pp. 396–408, 2019.

[23] C. Tsay, A. Kumar, J. Flores-Cerrillo, and M. Baldea, "Optimal demand response scheduling of an industrial air separation unit using data-driven dynamic models," *Computers & Chemical Engineering*, vol. 126, pp. 22–34, 2019.

[24] J. M. Simkoff and M. Baldea, "Stochastic scheduling and control using data-driven nonlinear dynamic models: application to demand response operation of a chlor-alkali plant," *Industrial & Engineering Chemistry Research*, vol. 59, no. 21, pp. 10031–10042, 2020.

[25] J. M. Morales, A. J. Conejo, H. Madsen, P. Pinson, and M. Zugno, *Integrating renewables in electricity markets: operational problems*, vol. 205. Springer Science & Business Media, 2013.

[26] G. Plancke, K. De Vos, R. Belmans, and A. Delnooz, "Virtual power plants: Definition, applications and barriers to the implementation in the distribution system," in *2015 12th International Conference on the European Energy Market (EEM)*, pp. 1–5, IEEE, 2015.

[27] A. Heshmati, S. Abolhosseini, J. Altmann, *et al.*, *The development of renewable energy sources and its significance for the environment*. Springer, 2015.

[28] N. Hatziargyriou, *Microgrids: architectures and control*. John Wiley & Sons, 2014.

[29] J. Ikäheimo, C. Evens, and S. Kärkkäinen, "Der aggregator business: the finnish case," *Technical Research Centre of Finland (VTT): Espoo, Finland*, 2010.

[30] N. Ruiz, I. Cobelo, and J. Oyarzabal, "A direct load control model for virtual power plant management," *IEEE Transactions on Power Systems*, vol. 24, no. 2, pp. 959–966, 2009.

[31] W. Tang and H.-T. Yang, "Optimal operation and bidding strategy of a virtual power plant integrated with energy storage systems and elasticity demand response," *IEEE Access*, vol. 7, pp. 79798–79809, 2019.

[32] Next-Kraftwerke, "Business model virtual power plant." https://www.next-kraftwerke.com/energy-blog/business-model-virtual-power-plant-vpp. Accessed: 2021-02-03.

[33] ENTSO-E, "Virtual power plants." https://www.entsoe.eu/Technopedia/techsheets/virtual-power-plants. Accessed: 2021-01-30.

[34] M. M. Othman, Y. Hegazy, and A. Y. Abdelaziz, "A review of virtual power plant definitions, components, framework and optimization," *International Electrical Engineering Journal*, vol. 6, no. 9, pp. 2010–2024, 2015.

[35] R. A. Van der Veen, A. Abbasy, and R. A. Hakvoort, "A comparison of imbalance settlement designs and results of germany and the netherlands," in *Young Energy Engineers & Economists Seminar (YEEES), 8-9 April 2010, Cambridge, UK*, Citeseer, 2010.

[36] Tennet, "Imbalance pricing system - how are the (directions of) payment determined?," tech. rep., TenneT TSO B.V., 2020.

[37] E. F. Camacho and C. B. Alba, *Model predictive control*. Springer science & business media, 2013.

[38] M. H. Albadi and E. F. El-Saadany, "Demand response in electricity markets: An overview," in *2007 IEEE power engineering society general meeting*, pp. 1–5, IEEE, 2007.

[39] P. Palensky and D. Dietrich, "Demand side management: Demand response, intelligent energy systems, and smart loads," *IEEE transactions on industrial informatics*, vol. 7, no. 3, pp. 381–388, 2011.

[40] W. Huang, N. Zhang, C. Kang, M. Li, and M. Huo, "From demand response to integrated demand response: Review and prospect of research and application," *Protection and Control of Modern Power Systems*, vol. 4, no. 1, pp. 1–13, 2019.

[41] M. Hussain and Y. Gao, "A review of demand response in an efficient smart grid environment," *The Electricity Journal*, vol. 31, no. 5, pp. 55–63, 2018.

[42] RVO, "Mja-sectorrapport 2016 koel- en vrieshuizen," tech. rep., Rijksdienst Voor Ondernemend Nederland, 2017.

[43] K. Fikiin, P. Mazzucchelli, A. Foster, J. Evans, S. Akterian, G. Alvarez, D. Leducq, M. Hoang, G. Garcia, L. Varga, *et al.*, "Energy mapping of large refrigerated warehouses co-located with renewable energy sources across europe," in *ICR 2019: The 25th IIR International Conference of Refrigeration*, 2019.

[44] S. David, M. Nance, P. Janie, K. Sila, C. Karin, S. Betty, M. Ralph, M. John, M. Lorin, G. Samuel, *et al.*, "Fast automated demand response to enable the integration of renewable resources," tech. rep., 2012.

[45] A. Grein and M. Pehnt, "Load management for refrigeration systems: Potentials and barriers," *Energy Policy*, vol. 39, no. 9, pp. 5598–5608, 2011.

[46] P. Grünewald and J. Torriti, "Demand response from the non-domestic sector: Early uk experiences and future opportunities," *Energy policy*, vol. 61, pp. 423–429, 2013.

[47] M. Akerma, H. M. Hoang, D. Leducq, C. Flinois, P. Clain, and A. Delahaye, "Demand response in refrigerated warehouse," in *2018 IEEE International Smart Cities Conference (ISC2)*, pp. 1–5, IEEE, 2018.

[48] C. Xavier and C. Oliveira, "Decarbonisation options for the dutch cement industry," tech. rep., PBL Netherlands Environmental Assessment Agency, 2021.

[49] R. T. Lidbetter and L. Liebenberg, "Load-shifting opportunities for a typical south african cement plant," in *2011 Proceedings of the 8th Conference on the Industrial and Commercial Use of Energy*, pp. 17–25, IEEE, 2011.

[50] D. L. Summerbell, D. Khripko, C. Barlow, and J. Hesselbach, "Cost and carbon reductions from industrial demand-side management: Study of potential savings at a cement plant," *Applied energy*, vol. 197, pp. 100–113, 2017.

[51] D. Olsen, "Opportunities for energy efficiency and demand response in the california cement industry," tech. rep., Lawrence Berkeley National Lab. (LBNL), Berkeley, CA (United States), 2011.

[52] X. Zhang, G. Hug, J. Z. Kolter, and I. Harjunkoski, "Demand response of ancillary service from industrial loads coordinated with energy storage," *IEEE Transactions on Power Systems*, vol. 33, no. 1, pp. 951–961, 2017.

[53] IEA, "Iron and steel technology roadmap," tech. rep., International Energy Agency, Paris, 2020.

[54] A. Keys, M. Van Hout, and B. Daniëls, "Decarbonisation options for the dutch steel industry," tech. rep., PBL Netherlands Environmental Assessment Agency, 2019.

[55] A. Feta, M. van Den Broek, W. Crijns-Graus, and G. Jägers, "Technical demand response potentials of the integrated steelmaking site of tata steel in ijmuiden," *Energy Efficiency*, vol. 11, no. 5, pp. 1211–1225, 2018.

[56] H. Kortes and T. Van Dril, "Decarbonisation options for the dutch aluminium industry," tech. rep., PBL Netherlands Environmental Assessment Agency, 2019.

[57] Aldel, "The invisible by-product of aldel: a more stable electricity grid." https://aldel.nl/the-invisible-by-product-of-aldel-a-more-stable-electricity-grid/, Dec 2019. Accessed: 2021-04-05.

[58] N. Depree, R. Düssel, P. Patel, and T. Reek, "The 'virtual battery'—operating an aluminium smelter with flexible energy input," in *Light Metals 2016*, pp. 571–576, Springer, 2016.

[59] H. C. Gils, "Assessment of the theoretical demand response potential in europe," *Energy*, vol. 67, pp. 1–18, 2014.

[60] E. Scherpbier and H. Eerens, "Decarbonisation options for the dutch chlor-alkali industry," tech. rep., PBL Netherlands Environmental Assessment Agency, 2020.

[61] K. Roh, L. C. Brée, K. Perrey, A. Bulan, and A. Mitsos, "Flexible operation of switchable chlor-alkali electrolysis for demand side management," *Applied Energy*, vol. 255, p. 113880, 2019.

[62] J. Baetens, J. D. De Kooning, G. Van Eetvelde, and L. Vandevelde, "A two-stage stochastic optimisation methodology for the operation of a chlor-alkali electrolyser under variable dam and fcr market prices," *Energies*, vol. 13, no. 21, p. 5675, 2020.

[63] H. Teichgraeber and A. R. Brandt, "Optimal design of an electricity-intensive industrial facility subject to electricity price uncertainty: Stochastic optimization and scenario reduction," *Chemical Engineering Research and Design*, vol. 163, pp. 204–216, 2020.

[64] Nouryon, "Akzonobel specialty chemicals to upgrade rotterdam chlor-alkali plant." https://www.nouryon.com/news-and-events/news-overview/2018/AkzoNobel-Specialty-Chemicals-to-upgrade-Rotterdam-chlor-alkali-plant/. Accessed: 2021-04-01.

[65] F. Klaucke, C. Hoffmann, M. Hofmann, and G. Tsatsaronis, "Impact of the chlorine value chain on the demand response potential of the chloralkali process," *Applied Energy*, vol. 276, p. 115366, 2020.

[66] K. Rademaker and M. Marsidi, *Decarbonisation Options for the Dutch Paper and Board Industry*. PBL Netherlands Environmental Assessment Agency;© ECN part of TNO, 2019.

[67] L. Herre, F. Tomasini, K. Paridari, L. Söder, and L. Nordström, "Simplified model of integrated paper mill for optimal bidding in energy and reserve markets," *Applied Energy*, vol. 279, p. 115857, 2020.

[68] F. Cell, H. J. Undertaking, F. Gérard, L. van Nuffel, T. Smit, J. Yearwood, O. Černỳ, J. Michalski, and M. Altmann, "Opportunities for hydrogen energy technologies considering the national energy & climate plans," 2020.

[69] S. Lensink and K. Schoots, "Eindadvies basisbedragen sde++ 2021," tech. rep., PBL Planbureau voor de Leefomgeving, 2020.

[70] M. M. Rashid, M. K. Al Mesfer, H. Naseem, M. Danish, *et al.*, "Hydrogen production by water electrolysis: a review of alkaline water electrolysis, pem water electrolysis and high temperature water electrolysis," *Int. J. Eng. Adv. Technol*, vol. 4, no. 3, pp. 2249–8958, 2015.

[71] IRENA, "Scaling up electrolysers to meet the 1.5 c climate goal," tech. rep., International Renewable Energy Agency, Abu Dhabi, 2020.

[72] Provincie Zuid-Holland, "Waterstofvisie en strategie - de rol van waterstof in de energie- en grondstoffentransitie in zuid-holland 2030 (-2050)," tech. rep., Provincie Zuid-Holland, Den Haag, 2020.

[73] M. Baldea, "Employing chemical processes as grid-level energy storage devices," in *Advances in energy systems engineering*, pp. 247–271, Springer, 2017.

[74] F. Sensfuß, M. Ragwitz, and M. Genoese, "The merit-order effect: A detailed analysis of the price effect of renewable electricity generation on spot market prices in germany," *Energy policy*, vol. 36, no. 8, pp. 3086–3094, 2008.

[75] H. Cui, F. Li, Q. Hu, L. Bai, and X. Fang, "Day-ahead coordinated operation of utility-scale electricity and natural gas networks considering demand response based virtual power plants," *Applied energy*, vol. 176, pp. 183–195, 2016.

[76] H. de Heer and M. van der Laan, *USEF: Workstream on Aggregator Implementation Models: Recommended Practices and Key Considerations for a Regulatory Framework and Market Design on Explicit Demand Response: Update 2017: Includes Residential Customer Segment.* USEF, 2017.

[77] S. Nolan and M. O'Malley, "Challenges and barriers to demand response deployment and evaluation," *Applied Energy*, vol. 152, pp. 1–10, 2015.

[78] Elia, "Solar power generation." https://www.elia.be/en/grid-data/power-generation/solar-pv-power-generation-data. Accessed: 2020-12-01.

[79] Elia, "Wind power generation." https://www.elia.be/en/grid-data/power-generation/wind-power-generation. Accessed: 2020-12-01.

[80] T. F. O'Brien, T. V. Bommaraju, and F. Hine, *Handbook of Chlor-Alkali Technology: Volume I: Fundamentals, Volume II: Brine Treatment and Cell Operation, Volume III: Facility Design and Product Handling, Volume IV: Operations, Volume V: Corrosion, Environmental Issues, and Future Developments*, vol. 1. Springer Science & Business Media, 2007.

[81] Eurochlor, "Chlor-alkali industry review 2019-2020," tech. rep., Eurochlor, a sector group of Cefic, 2020.

[82] J. I. Otashu and M. Baldea, "Corrigendum to "demand response-oriented dynamic modeling and operational optimization of membrane-based chlor-alkali plants"[computers and chemical engineering 121 (2019) 396–408]," *Computers & Chemical Engineering*, vol. 145, p. 107171.

[83] P. S. Agachi, Z. K. Nagy, M. V. Cristea, and Á. Imre-Lucaci, *Model based control: case studies in process engineering.* John Wiley & Sons, 2007.

[84] T. Budiarto, E. Esche, J.-U. Repke, and E. Leksono, "Dynamic model of chloralkali membrane process," *Procedia engineering*, vol. 170, pp. 473–481, 2017.

[85] M. Espinosa-López, C. Darras, P. Poggi, R. Glises, P. Baucour, A. Rakotondrainibe, S. Besse, and P. Serre-Combe, "Modelling and experimental validation of a 46 kw pem high pressure water electrolyzer," *Renewable Energy*, vol. 119, pp. 160–173, 2018.

[86] J. Webster and C. Bode, "Implementation of a non-discretized multiphysics pem electrolyzer model in modelica," in *Proceedings of the 13th International Modelica Conference, Regensburg, Germany, March 4–6, 2019*, no. 157, Linköping University Electronic Press, 2019.

[87] E. Wolf, "Large-scale hydrogen energy storage," in *Electrochemical energy storage for renewable sources and grid balancing*, pp. 129–142, Elsevier, 2015.

[88] ENTSO-E, "Day-ahead prices." https://transparency.entsoe.eu/transmission-domain/r2/dayAheadPrices/. European Network of Transmission System Operators for Electricity. Accessed: 2021-02-01.

[89] M. Baldea, J. Du, J. Park, and I. Harjunkoski, "Integrated production scheduling and model predictive control of continuous processes," *AIChE Journal*, vol. 61, no. 12, pp. 4179–4190, 2015.

[90] M. T. Kelley, R. C. Pattison, R. Baldick, and M. Baldea, "An milp framework for optimizing demand response operation of air separation units," *Applied energy*, vol. 222, pp. 951–966, 2018.

[91] J. M. Simkoff and M. Baldea, "Parameterizations of data-driven nonlinear dynamic process models for fast scheduling calculations," *Computers & Chemical Engineering*, vol. 129, p. 106498, 2019.

[92] M. Ławryńczuk, "Nonlinear predictive control for hammerstein–wiener systems," *ISA transactions*, vol. 55, pp. 49–62, 2015.

[93] F. Scheepers, M. Stähler, A. Stähler, E. Rauls, M. Müller, M. Carmo, and W. Lehnert, "Temperature optimization for improving polymer electrolyte membrane-water electrolysis system efficiency," *Applied Energy*, vol. 283, p. 116270, 2021.

[94] M. Carmo, D. L. Fritz, J. Mergel, and D. Stolten, "A comprehensive review on pem water electrolysis," *International journal of hydrogen energy*, vol. 38, no. 12, pp. 4901–4934, 2013.

[95] D. Olsen, S. Kiliccote, M. Sohn, L. Dunn, M. Piette, *et al.*, "Taxonomy for modeling demand response resources," tech. rep., Lawrence Berkeley National Lab.(LBNL), Berkeley, CA (United States), 2014.

[96] S. M. Alia, S. Stariha, and R. L. Borup, "Electrolyzer durability at low catalyst loading and with dynamic operation," *Journal of the Electrochemical Society*, vol. 166, no. 15, p. F1164, 2019.

[97] A. Weiß, A. Siebel, M. Bernt, T.-H. Shen, V. Tileli, and H. Gasteiger, "Impact of intermittent operation on lifetime and performance of a pem water electrolyzer," *Journal of The Electrochemical Society*, vol. 166, no. 8, p. F487, 2019.

[98] L. Bertuccioli, A. Chan, D. Hart, F. Lehner, B. Madden, and E. Standen, "Study on development of water electrolysis in the eu," *Fuel cells and hydrogen joint undertaking*, pp. 1–160, 2014.

[99] A. Buttler and H. Spliethoff, "Current status of water electrolysis for energy storage, grid balancing and sector coupling via power-to-gas and power-to-liquids: A review," *Renewable and Sustainable Energy Reviews*, vol. 82, pp. 2440–2454, 2018.

[100] P. Patrinos, D. Bernardini, A. Maffei, A. Jokic, and A. Bemporad, "Two-time-scale mpc for economically optimal real-time operation of balance responsible parties," *IFAC Proceedings Volumes*, vol. 45, no. 21, pp. 741–746, 2012.

[101] B. Hylkema, "Determinants of profitability in the dutch positive balancing power market: A case study at akzonobel," Master's thesis, Delft University of Technology, 2017.

[102] M. J. Vasallo, J. M. Bravo, E. G. Cojocaru, and M. E. Gegúndez, "Calculating the profits of an economic mpc applied to csp plants with thermal storage system," *Solar Energy*, vol. 155, pp. 1165–1177, 2017.

[103] M. Killian and M. Kozek, "Ten questions concerning model predictive control for energy efficient buildings," *Building and Environment*, vol. 105, pp. 403–412, 2016.

[104] E. Mohammadi and M. Montazeri-Gh, "A new approach to the gray-box identification of wiener models with the application of gas turbine engine modeling," *Journal of Engineering for Gas Turbines and Power*, vol. 137, no. 7, p. 071202, 2015.

[105] V. Adetola, D. DeHaan, and M. Guay, "Adaptive model predictive control for constrained nonlinear systems," *Systems & Control Letters*, vol. 58, no. 5, pp. 320–326, 2009.

[106] N. Zecevic and N. Bolf, "Advanced operation of the steam methane reformer by using gain-scheduled model predictive control," *Industrial & Engineering Chemistry Research*, vol. 59, no. 8, pp. 3458–3474, 2020.

[107] X. Wang, H. Teichgraeber, A. Palazoglu, and N. H. El-Farra, "An economic receding horizon optimization approach for energy management in the chlor-alkali process with hybrid renewable energy generation," *Journal of Process Control*, vol. 24, no. 8, pp. 1318–1327, 2014.

[108] P. Fragiacomo and M. Genovese, "Numerical simulations of the energy performance of a pem water electrolysis based high-pressure hydrogen refueling station," *International Journal of Hydrogen Energy*, vol. 45, no. 51, pp. 27457–27470, 2020.

[109] A. Midilli, S. Inac, and M. Ozsaban, "Exergetic sustainability indicators for a high pressure hydrogen production and storage system," *International Journal of Hydrogen Energy*, vol. 42, no. 33, pp. 21379–21391, 2017.

[110] E. Taibi, H. Blanco, R. Miranda, and M. Carmo, "Green hydrogen cost reduction; scaling up electrolysers to meet the 1.5 c climate goal," tech. rep., International Renewable Energy Agency, Abu Dhabi, 2020.